Dissertation
submitted to the
Combined Faculty of Natural Sciences and Mathematics
of the Ruperto Carola University Heidelberg, Germany
for the degree of
Doctor of Natural Sciences

Presented by
MSc Diana Martins Bordalo
born in: Sezulfe, Portugal
Oral examination: 26 November 2019

Loss of Filamin A leads to heart failure in zebrafish

Referees:
Prof. Dr. Marc Freichel
Prof. Dr. med. Benjamin Meder

"*A ship in harbor is safe, but that is not what ships are built for.*"

— John Augustus Shedd, Salt from My Attic

Abstract

Dilated Cardiomyopathy (DCM) is frequently leading to heart failure. Familial analysis revealed 30% - 60 % of cases to be of genetic cause, predominantly occurring in genes encoding for structural proteins. The underlying mechanisms and signalling events that translate DCM causing mutations into the clinical phenotype are poorly understood. Previously, our group identified the Core-Binding Factor β (CBFβ) to be an essential factor for maintaining the sarcomeric Z-disc structure of the heart muscle. CBFβ is mainly located in the sarcomere and is retained in the cytoplasm via the interaction with Filamin A (FLNA). However it is hypothesized that under stress conditions, CBFβ is translocated to the nucleus, where it regulates the expression of several genes. To analyze the contribution of FLNA to the development of heart failure we created a transient and a stable loss-of-function model of FLNA in zebrafish.

FLNA transient knockdown (MO-*flna*) resulted in systolic dysfunction, defects in re-absorption of cardiac matrix, a dilated atrium, blood regurgitation and maturation defects shown by uncompleted heart looping. We observed a significantly reduced heart rate (MO-*control* vs MO-*flna*; mean±SD: 148±6.9 vs 108±25.1 beats/min, respectively; $p<0.05$) and fractional shortening (MO-*control* vs MO-*flna*; mean±SD: 64.7±4.0 vs 19.3±10.8 beats/min, respectively; $p<0.0001$). We further established the CRISPR-CAS9 mediated FLNA stable knockout (FLNA KO). Indeed, in F0 embryos we observed a significantly reduced heart rate (wildtype vs FLNA KO; mean±SD: 144±17.6 vs 106±12.3 beats/min, respectively; $p<0.0001$) and fractional shortening (wildtype vs FLNA KO; mean±SD: 64±8.9 % vs 43±8.8 %, respectively; $p<0.0001$), as observed for the FLNA knockdown. F0 mosaic embryos were grown to adulthood and outcrossed with wildtype fish. Two FLNA KO lines (with a predicted stop codon on *flna* exon 4) were selected for propagation. Heterozygous adults from both lines showed a significantly reduced ejection fraction (wildtype vs FLNA KO; mean±SD: 62±6.9 % vs 41±12.2 %, respectively; $p<0.01$) and increased ventilation frequency (wildtype vs FLNA KO; mean±SD: 7±4.2 vs 15±7.0 buccal movements, respectively; $p<0.001$). Compound heterozygous, with both lines mutations, developed a pericardial edema with a dilated heart, stressing the potential role of FLNA in maintaining heart function. Homozygous embryos from one of the lines, did not show a heart failure phenotype. In accordance, *flnb* was shown to be up-regulated in FLNA KO adults, illustrating possible compensatory mechanisms activation. In regard to CBFβ translocation mechanism, for the first time, β-adrenergic stress was identified as a trigger for CBFβ translocation to the nucleus.

In conclusion, FLNA knockdown and knockout in zebrafish leads to a heart failure phenotype. By deeply investigating FLNA regulation (such as cleavage, phosphorylation, response to external cellular stress, etc) and its interacting partners (such as CBFβ), we will further our understanding of the genetic pathogenic pathways involved in heart failure.

Zusammenfassung

Dilatative Kardiomyopathie (DCM) führt häufig zu Herzinsuffizienz. In familiären Untersuchungen wurde festgestellt, dass 30 % - 60 % der Kardiomyopathien genetische Ursachen haben, die überwiegend in den Genen, für Strukturproteine kodierend, vorkommen. Die zugrundeliegenden Mechanismen, sowie Signalkaskaden, die dazu führen, dass DCM-assoziierte Mutationen zu einem klinischen Phänotyp führen, sind noch nicht ausreichend untersucht. In vorangegangenen Studien hat unsere Arbeitsgruppe den Core-Binding Factor β (CBFβ) als möglichen essentiellen Faktor identifiziert, um die sarkomerische Z-Disk-Struktur im Herzmuskel aufrecht erhalten zu können. CBFβ ist im Sarkomer lokalisiert und wird durch die Interaktion mit Filamin A (FLNA) im Zytoplasma gehalten. Allerdings wird angenommen, dass unter Stressbedingungen CBFβ in den Nukleus transportiert wird und dort die Genexpression verschiedener Zielgene reguliert. Um die Rolle von FLNA in der Entwicklung von Herzinsuffizienz zu analysieren, wurde ein stabiles und transientes *loss-of-function* Modell in Zebrabärblingen etabliert.

Der transiente FLNA *knockdown* (MO-*flna*) zeigt eine systolische Dysfunktion, Defekte in der Reabsorption der kardialen Matrix, einem dilatiertem Atrium, Blutrückfluss, sowie Defekte in der Herzentwicklung, welches sich durch eine unvollständig ausgebildete Herzschleife zeigt. Wir konnten eine reduzierte Herzfrequenz beobachten (MO-*control* vs MO-*flna*; Mittelwert±SD: 148±6.9 vs 108±25.1 Schläge/min; $p<0.05$) sowie eine veränderte linksventrikuläre Verkürzungsfraktion (MO-*control* vs MO-*flna*; Mittelwert±SD: 64.7 ±4.0 vs 19.3±10.8 Schläge/min; $p<0.0001$). Des Weiteren wurde eine stabile FLNA CRISPR-CAS9 *knockout* Mutante (FLNA KO) etabliert, welche im Einklang mit der FLNA *knockdown* Mutante steht und für die F0 Embryonen eine signifikant reduzierte Herzfrequenz (Wildtyp vs FLNA KO; Mittelwert±SD: 144±17.6 vs 106±12.3 Schläge/min; $p<0.0001$) sowie linksventrikuläre Verkürzungsfraktion (Wildtyp vs FLNA KO; Mittelwert±SD: 64±8.9 % vs 43±8.8 %; $p<0.0001$) zeigten. F0 Mosaik Embryonen wurden zu adulten Zebrabärblingen herangezüchtet und mit einer Wildtyplinie ausgekreuzt. Zwei der FLNA KO Linien (mit einem Stopp Kodon ins *flna* Exon 4) wurden zur Fortpflanzung ausgewählt, um die Linie zu erhalten. Heterozygote adulte Fische von beiden Linien zeigten eine signifikant reduzierte Ejektionsfraktion (Wildtyp vs FLNA KO; Mittelwert±SD: 62±6.9 % vs 41±12.2 %; $p<0.01$) und eine erhöhte Atemfrequenz (Wildtyp vs FLNA KO; Mittelwert±SD: 7±4.2 vs 15±7.0 Mundöffnungen; $p<0.001$). Compound-Heterozygote Fische, mit Mutationen beider Linien, entwickelten ein perikardiales Ödem mit Herzdilatation, welches die Rolle von FLNA in der Herzfunktion untermalt. Auffällig ist, dass die homozygoten Embryonen einer Linie den Phänotyp einer Herzinsuffizienz nicht zeigten. In Übereinstimmung damit, wurde eine Hochregulation von *flnb* in FLNA KO adulten Fischen gezeigt, was eine mögliche Aktivierung von Kompensations-mechanismen zeigt. Abschließend wurde in Hinblick auf den CBFβ Translokationsmechanismus, adrenerger Stress zum ersten Mal als ein Auslöser für CBFβ Translokation in den Nukleus identifiziert.

Zusammenfassend führt der FLNA *knockdown* und *knockout* im Zebrabärbling zu einem Phänotyp der Herzinsuffizienz. Bei weiteren Untersuchungen in Hinblick auf Regulationsmechanismen von FLNA (wie Proteinspaltung, Phosphorylierung, Stressantwort auf extrazelluläre Einflüsse *etc.*) und dessen Interaktionspartnern (wie CBFβ) werden wir unser Verständnis von genetisch pathogenen Reaktionswegen, die in die Herzinsuffizienz Enwicklung involviert sind, vertiefen.

Table of Contents

1 | Introduction

1.1 Cardiomyopathies

Heart failure (HF) affects 40 million people worldwide, with an increasing prevalence due to the ageing population (Morales and Hershberger, 2017; Czepluch, Wollnik, and Hasenfuß, 2018). Defined as an insufficient cardiac output for appropriate end-organ perfusion, HF mortality rates exceed 40% at 5-year follow-up (Cahill, Ashrafian, and Watkins, 2013; Hobbs et al., 2007). HF strongly reduces the quality of life by affecting exercise tolerance and multi-organ function (Czepluch, Wollnik, and Hasenfuß, 2018). Furthermore, HF itself represent the final phenotype of multiple pathways derived from genetic and/or environmental influences.

Genetic contribution to heart failure is very complex and ranges from monogenic HF syndromes, with high penetrance, to less penetrant and cumulative genetic variants. Cardiomyopathies can derive from such genetic alterations.

According to the *American Heart Association* (AHA), "cardiomyopathies are a heterogeneous group of diseases of the myocardium associated with mechanical and/or electrical dysfunction that usually (but not invariably) exhibit inappropriate ventricular hypertrophy or dilation and are due to a variety of causes that frequently are genetic. Cardiomyopathies either are confined to the heart or are part of generalized systemic disorders, often leading to cardiovascular death or progressive heart failure-related disability" (Maron et al., 2006).

Cardiomyopathies can be classified as primary (the patient does not have other conditions that lead to a weakened myocardium) or secondary (if the myocardium is affected as a result of a systemic or multiple organ disease). Furthermore, according to AHA, primary cardiomyopathies are divided into three categories: genetic, mixed or acquired (**Figure 1.1**) (Maron et al., 2006).

Hypertrophic cardiomyopathy (HCM) is the most common primary genetic cardiomyopathy, with a prevalence of 1 in 500 in the general population (Bonow, 2017). HCM is one of the most frequent causes of sudden cardiac death in young and asymptomatic athletes (Maron, Pelliccia, and Spirito, 1995). In its typical form, it is characterized by a disproportional thickening of the ventricular septum relative to the ventricle free wall (**Figure 1.2**) due to massive myocardial hypertrophy. Patients with HCM often exhibit a reduced stroke volume due to impaired diastolic filling as a consequence of reduced chamber size and compliance of the hypertrophied left ventricle. HCM arises from autosomal dominant mutations, mainly in genes such as β myosin heavy chain (MYH), cardiac troponin-T (TNNT), α-tropomyosin (TPM1) and myosin binding protein C (MYBPC) (Aster, 2014).

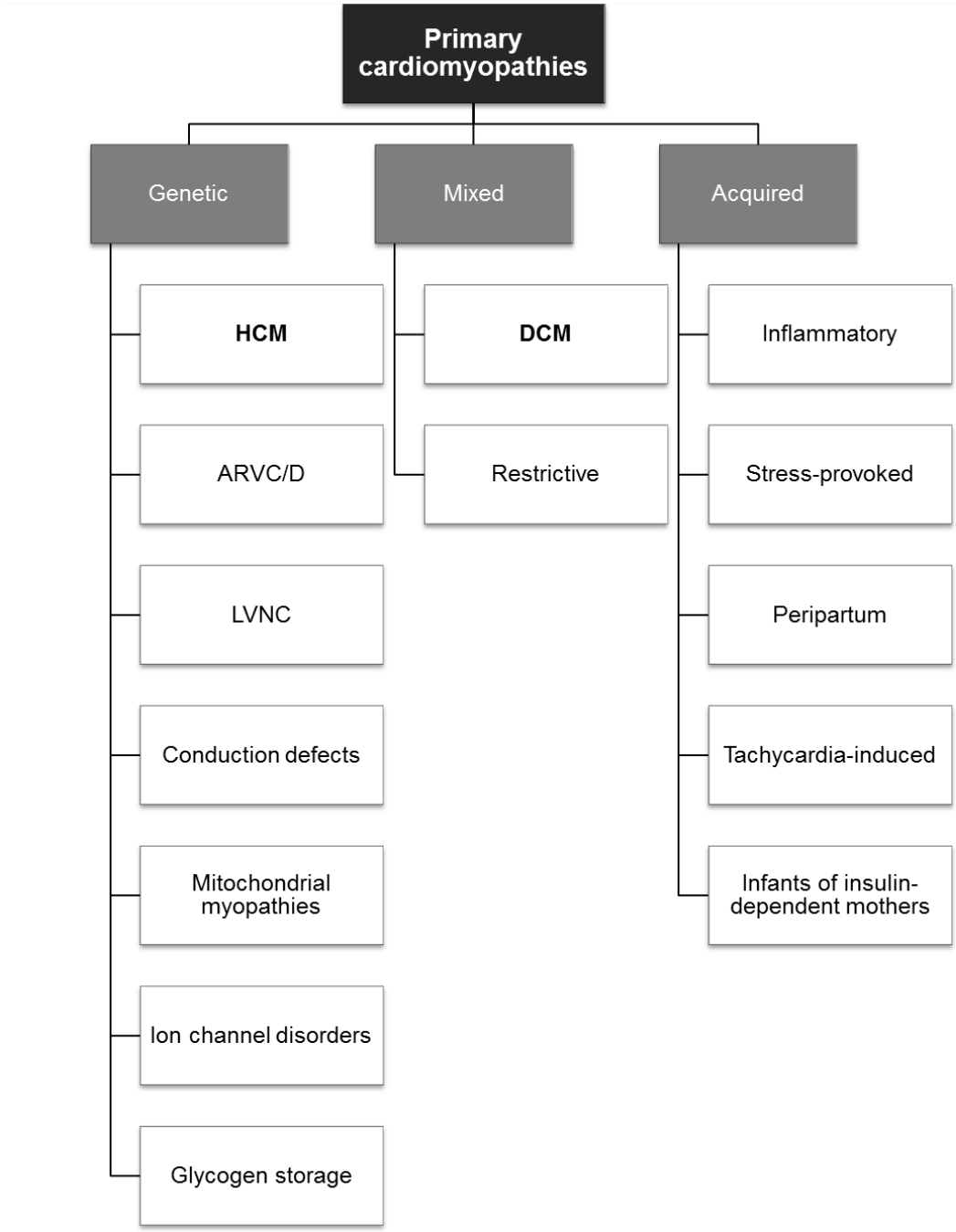

Figure 1.1: **Classification of primary cardiomyopathies.** Adapted from *American Heart Association* Scientific Statement, Maron et al., 2006.

Dilated cardiomyopathy (DCM) with a prevalence of 1:250 (Hershberger, Hedges, and Morales, 2013), is one of the most frequent causes for heart failure (Mestroni et al., 2014) and heart transplantation at young age (Towbin et al., 2006). This disease is commonly characterized by progressive signs and symptoms of heart failure with systolic contractile dysfunction and cardiac dilation (**Figure 1.2**). Patients are affected with cardiac stress caused by volume overload and high end-diastolic pressure that results in reduced left ventricular ejection fraction (which translates to decreased cardiac output). DCM is a multifactorial disease that can arise from genetic mutations, myocarditis, chronic alcohol consumption, iron overload, among others. However, familial analysis revealed that 30% to 50% of DCM are familial cases, with mutations occurring in a wide variety of genes (from cytoskeleton to sarcolemma and nuclear envelop genes; Aster, 2014; Haas et al., 2015). Nevertheless, in most cases the family size is too small to draw conclusions on heritage of genetic variants. The underlying mechanisms and signalling events that translate DCM causing mutations into the clinical phenotype are poorly understood.

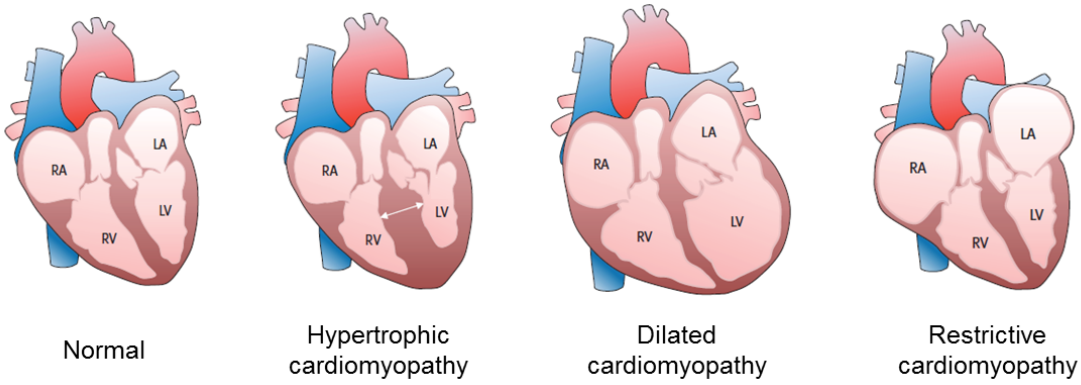

Figure 1.2: **Morphology of the most common primary cardiomyopathies.** Most left is shown a normal heart with represented right atrium (RA), right ventricle (RV), left atrium (LA) and left ventricle (LV). Adapted from Genetische Diagnostik von Kardiomyopathien, Meder, 2017.

Other cardiomyopathies have been reported such as restrictive cardiomyopathy (RCM, **Figure 1.2**, Aster, 2014), Arrhythmogenic Right Ventricle Cardiomyopathy (ARVC, Aster, 2014) and Left Ventricular Non-Compaction (LVNC, Sedaghat-Hamedani et al., 2017) but with a much lower prevalence in the general population.

Nearly 100 genes were associated with primary cardiomyopathies (Czepluch, Wollnik, and Hasenfuß, 2018). However, further research is needed to enlighten the mechanisms leading to the genetic and phenotypic heterogeneity observed. Different variants within an individual gene can produce contrasting cardiomyopathies and, on the contrary, different genetic mutations can lead to the same cardiomyopathy. Furthermore, even within the same family, penetrance and expressivity vary greatly, suggesting that multiple factors (such as genetic, epigenetic or environmental modifiers) contribute to the phenotype. Future research should be directed to identify pathogenic mutations and variants, as well as defining the cellular and molecular mechanisms of genetic cardiomyopathies. In this setting, understanding the contribution of multiple genes to a phenotype, will allow targeted genetic testing of families, enabling early risk stratification and treatment before cardiac decompensation or remodelling has occurred.

1.2 Zebrafish in cardiovascular research

Since George Streisinger's initial use of zebrafish in the early nineteens, zebrafish has been developed into a widely used model organism (Grunwald and Streisinger, 1992). Zebrafish possess several advantages, such as very fast development, with most of organ primordia formed at 24 hours post-fertilization (hpf), translucent embryos, high egg abundance, small-sized embryos and established pipelines of high-throughput molecular and drug screening (Poon and Brand, 2013). It is an appealing model in cardiovascular research, given the high homology with humans [82% of human disease-related genes listed in the *Online Mendelian Inheritance in Man* (OMIM) have at least one orthologue in zebrafish, Howe et al., 2013]. The genetic pathways of heart development are highly conserved between humans and zebrafish (Poon and Brand, 2013).

In the teleost fish, cardiac progenitors are specified at 5 hours post-fertilization (hpf, **Figure 1.3 - A**). At 22 hpf, a cardiac cone is formed by the fusion of the bilateral heart fields. This cone extends anteriorly and is reshaped into a primitive heart tube. By 24 hpf, the linear heart tube has an outer myocardial and an inner myocardial layer, separated by "cardiac jelly" (the extracellular matrix). At this point, the heart tube exhibits peristaltic contractile movements (**Figure 1.3 - B**). At 33 hpf, the heart tube acquires an S-shaped configuration by looping of the chambers. At 36 hpf, the onset of the cardiac conduction system is outlined by the change in the slow peristaltic contractions to a sequential chamber contraction (**Figure 1.3 - C**). At 37 hpf, the atrioventricular myocardium undergoes a genetic identity shift, which triggers endocardial cell morphology changes. By 48 hpf, the ventricular chambers balloons, displaying an outer curvature with big elongated myocardial cells that are able to conduct electrical activity thrice as fast than cells in the inner curvature (**Figure 1.3 - D**). At 72 hpf, the endocardial cells form the primitive valve leaflets, which block the retrograde blood flow from the ventricle to the atrium (**Figure 1.3 - E**).

In an adult zebrafish heart, the atrium only has a thin layer of myocardial cells, whereas the ventricle has trabeculae that thickens its walls (**Figure 1.3 - F**). The pacemaker site is located at a ring-like structure, at the border between the sinus venosus and the atrium (Poon and Brand, 2013, Asnani and Peterson, 2014, Bakkers, 2011).

Zebrafish is also a relevant model in cardiomyopathy research (Asnani and Peterson, 2014). Mutants like *silent heart* (*tnnt2* gene disruption, Chen et al., 1996; Sehnert et al., 2002; Stainier et al., 1996) and *pickwick*$^{\mathrm{m171}}$ (*ttn* truncating variant, Driever et al., 1996; Xu et al., 2002) have shown that parallels can be drawn between genes relevant for primary cardiomyopathies in humans and zebrafish (Vogel et al., 2009). Furthermore, JunB is a transcriptional factor responsible for the activation of *core-binding factor* β (*cbf*β) gene transcription in the heart and skeletal muscle cells. JunB and CBFβ have been correlated with heart failure in zebrafish (Meder et al., 2010).

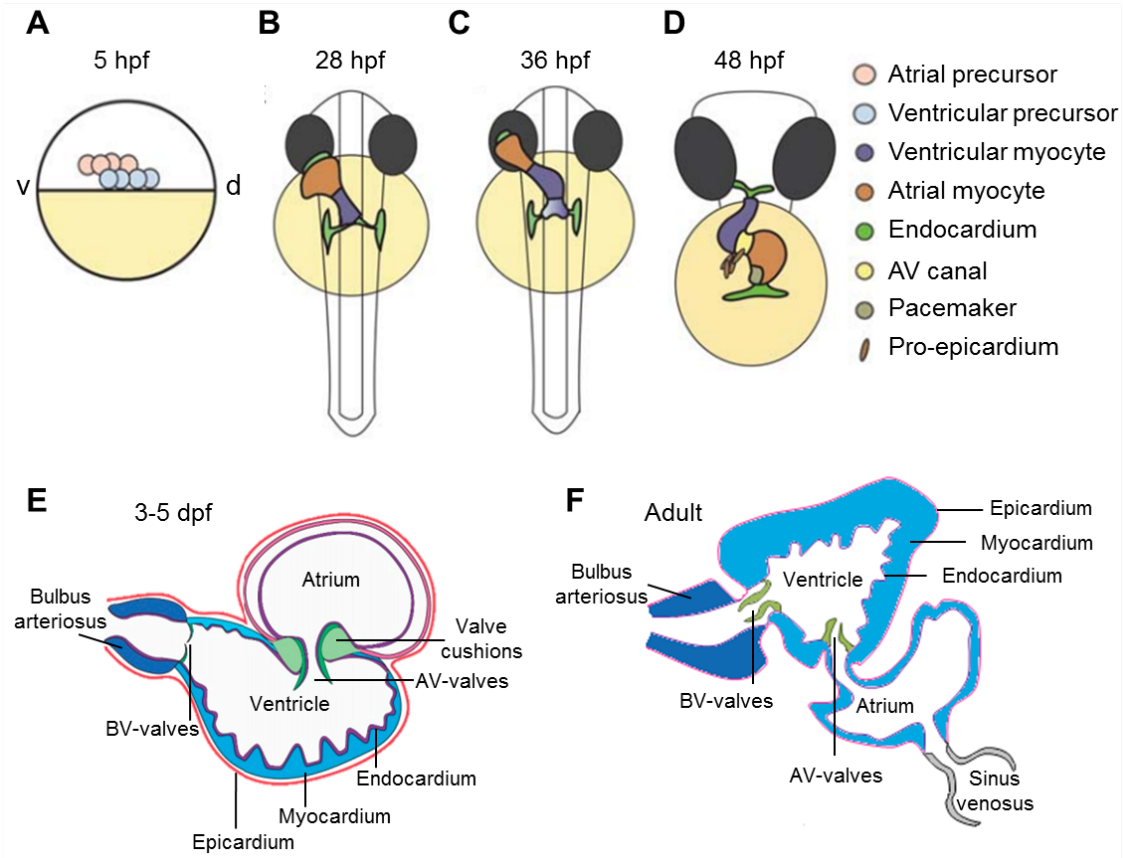

Figure 1.3: **Stages of cardiac development in zebrafish.** A - at 5 hours post-fertilization (hpf), the cardiac progenitor cells are located bilaterally in the lateral marginal zone. Atrial progenitor cells (pink) are located more ventral than the ventricle progenitor cells (light blue), cardiogenic differentiation is initiated in the future ventricle myocardial cells by the expression of cardiac myosins. B - at 28 hpf, the linear heart tube has formed. C - new cardiomyocytes are added to this region (purple gradient). At 36 hpf, cardiac looping has started, with a displacement of the ventricle towards the mid-line and the constriction at the position of the atrioventricular canal. D - the heart tube continues to loop and forms an S-shaped loop. Ellipsoid extracardiac pro-epicardial cells (brown) are located near the atrioventricular canal (yellow), from where they start to cover the myocardium with an epicardial layer. The pacemaker is present in the inner curvature of the atrium near the venous pole (green). Adapted from Bakkers, 2011. E - cross-section of the embryonic heart with 3 to 5 days post-fertilization (dpf). BV - bulboventricular; AV - atrioventricular. Adapted from Brown et al., 2016. F - schematic representation of adult zebrafish heart anatomy. BV - bulboventricular; AV - atrioventricular. Adapted from Poon and Brand, 2013.

1.3 Runx family

RUNX proteins belong to the Runx family which is deeply involved in development regulation. These transcriptional factors are characterized by a highly conserved Runt domain, first described in *Drosophila melanogaster* (Gergen and Butler, 1988). This domain is located at the N-terminus and contains 128 amino acids (Ito, 2004) that can specifically recognize the sequence PyGPyG-GTPy (Py = pyrimidine) (Kamachi et al., 1990).

This family has three members: RUNX1, RUNX2 and RUNX3 (**Figure 1.4**). Research using the mouse model revealed a non-redundant and tissue specific role for each of the Runx genes: *runx1* knockout led to a lack of definitive hematopoiesis (Bee et al., 2010); no bone formation was observed in the *runx2* knockout (Komori et al., 1997) and *runx3* knockout was associated with defects in cytotoxic T cell development (Ito et al., 2008), neural and gastrointestinal disorders (Inoue et al., 2002 and Li et al., 2002, respectively).

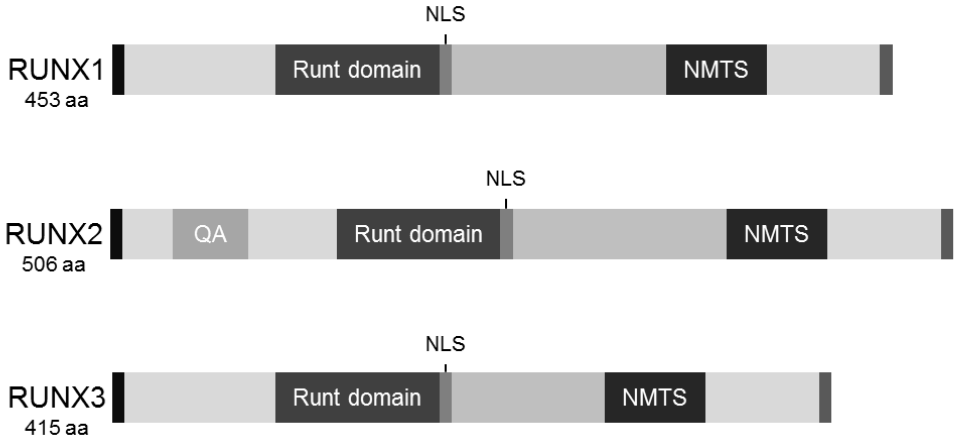

Figure 1.4: **Structure of the RUNX protein family.** The conserved Runt domain is responsible for the recognition and binding of DNA. All members possess a Nuclear Matrix Targeting Signal (NMTS) and a Nuclear Localization Signal (NLS); however, only RUNX2 includes a QA domain containing a stretch of Glutamine and Alanine residues. Adapted from Camacho, 2011.

Although the Runt domain can recognize and bind to a specific DNA sequence, this protein-DNA interaction can be increased and stabilized by CBFβ.

1.4 Core Binding Factor β (CBFβ)

CBFβ binds the Runt domain of all Runx family members and, besides enhancing its affinity to DNA (Bartfeld et al., 2002; Nagata et al., 1999), it can also protect RUNX proteins from ubiquitin-proteasome degradation (Huang et al., 2001). Interestingly, it was shown that CBFβ itself does not bind the DNA directly (Nagata et al., 1999) and neither does it possess a nuclear localization sequence (NLS, Blyth, Cameron, and Neil, 2005). Under which circumstances CBFβ is localized in the nucleus is still poorly studied. However, despite the nuclear localization of CBFβ, it has been reported by Meder *et al.* (2010) that CBFβ is also a structural protein of the sarcomeric Z-disc, essential to maintain its functional structure. In different model systems, it has been shown that genetic abnormalities in genes involved in mechanical Z-disc stabilization lead to heart failure, stressing the need for detailed CBFβ research in this context.

1.4.1 CBFβ loss-of-function models

In the zebrafish CBFβ loss-of-function model, heart function is impaired, with reduced heart rate and fractional shortening (Meder et al., 2010). Furthermore, upon tactile stimulation, CBFβ morphants showed weak or complete absence of skeletal muscle response. These findings were consistent with the sarcomeric disarray observed in these morphants (Meder et al., 2010).

To better understand the phenotype of CBFβ null mutants both in mouse and zebrafish, it is crucial to have a basic understanding of the hematopoiesis process. During embryonic development, several waves of hematopoiesis occur in separate locations. The first wave is defined by the migration of both the primitive myeloid progenitors (later differentiating into macrophages and neutrophils) and erythromyeloid progenitors (later generating erythrocytes, mast cells and neutrophils) from the anterior and posterior lateral mesoderm, respectively. In a second wave, the hematopoietic stem and progenitor cells (HSPC) are formed in the dorsal aorta or aorta-gonad-mesonephros, in mouse and zebrafish, respectively. The HSPC suffer an endothelial hematopoietic transition after which they enter circulation and colonize several organs (Bresciani et al., 2014; Forrester, Berman, and Payne, 2012).

In the mouse CBFβ null mutant ($cbf\beta^{-/-}$) the embryos showed a total lack of multipotent hematopoietic progenitors and died prematurely due to hemorrhages into the central nervous system (Sasaki et al., 1996). Of note, $cbf\beta^{-/-}$ showed a similar phenotype to $runx1^{-/-}$. In both models, the absence of definitive hematopoietic lineages suggests that both genes are necessary for HSPC specification (Sasaki et al., 1996). Further studies in zebrafish could elucidate distinct functions for CBFβ and RUNX1 (Bresciani et al., 2014). Bresciani *et al.* 2014 showed that RUNX1 is necessary for the emergence of HSPC, while CBFβ is pivotal for the release of HSPC from the aorta-gonad-mesonephros region in a later stage of development.

Until now, the function of CBFβ was analysed in early development by the characterization of loss-of-function morphants (Meder et al., 2010). Understanding the phenotype of disease causing CBFβ mutations in humans, might further elucidate CBFβ dependent mechanisms.

1.4.2 CBFβ associated diseases

Translocations in chromosome 16 have been found to produce a fusion protein between CBFβ and smooth-muscle myosin-heavy-chain (MYH11). This CBFβ-MYH11 isoform has been associated with acute myeloid leukemia (Liu et al., 1993) and extensively studied. Less studied is the contribution of CBFβ to cleidocranial dysplasia (Machol, Mendoza-Londono, and Lee, 2006), a congenital disease characterized by skeletal defects. Mouse studies where CBFβ was ablated in skeletal cells showed that CBFβ is necessary for bone ossification, chondrocyte and osteoblast proliferation and maturation (Chen et al., 2014).

In the sarcomere, CBFβ is primarily encountered as a structural protein but, as described before, it can also be found in the nucleus interacting with the RUNX proteins. The translocation of CBFβ from the sarcomere to the nucleus was studied by Yoshida *et al.* (2005), who showed that CBFβ is retained in the sarcoplasm through the interaction with the protein Filamin A (FLNA). In which circumstances is this interaction disturbed to allow CBFβ translocation to the nucleus and how it is regulated remains unclear.

1.5 Filamin family

The cytoskeleton is an essential cell component determining cellular movement, shape, division and signal transduction in response to the external environment. The defining activity of filamins is the capacity to transform a population of non-linked F-actin filaments into a dynamic orthogonal network (Wang and Singer, 1977).

The filamin family consists of three isoforms: filamin A (FLNA), filamin B (FLNB) and filamin C (FLNC) (**Figure 1.5**). FLNA is ubiquitously expressed in all tissues. FLNB, with the exception of retinal epithelium where it is highly expressed, is expressed at much lower levels but also ubiquitously. FLNC is expressed in skeletal and cardiac muscle cells (Stossel et al., 2001 and Feng et al., 2006). In human and mice, *flna* is located on the X chromosome, while *flnb* and *flnc* are located on chromosome 3 and 7, respectively.

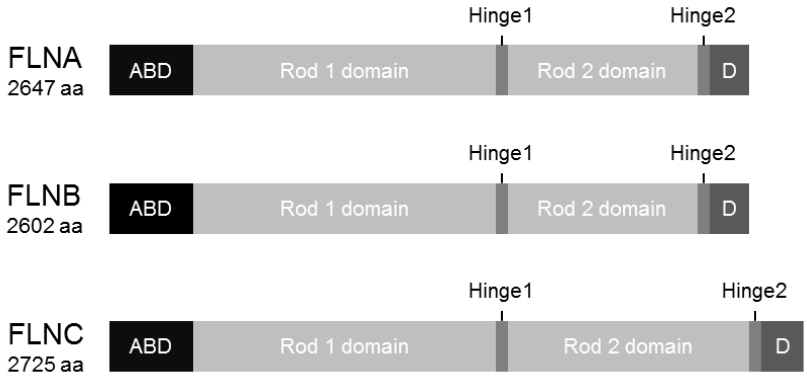

Figure 1.5: **Structure of the filamin family proteins.** Filamin comprise a highly conserved actin binding domain (ABD), rod 1 and 2 domains composed of immunoglobulin-like repeats, flexible hinges between repeats 15-16 and 23-24 and the self-association domain (D) (Stossel et al., 2001, Nakamura, Stossel, and Hartwig, 2011).

Filamins contain an N-terminal actin binding domain (ABD), which is highly conserved between actin binding proteins (Clark et al., 2009; Sawyer et al., 2009). This 30 kDa domain comprises two calponin homology (CH) domains, required for F-actin binding (Bresnick, Warren, and Condeelis, 1990). The ABD is followed by a rod region of filamin repeat domains that adopt an immunoglobulin-like (Ig-like) configuration. With a total of 58 nm contour length, the rod 1 domain encompasses 1 to 15 Ig-like repeats. With only 19 nm due to pairing of neighbouring Ig-like repeats, rod 2 encompasses repeats 16 to 23 (Nakamura, Stossel, and Hartwig, 2011) and it is separated from rod 1 by a hinge. Another hinge separates rod 2 from the C-terminal self-association domain (encompassing Ig-like repeat 24). It is not fully understood if filamins can form heterodimers, however the detection of FLNB and FLNC heterodimer was reported in *in vitro* cross-linking assays (Himmel et al., 2003). While no evidence was shown or hypothesis formed proposing the heterodimerization of FLNA and FLNC (Himmel et al., 2003), data indicates that FLNA could heterodimerise with FLNB to compensate for dysfunctional FLNA homodimers (Sheen et al., 2002).

1.5.1 Filamin A (FLNA)

Filamin A, with approximately 280 kDa, consists of 2647 amino acids. It is composed of an N-terminal actin-binding domain (ABD) and a long rod-like domain of 24 repeats discontinued by two hinge domains (30 amino acid flexible loop). The ABD comprises two calponin homology domains and the filamin repeat 24 functions as the homo-dimerization domain (Savoy and Ghosh, 2013).

Besides binding actin filaments, FLNA interacts with more than 90 different proteins from different pathways, mainly through its rod 2 domain (Popowicz et al., 2006 and Nakamura, Stossel, and Hartwig, 2011). Several studies suggest that FLNA modulates the subcellular localization of its interacting partners, thus regulating multiple signalling cascades of different pathways (Camacho, 2011).

The interaction of FLNA with actin but also with other proteins, can be regulated through different factors. Nakamura *et al.* (2011) summarized it into (1) mechanical forces, (2) phosphorylation, (3) proteolysis, (4) competition between binding partners and/or (5) multimerization of partners. Importantly, Savoy *et al.* (2013) highlighted the different functional roles of complete FLNA located in the cytoplasm and cleaved FLNA shuttling to the nucleus. Depending on the location of FLNA, defined by its protein length (cleaved or complete) and also possibly its interacting partners, different signalling pathways are activated. All these are important factors to investigate in the context of cardiomyopathies.

1.5.2 FLNA loss-of-function models

Filamin-deficient mice showed an incomplete septation of the heart outflow tract, atrial and ventricular septal defects, small right ventricle, hemorrhages, thickening of the mitral valve and skeletal fusion defects (Hart et al., 2006). This led to male lethality in embryonic stages. A different FLNA loss-of-function model exhibit abnormal epithelial and endothelial organization, as well as aberrant adherens junctions (Feng et al., 2006). This was accompanied by an abnormal cardiovascular aortic arch, a thickened and malformed outflow tract valve, septal and atrial defects and also abnormal angiogenesis (Feng et al., 2006; Zhou et al., 2007). Likewise, in this model, embryos died prematurely. Currently, all the FLNA loss-of-function models created have high embryonic lethality, hindering studies throughout development until adulthood.

Curiously, no major heart defects were detected in FLNB (Zhou et al., 2007; Lu et al., 2007) or FLNC (Dalkilic et al., 2006) loss-of-function models. Moreover, up to date, no FLNA loss-of-function model in zebrafish have been described. In addition, examining the phenotype of FLNA mutations in humans, will broaden our understanding of FLNA complex function.

1.5.3 FLNA associated diseases

A nonsense mutation was identified in FLNA and shown to hinder the migration of neurons to the central nervous system in humans (Fox et al., 1998). Males with this mutation, occasionally displayed aortic dilatation and died from massive hemorrhage during the neonatal period, while the ones surviving until adolescent years died of abdominal aortic aneurysms. Females manifested a high incidence of strokes, congenital heart defects such as patent ductus arteriosus and aortic

aneurysms (Fox et al., 1998; Zhou et al., 2007). Multiple FLNA mutations were associated with skeletal (such as otopalatodigital syndrome) and cardiac malformations that often lead to perinatal death. Kindt *et al.* linked FLNA mutations to familial cardiac valvular dystrophy (X-linked myxomatous valvular dystrophy, Kyndt et al., 2007; Goodwin et al., 2012). Missense mutations affecting the actin-binding site of FLNA which results in frontometaphyseal dysplasia, with accompanying extraskeletal features such as cardiac, tracheobronchial and urologic malformations leading to perinatal death have also been reported (Robertson et al., 2006).

There are several hints for an impact of FLNA mutations on myocardial function, however this hypothesis was never clearly investigated in heart failure.

1.6 CBFβ and FLNA interaction

As mentioned before, CBFβ is primarily encountered in the sarcomere, however is known that it translocates to the nucleus to interact with RUNX proteins. This particularity of CBFβ to translocate to the nucleus is of utmost importance given that CBFβ might act as a stress signal transducer from the sarcomere to the nucleus. Progressively more evidence is provided about the role of several Z-disc structural proteins that convey information from the Z-line to the nucleus, therefore uncovering their intracellular signaling function in addition to their structural function in the sarcomere (Knöll, Hoshijima, and Chien, 2002). Yoshida *et al.* (2005) showed that CBFβ translocation is partially regulated by the interaction with FLNA, which retains CBFβ in the sarcoplasm of HeLa cells.

CBFβ interacts with FLNA through the repeat 23, hinge 2 and the self-association domain (repeat 24). On the other hand, FLNA binds CBFβ between the residues 68 to 93 (Yoshida et al., 2005).

The interaction between FLNA and CBFβ was investigated in the context of osteoarthritis by Johnson *et al.*, 2012. The authors identified FLNA as an interacting partner by cross-linking kartogenin (KGN) to its potential cellular interacting partners. Curiously, KGN and CBFβ compete for the same FLNA binding region. In essence, KGN binds FLNA and disrupts CBFβ interaction, promoting CBFβ translocation to the nucleus and chondrogenesis stimulation (Johnson et al., 2012).

It is important to consider that possibly any protein binding to the same region as CBFβ might interfere with its binding to FLNA. In **Supplement Table S1** known interaction partners of FLNA, that bind the repeats 23 to 24, are listed.

In summary, a deep understanding of the FLNA interactome will elucidate one of the possible mechanisms that regulate CBFβ translocation to the nucleus. Furthermore, it would be relevant to explore the response of FLNA and its interacting partners to stress factors present in the context of cardiomyopathies.

2 | Research objectives

FLNA is an actin-binding cytoskeletal protein, involved in different cellular and stress response mechanisms. The correct functioning of FLNA is essential for cells demonstrated by several malformations being associated with diverse human diseases. CBFβ was identified by our group as an important gene in heart failure pathogenesis. In particular, CBFβ acts as a transcriptional factor interacting with FLNA thereby regulating the expression of important heart failure-related downstream genes. FLNA functions has been proposed to act as a regulatory layer of CBFβ shuttling. This project aims to assess the genomic and functional mechanism by which FLNA contributes to heart failure.

Using zebrafish as a model system, the objectives of this research were as follows:

I Analyse embryonic heart function in a transient FLNA loss-of-function model.

II Establish CRISPR-CAS9 methodology for the generation of zebrafish knockout lines.

III Understand the role of FLNA in the progression of heart failure using a stable FLNA loss-of-function model.

IV Define FLNA and CBFβ cellular localization in wildtype and understand if cardiac-relevant stress affects CBFβ cellular localization.

3 | Materials and Methods

Materials

3.1 Equipment

The equipment used for the experiments in this thesis is listed in **Table 3.1**.

Table 3.1: **Equipment.**

Equipment	Model	Manufacturer
Embryos manipulation		
Dual-Stage Glass Micropipette Puller	PC-10	Narishige
Stereoscope	MZFLIII	Leica
Stereoscope camera	DFC310 FX	Leica
Inverted microscope	DMIRB	Leica
Inverted microscope camera	DFC360 FX	Leica
Microinjector	FemtoJet4i	Eppendorf
Incubator	Heraeus	Thermo Fisher Scientific
Imaging		
Fluorescence microscope	Axioskop 2 plus	Zeiss
Fluorescence microscope	Ni-E	Nikon
Fluorescence microscope camera	AxioCam MRc	Zeiss
Confocal microscope	DMi8	Leica
Luminescense imaging system	Isogen Life Sciences	Proxima
Molecular Biology		
Centrifuge	5430R	Eppendorf
Centrifuge	5417R	Eppendorf
Table top centrifuge	D-6015	Neolab
Table top centrifuge	MiniStar	VWR
Thermomixer	Comfort	Eppendorf
Vortex mixer	Reax 2000	Heidolph
Heat plate	RCT basic	IKAwerke

Equipment	Model	Manufacturer
Molecular Biology		
Lateral shaker	DuoMax 2030	Heidolph
Tube roller	SU 1400	SunLab
Weighing scale	CP142S	Sartorius
Microwave	NN-SD452W	Panasonic
Electrophoresis chamber	PerfectBlue Mini L	Peqlab
Electrophoresis power supply	EPS 301	Amersham Pharmacia Biotech
UV transilluminator	UST-20S-8E	Biostep
Digital graphic printer	UP-D895	Sony
Spectrophotometer	SmartSpec Plus	BioRad
HistoCore	Pearl	Leica
HistoCore	Arcadia H	Leica
Microtome	RM 2145	Leica
pH/mV bench meter	pH 211	Hanna Instruments
Real-time PCR system	ViiA 7	Applied Biosystems
Thermocycler	Mastercycler ep gradient S	Eppendorf
Thermocycler	SimpliAmp	Applied Biosystems
X-ray film processor	Cawomat 2000 IR	Wiroma
Spectrophotometer	Nanodrop Lite	Thermo Fisher Scientific
Fragment Analyser	-	Advanced Analytical Technologies

3.2 Buffers and solutions

All buffers and solutions used in the experiments that were not provided by the equipment/reagent manufacturer can be seen in **Table 3.2**.

Table 3.2: **Composition of buffers and solutions.**

Name	Composition
E3 buffer	5 mM NaCl 0.17 mM KCl 0.33 mM $CaCl_2$ 0.33 mM $MgSO_4$ 1 % methylene blue
Dent's fixative solution	80 % methanol 20 % DMSO
Dent's bleach solution	70 % methanol 10 % H_2O_2 20 % DMSO
PBS	1:10 dilution of 10X PBS (Gibco) with dH_2O

Name	**Composition**
PBT	1X PBS 0.1 % Tween-20 (Roth)
PBST	1X PBS 1 % Tween-20 (Roth)
TNN lysis buffer	50 mM Tris-HCl, pH 7.5 120 mM NaCl 0.1 % NP-40
TNN working buffer	TNN lysis buffer 1 mM DTT 1 mM $NaVO_3$ 1 mM NaF 0.2 mM PMSF 1X Protease Inhibitor Cocktail Tablets (Roche) 1X PhosSTOP (Roche)
Deyolking buffer	55 mM NaCl 1.8 mM KCl 1.25 mM $NaHCO_3$
Washing buffer	10 mM Tris-HCl, pH 8.5 110 mM NaCl 3.5 mM KCl 2.7 mM $CaCl_2$
TBS buffer	50 mM Tris-HCl, pH 7.4 150 mM NaCl
TBST buffer	50 mM Tris-HCl, pH 7.4 150 mM NaCl 0.05 % Tween-20
Running buffer	25 mM Tris 192 mM Glycine 0.1 % SDS
Blotting buffer	19 mM Tris-HCl 144 mM Glycine 15 % Methanol
Blocking buffer	TBST buffer 5 % Milk powder or 5 % BSA

Name	Composition
LB medium	10g Tryptone 10g NaCl 5g Yeast extract in 1L dH_2O

3.3 Biological material

3.3.1 Zebrafish lines

All *Danio rerio* experiments were performed in accordance with the guidelines of the government of Baden-Württemberg and have been approved by the Regierungspräsidium Karlsruhe (permit number 35-9785.81/G-1/15). The project involving genetically modified fish (number G-126/15) was approved by the "Deutsches Zentrum zum Schutz von Versuchstieren". The AB strain (European Zebrafish Research Center, ZDB-GENO-960809-7) was used as the wildtype reference.

3.3.2 Bacteria strains

One Shot TOP10 (Thermo Fisher scientific) bacteria strain with the following genotype: *F- mcrA* Δ *(mrr-hsdRMS-mcrBC)* Φ *80lacZ* Δ *M15* Δ *lacX74 recA1 araD139* Δ *(araleu)7697 galU galK rpsL (StrR) endA1 nupG* was used for TA and DNA Ligase cloning.

3.4 Ensembl genome browser IDs

DNA sequences were retrieved from the *Ensembl genome browser 97*, using the zebrafish genome version GRCz11 (**Table 3.3**).

Table 3.3: **Ensembl IDs used.**

Gene name	Gene ID	Transcript Name	Transcript ID	% similarity with human orthologues
flna	ENSDARG00000074201	flna-202	ENSDART00000135820.3	82 %
cbfβ	ENSDARG00000040917	cbfβ-203	ENSDART00000171871.3	81 %
flnb	ENSDARG00000098374	flna-202	ENSDART00000164423.2	66 %
rplp0	ENSDARG00000051783	rplp0-201	ENSDART00000073462.5	90 %

Taken from http://www.ensembl.org. Last accessed 19th September 2019.

3.5 Oligonucleotides

3.5.1 DNA oligonucleotides

DNA oligonucleotide primers for gRNA cloning, PCR and qRT-PCR were obtained from Sigma and are listed in **Table 3.4** below.

Table 3.4: **Oligonucleotides.**

Primer target	Sequence	Sense/Antisense	Amplicon
CRISPR gRNA cloning			
gRNA targeting *flna* exon 2	5' TAGGAAAGCCCTTGGCGCTCTGG 3'	Sense	-
gRNA targeting *flna* exon 2	5' AAAGCCCTTGGCGCTCTGGGTTT 3'	Antisense	-
CRISPR founders' PCR screening			
flna exon 2	5' CCTGGGTCTGATATGGACTCTT 3'	Sense	276 bp
flna exon 2	5' GGACCTATCAAACCCTGAGAAC 3'	Sense	276 bp
CRISPR off-targets' PCR screening			
ccdc22	5' GCTCAGCAGGAAGCTGAACT 3'	Sense	459 bp
ccdc22	5' GCAACCATGGACATTTTGAA 3'	Antisense	459 bp
nnt	5' GACCGTGGACCACAAAAAGT 3'	Sense	544 bp
nnt	5' CACATCAATCTTTGGCTGGA 3'	Antisense	544 bp
cnih2	5' GGAGGAGGTTGCAGATTCTCT 3'	Sense	457 bp
cnih2	5' AGCAGGGAGGAAGAACATGA 3'	Antisense	457 bp
caska	5' TGCGCATAAAAACGATTGAT 3'	Sense	542 bp
caska	5' TTTTGCCGTGTTTGTTTTCA 3'	Antisense	542 bp
smurf2	5' GGAATGCAGCATCCAGAAAT 3'	Sense	446 bp
smurf2	5' GGAATGCAGCATCCAGAAAT 3'	Antisense	446 bp
znf1140	5' CTCAACCAAAAGGTTTCTCCA 3'	Sense	446 bp
znf1140	5' AGTCCAACACCGTGATCCAT 3'	Antisense	446 bp
Clone sequencing			
M13	5' GTAAAACGACGGCCAGT 3'	Sense	Variable
M13	5' CATGGTCATAGCTGTTTCC 3'	Antisense	Variable
qRT-PCR			
flna	5' CTGACAGCCACACTCACCAC 3'	Sense	80 bp
flna	5' ATTCCCACATGCCCATTTCT 3'	Antisense	80 bp
cbfβ	5' GACGGGAAAGGTGTACCTGA 3'	Sense	78 bp
cbfβ	5' TGAAGATCAAGCCAGCCTCT 3'	Antisense	78 bp
flnb	5' TACGGTCCAGGTATTGAGCC 3'	Sense	73 bp
flnb	5' CACTGAACGTGTCCACAGTGA 3'	Antisense	73 bp
rplp0	5' TGGAAAACAACCCAGCTCT 3'	Sense	75 bp
rplp0	5' CTCCTTGGTGAAGACGAAGC 3'	Antisense	75 bp

3.5.2 Morpholinos

The morpholino (MO) modified antisense oligonucleotides were purchased from GeneTools, LLC. All morpholinos were reconstituted in 200 mM KCl, pH 7.5 to a final concentration of 1 mM. The MO targets, sequences and the titrated optimized concentrations can be found in **Table 3.5**.

Table 3.5: **Morpholino-modified antisense oligonucleotides.**

Morpholino target	Sequence	Concentration
none	5' CCTCTTACCTCAGTTACAATTTATA 3'	Variable
start-*flna*	5' GTGTGTTGACTCATTTTTATCGACT 3'	270 μM
start-*cbfβ*	5' GACCACCCGAGGCATCTTGAACG 3'	650 μM

3.5.3 Plasmids

The pT7-gRNA plasmid (46759, Addgene) was used to clone the gRNA for CRISPR gene editing. The pCR4-TOPO (from the TOPO cloning kit, K457502, Thermo Fisher Scientific) was used to clone PCR fragments for further Sanger sequencing.

3.6 Antibodies

Antibodies used for immunoblotting and fluorescent immunohistochemistry staining are listed in **Table 3.6** and **Table 3.7**.

Table 3.6: **Primary antibodies.**

Antibody target	Host	Concentration	Blocking	Catalog number	Manufacturer
Immunoblotting					
Anti-FLNA	Rabbit	1:250,000	5 % filtered milk	LS-B6554	LifeSpan Biosciences
Anti-CBFβ	Rabbit	1:500	5 % filtered milk	ab33516	Abcam
Anti-TUBB	Rabbit	1:500	5 % filtered milk	ab6046	Abcam
Anti-GAPDH	Mouse	1:500	5 % filtered milk	H86504M	Meridian Sciences
Immunostaining					
Anti-FLNA	Rabbit	1:50	1X Power Block	LS-C409442	LifeSpan Biosciences
Anti-CBFβ	Rabbit	1:50	1X Power Block	ab33516	Abcam

Table 3.7: **Secondary antibodies.**

Antibody target	**Host**	**Concentration**	**Blocking**	**Catalog number**	**Manufacturer**
Immunoblotting					
Anti-mouse, HRP linked	Horse	1:3000	1X TBST	# 7076	Cell Signalling
Anti-rabbit, HRP linked	Goat	1:3000	1X TBST	# 7074	Cell Signalling
Immunostaining					
Anti-mouse FITC	Goat	1:200	1X Power Block	1070-02	Southern Biotech
Anti-mouse TRITC	Goat	1:200	1X Power Block	1070-03	Southern Biotech
Anti-rabbit FITC	Goat	1:200	1X Power Block	F1262	Sigma

Methods

3.7 Zebrafish methods

3.7.1 Husbandry

Zebrafish maintenance and breeding was carried out as described by Westerfield (Westerfield, 1995).

Breeding and embryo maintenance

Sexually mature zebrafish were kept overnight in mating tanks, separated by a partition plate. The partition was removed in the beginning of the light phase and spawning began shortly after. Eggs were collected, rinsed and placed in a petri dish with 1X E3 buffer. Embryos were raised in an incubator at 28.5 °C until 7 days post fertilization (dpf), upon which they were transferred to the fish room system (Aqua Schwarz, Germany).

Adult maintenance

Adult zebrafish were maintained on a 14-hour light and 10-hour dark cycle at 28.5 °C in a recirculation system (Schwarz Ltd Germany, Mueller and Pfleger Ltd Germany). Mature fish were fed daily with a combination of freshwater aquarium flake food (TetraWerke, Melle, Germany) and live artemia shrimps (Sanders, Great salt lake, Artemia cysts). The care and treatment of the animals were conducted in accordance with the guidelines established by the Seoul National University Institutional Animal Care and Use Committee (Approval No. SNU-050418-2).

3.7.2 Embryo handling and manipulation

One-cell stage embryos were aligned in the grooves of injection ramps [in a petri dish, the mold TU-1 (Adaptative Science Tools) was used to shape 3 % agarose (16500500, Invitrogen) in 1X E3 buffer]. Prior to embryo injections, needles were created from 1 mm glass capillaries (World Precision Instruments) using a glass micropipette puller at 68.3 °C and 70.1 °C temperature cycles. Injections were done using a microinjector with a compensation pressure (P_c) of 15 hPa and an injection time (t_i) of 0.1 sec. The injection pressure (P_i) was adjusted for each needle. At 24 hours post-fertilization (hpf) the 1X E3 buffer was replaced with 1-phenyl-2-thiourea (PTU; 0.2 mM) to prevent melanization, thereby facilitating the imaging process.

Morpholino gene knockdown

Wildtype embryos were injected with a control morpholino-modified antisense oligonucleotide (MO) in order to exclude unspecific toxic effects from a given injected concentration. The MOs were complementary to the *flna* and *cbfβ* start site, therefore blocking translation. All MOs were injected in one-cell stage embryos. Morpholino titrated optimized concentrations were injected as described in **Table 3.5**.

Isoproterenol exposure

Isoproterenol (ISO) is a non-selective beta adrenoreceptor agonist that is an analog of epinephrine (adrenaline). All Isoproterenol (I6504, Sigma) dilutions were freshly prepared in 1X E3 buffer to a final concentration of 1 mM. Embryos were incubated with 1 mM ISO for 100 min at 28.5 °C.

3.7.3 CRISPR gene knockout

Target site selection and gRNA production

Potential target sites were identified using the CHOPCHOP online tool (Montague et al., 2014, Labun et al., 2016). A guide RNA (gRNA) targeting exon 2 of FLNA transcript 202 (*Danio rerio* GRCz11, ENSDART00000135820.3) was selected (sequence is listed on **Table 3.4**). The DNA oligonucleotides were cloned into a pT7-gRNA plasmid via T4 DNA ligation cloning (1048122001, Roche). The gRNA was produced using the *in vitro* transcription kit T7 MEGAshortscript (AM1354, Thermo Fisher Scientific). Possible off-targets were determined with the CCTop tool (del Sol Keyer et al., 2015) and primer sequences can be found in **Table 3.4**.

Embryo microinjections

The CRISPR-CAS9 (Clustered Regularly Interspaced Short Palindromic Repeats Associated Protein 9) protein (C15111835, ToolGen) was reconstituted in nuclease-free water to a final concentration of 20 μM. The components were added to a 1.5 mL tube as follows: 1 μL of CAS9 protein, 1 μL of 750 ng/μL gRNA and 1 μL of 1 M KCl. The mixture was incubated at 37 °C for 20 min to allow the protein and the gRNA to form complexes. The needle was calibrated using a calibration slide (05A01040, Pyser-sgi) to a final injection volume of 1 nL. The embryos were aligned in the injection ramps and the gRNAs were injected directly into the cell.

Genotyping and line propagation

Genotyping was performed in 24 hpf embryos or in adult zebrafish. Both embryos and adults were exposed to tricaine methanesulfonate (E10521, Sigma-Aldrich) until there was no touch response. In summary, the embryo or the adult fin was transferred to 100 μL of 50 mM NaOH and dissolved rigorously at 95 °C for 20 minutes. The solution was neutralized by adding 10 μL 1 M Tris-HCl, pH 8 and centrifuged at 14,000 for 15 min. The supernatant was used as a template for polymerase chain reaction (PCR) as described in *Section 3.8.1.*

3.7.4 Embryo assessment

Embryo tissue harvesting

Embryos were immersed in concentrated tricaine methanesulfonate water and kept in this solution for at least 10 min following cessation of opercular movement. In order to evaluate tissue specific

gene or protein expression, as well as, the sarcomere structure; embryonic hearts were dissected using a 0.5 nm needle. Embryo tail and head tissues were collected using forceps and scalpels.

Electron microscopy analysis

Embryos were immersed in concentrated tricaine methanesulfonate water and kept in this solution for at least 10 min following cessation of opercular movement. Embryo skeletal muscle samples were sent to the Electron Microscope Core Facility of Heidelberg University (EMCF). Sample processing was performed by Charlotta Funaya, Steffi Gold and Sebastian Wurzbacher at the EMCF.

Phenotype analysis

To document embryos, these were anaesthetised with 0.02 % tricaine methanesulfonate. Embryos were transferred to 2.5 % methylcellulose (64632, Fluka) dissolved in 1X E3 buffer and imaged with a Leica MZFIII stereoscope. Video documentation was performed using the Leica DM IRB inverted microscope with a 20X objective, at room temperature. For the latter, the software Virtual Dub (version 1.7) was used to record 10 sec video frames of the beating heart. The heart rate was determined by counting the heart beats in a period of 5 seconds and extrapolating to 1 min. Fractional ventricular shortening was calculated by measuring the inner heart wall in the diastole and the systole [using Fiji (Schindelin et al., 2012) and using the following formula: FS = (VEDD - VESD) / VEDD * 100 % [FS - fractinonal shortening, VEDD - ventricle end-diastolic dimension (pixels), VESD - ventricle end-systolic dimension (pixexls)].

3.7.5 Adult assessment

Genotyping

Adult zebrafish were genotyped by clipping the fin and extracting DNA using the NaOH protocol, as mentioned in *Section 3.7.3*.

Behavioural analysis

Individual tanks containing adult zebrafish were transferred to the mating area and let to rest for 5 minutes. Zebrafish behaviour was assessed by determining the frequency of buccal movements during three minutes (Jonz and Nurse, 2005).

Echocardiography (ECG)

The Vevo 2100 imaging system was used with the MS700 transducer to perform echocardiographies. This transducer has 256 crystals displayed in a linear array that emitted waves with a frequency between 30 and 70 MHz, reflected back from the zebrafish, hence allowing a visualization of the different body structures, in particular the heart. Echocardiographies were performed in adult zebrafish, with similar age and size. Echocardiographies were executed according to Hein et al., 2015.

Zebrafish dissection and tissue harvesting

Adult zebrafish were immersed in concentrated tricaine water until cessation of gill movement could be observed. To excise the heart, the zebrafish were placed ventral side up in the groove of a sponge under a dissecting stereoscope. In order to isolate the brain, the zebrafish were placed ventral side down. The skeletal muscle and fin were removed with the zebrafish laying laterally.

3.8 Molecular methods

3.8.1 Polymerase chain reaction (PCR)

DNA was isolated from zebrafish embryos or adult fin using the NaOH protocol described in *Section 3.7.3*. Polymerase chain reactions were performed using Taq Polymerase (201203, Qiagen) and according to manufacturer's instructions. Primers used are listed on *Section 3.5.1*.

3.8.2 Gel electrophoresis and gel extraction

To separate the DNA fragments by size, they were run on 1.0 % to 1.5 % agarose gels [(15510-0227, Invitrogen) solved in 1X TBE buffer (A4686, AppliChem)]. Ethidium bromide (22182, Roth) was added to the liquid agarose for later visualization of the bands. DNA loading dye (R0611, Thermo Fisher Scientific) was added to a final concentration of 1X to each sample. The DNA fragment size marker quick load 2-log DNA ladder (N0469, New England Biolabs) was added to the gel. Negatively charged DNA fragments were separated using an electric current of 400 mA at 120 V for 90 min. Bands were visualized using a UV transilluminator (Biostep). Individual bands were cut from the gel using a scalpel, DNA was extracted using the QIAquick gel extraction kit according to manufacturer's instructions (28706, Qiagen). Extracted DNA was stored in dH_2O in 1.5 mL tubes at -20 °C.

3.8.3 RNA extraction

RNA was extracted from zebrafish embryos and adult tissues using miRNeasy Mini kit according to manufacturer's instructions (217004, Qiagen). The RNA quality and concentration was measured using the fragment analyser (Advanced Analytical Technologies).

3.8.4 Reverse Transcription - quantitative PCR (qRT-PCR)

The Luna Universal One-Step RT-qPCR kit (E3005L, Biolabs) was used to analyse *flna*, *flnb* and *cbfβ* mRNA expression level. For each reaction 100 ng of total RNA was used. The reaction program used is listed in **Table 3.8**.

Table 3.8: **RT-qPCR reaction program using ViiA 7 from Applied Biosystems.**

Stage name	Temperature	Time	Transition	Cycles
Hold stage	55 °C	20 s	-	1
Reverse transcription	55 °C	10 min	Increasing 2.63 °C/s	1
PCR cycle	95 °C	1 min	-	1
	95 °C	10 s	-	
	-	-	Decreasing 2.42 °C/s	40
	60 °C	30 s	-	
Melt curve	95 °C	15 s	Decreasing 2.42 °C/s	1
	60 °C	1 min	Increasing 0.1 °C/s	1
	95 °C	15 s	-	1

3.8.5 Zebrafish protein extraction and quantification

To analyse the protein concentrations of FLNA and CBFβ in zebrafish, different tissues were isolated as described in *Section 3.7.4* and *Section 3.7.5*.

Protein extraction

Whole embryo For protein isolation of whole zebrafish embryos, 72 hours post-fertilization (hpf) fish (n=30) were anaesthetised with 1 % tricaine methanesulfonate and collected in a 2 mL tube. To remove the zebrafish yolk, embryos were washed with 1 mL deyolking solution. Then, the embryos were washed with 1 mL washing buffer. Washing buffer was removed completely and TNN working buffer was added (5μL per embryo added). Embryos were homogenized with 0.6 mm and 0.4 mm needles (300700, 302200, respectively, BD microlance 3). Embryo lysates were incubated on ice for 15 min and centrifuged for 15 min at 14,000 rpm in a temperature-controlled centrifuge at 4°C. The supernatant was collected in a new 1.5 mL tube and stored at -80 °C.

Embryonic tissues A minimum of fifty 72 hpf embryonic hearts were collected per 2 mL tube. Samples were centrifuged for 5 min at 14,000 rpm at 4 °C and the supernatant was removed. 1X Laemmli (161-0747, BioRad) diluted in TNN working buffer was added directly to the tubes. The samples were boiled at 95 °C for 5 min. At this time point, samples could be stored at -20 °C. After collecting a minimum of 50 embryonic zebrafish heads and 50 embryonic zebrafish tails in Precellys tubes containing 1.4 mm ceramic beads (Precellys lysing kit, KT03961-1-009.2, Precellys), the samples were centrifuged for 5 min, 14,000 rpm at 4 °C and the supernatant was removed. 150 μL of TNN working buffer was added to each sample and samples were homogenized using the Precellys mill (program: 2x 5,000 rpm 20 s, 10 s pause). Samples were incubated on ice for 15 min and centrifuged for 15 min, 14,000 rpm at 4°C. The supernatant was collected in a new 1.5 mL tube and stored at -80 °C.

Adult tissues For protein isolation, Precellys tubes containing 1.4 mm ceramic beads (Precellys lysing kit, KT03961-1-009.2, Precellys) were used. Following the addition of 150 μL of TNN working buffer to each sample, these were homogenized using the Precellys mill (program: 2x

5,000 rpm 20 s, 10 s pause). Samples were incubated on ice for 15 min and then centrifuged for 15 min, 14,000 rpm at 4°C. The supernatant was collected in a new 1.5 mL tube and stored at -80°C.

Bradford protein assay

A Bradford assay was performed to measure sample protein concentration. According to Pierce Coomassie (Bradford) protein assay kit instructions (23200, Thermo Fisher Scientific), 2 μL of protein sample were added to 998 μL of 1X Bradford solution (diluted with dH_2O). Sample absorbance was measured at 595 nm wavelength using a spectrophotometer (BioRad). Total protein concentration was extrapolated from a comparison with the standard curve (previously created using defined BSA samples diluted in TNN working buffer).

3.8.6 Western blot

Proteins were separated by SDS-PAGE (Sodium Dodecyl Sulfate-Polyacrylamide Gel Electrophoresis) using precast gels (456-1094, BioRad). Proteins were transferred to a polyvinylidene fluoride (PVDF) membrane by wet blotting. The membranes were blocked in 5 % filtered (40 μm sterile, 542040, EASYstrainer, Greiner bio-one) milk dissolved in 1X TBST for at least 1h. These were incubated in 50 mL falcon overnight at 4 °C with primary antibody (see **Table 3.6**). To ensure constant and uniform sample agitation the tubes were incubated overnight in a tube roller device (SunLab). The membrane was washed three times in 1X TBST and incubated with horseradish peroxidase (HRP)-coupled secondary antibody for 2 h at room temperature (see **Table 3.7**). Proteins bound by HRP-coupled secondary antibody were visualized by the use of ECL (Enhanced Chemiluminescence) substrate (32106, Thermo Fisher Scientific). For low abundance proteins a high sensitivity ECL substrate was used (GERPN2235, Merck).

3.8.7 Immunohistochemistry

At 72 hpf, embryos were collected in a 2 mL tube and fixed in Dent's fixative (see **Table 3.2**) overnight at room temperature. The next day, the embryos were transferred to Dent's bleach (see **Table 3.2**) and incubated overnight at room temperature. At this time point, the samples could be stored in 100 % methanol or alternatively, the dehydration protocol could be followed directly (see below).

Dehydration and paraffin embedding

The previously fixed and bleached embryos were transferred to a cassette (One-Piece Microbiopsy Cassettes, 3802751, Leica). Using the HistoCore Pearl, the embryos were dehydrated and embedded as described in **Table 3.9**.

Table 3.9: **Dehydration and paraffin embedding protocol.** All steps were performed under pressure and vacuum conditions to ensure enough tissue penetration by the reagents.

Solution	Time	Temperature
70 % ethanol	30 min	40 °C
80 % ethanol	30 min	40 °C
95 % ethanol	45 min	40 °C
100 % ethanol	45 min	40 °C
100 % ethanol	45 min	40 °C
100 % ethanol	45 min	40 °C
Xylene	45 min	40 °C
Xylene	45 min	40 °C
Paraffin	1 h	65 °C
Paraffin	1 h	65 °C
Paraffin	1 h	65 °C

Using the HistoCore Arcadia H paraffin machine, the embryos were aligned and the paraffin was let to solidify in the cold plate for 10 min. The paraffin blocks were stored overnight at -20 °C. The blocks were cut into 5 μm histological sections using the microtome (Leica). Histological slices were added to microscope slides (1000200, Marienfeld) and dried on a hot plate (Hl1220, Leica) for at least 2 hours (h) at 37 °C. The samples were stored at room temperature.

Fluorescent immunostaining

Paraffin was removed from specimens by washing with ethanol as follows: 2 x 5 min Xylene (534056, Sigma), 2 x 5 min 100 % ethanol (603-002-00-5, Zentralbereich), 5 min 96 % ethanol, 5 min 70 % ethanol, 5 min 1X PBS. After unmasking the antigens (2 x 5 min in the microwave at 1000 W, with 0.01 M Sodium Citrate pH 8.0 adjusted with 1 M NaOH) the slides were washed 2 x 5 min in 1X PBS and 2 x 5 min in 1X PBST. The tissue sections were encircled with an ImmEdge hydrophobic barrier pen (H-4000, Vector Labs). To reduce nonspecific binding sites, the slides were incubated with 1X Power Block (HK 085-5K, Biogenex) for 30 min at 4°C. The samples were incubated with the primary antibody (1:50 in 1X Power Block) at 4 °C in the humidity chamber, overnight. The slides were washed 3 x 2 min 1X PBS, with lateral shaking. In case of a double staining, the second primary antibody (1:50 in 1X Power Block) was added and samples were incubated overnight at 4 °C in a in-house made humidity chamber. The slides were washed 3 x 2 min 1X PBS and then incubated with the secondary antibody (1:200 in 1X Power Block) for 2 h at 4 °C. In case of a double staining, both secondary antibodies were diluted in the same solution. The slides were washed 3 x 2 min 1X PBS, with lateral shaking. In order to reduce the unspecific background signal, slides were treated with the Vector TrueVIEW autofluorescence quenching kit (VEC-SP-8400, Vector). For DAPI (4',6-diamidino-2-phenylindole) staining samples were incubated with 1 μg/mL Hoechst (H3570, Thermo Fisher Scientific) for 10 min. After washing 2 x 2 min with 1X PBS, the sections were covered with mounting medium (included in the Vector TrueVIEW kit) and documented using a 40X objective (Numerical Aperture of 0.95 and a working distance of 0.23 - 0.17 mm) from the Nikon Ni-E motorized high-end upright microscope (at the Nikon Imaging Center, core facility for light microscopy at the University of Heidelberg, Germany). The filter cubes used can be visualized in **Table 3.10**.

Table 3.10: **Filter cubes used in the Ni-E microscope, with the 40 X Nikon objective.**

Filter	Excitation Wavelength	Dichroic Mirror	Emission Wavelength
DAPI	390 nm	416 nm	460 nm
EGFP	472 nm	495 nm	520 nm
TRITC	543 nm	562 nm	593 nm

3.8.8 Cloning

Topo TA

For a clear single peak Sanger sequencing result, PCR products were cloned into a pCR4-TOPO TA Vector using the TOPO TA cloning kit (450071, Thermo Fisher Scientific) following the manufacturer's instructions. Plasmids were transformed in *Escherichia coli* One Shot Top10 chemically competent cells (C404010, Invitrogen) and plasmids were extracted using the plasmid miniprep kit (732-2780, Peqlab).

T4 DNA ligase cloning

To incorporate the gRNA into a vector suitable for *in vitro* transcription, T4 DNA Ligase (10 487 220 001, Roche) was used. As in TOPO TA cloning, plasmids were transformed in *E. coli* One Shot Top10 chemically competent cells (C404010, Invitrogen) and plasmids were extracted using the plasmid miniprep kit (732-2780, Peqlab).

3.8.9 Next generation sequencing

For heart transcriptome analysis, RNA was collected from zebrafish adults and embryos as described in *Section 3.8.3*. Regarding embryonic material harvesting, 300 whole embryos were pooled per condition and 500 hearts were also pooled per condition. Adult samples were not pooled, each sample represents one individual heart. The samples description can be found in **Table 3.11**. FLNA knockout adult samples origin can be understood with help from **Figure 4.10**. Sequencing was performed with IlluminaHiSeq 2000, using the TruSeq SBS Kit v3 (FC-401-3001, Illumina) and reading 2x 100 bp for paired-end sequencing, on five lanes of a sequencing flow cell.

Table 3.11: **Total RNA sequencing samples from embryos FLNA knockdown and adult FLNA knockout.** Quality is measured in terms of RNA Quality Number (RQN) score and ranges from 1 to 10 (1 being low-quality and 10 being high-quality RNA).

Sample description	**Sample ID**	**Concentration (ng/μL)**	**RQN score**
Whole embryos			
Wildtype	10722	27.65	9.5
FLNA knockdown	10721	17.69	9.8
Embryonic hearts			
Wildtype	10722	3548.38	9.3
FLNA knockdown	10721	1540.94	10.0
Wildtype controls - Adult hearts			
Male 1	10484	19.99	9.0
Male 2	10485	26.65	8.3
Male 3	10486	25.21	7.9
Female 1	10487	41.78	6.2
Female 2	10488	23.77	8.0
Female 3	10489	15.61	8.1
Female 4	10490	22.49	7.4
Female 5	10491	22.87	8.2
Line 1 - Adult hearts			
I:2	13890	7.13	1.5
II:3	13892	15.25	8.9
III:3	13893	6.71	8.5
Line 2 - Adult hearts			
I:2	13894	11.86	8.1
II:4	13895	18.11	8.0
III:3	13897	18.46	8.1

3.9 Statistical analysis

Statistical analysis was conducted with GraphPad Prism 5 Software (GraphPad software, Inc., USA). All group data are presented as mean ± standard deviation (SD). Two-group comparisons were made using Student's t-test. If the data had a Gaussian distribution the unpaired t-test was performed, otherwise the Mann-Whitney test was used. Null hypothesis was rejected at *$p<0.05$ (higher significance levels were denoted by **$p<0.01$ or ***$p<0.001$).

4 | Results

4.1 CBFβ and FLNA transient loss-of-function model

To elucidate the function of FLNA and CBFβ, different transient gene knockdowns in piscine embryos were established.

4.1.1 FLNA and CBFβ protein domains are highly conserved between human and zebrafish

Considering that gene and protein conservation between humans and zebrafish is key to be able to draw a significant parallel between the two organisms, both human and zebrafish amino acid sequences were aligned.

Taken the amino acid sequence into account, zebrafish and human CBFβ share 86% similarity, with a highly conserved domain (**Figure 4.1 - A**). The complete amino acid (**Supplement Figure S1**) alignment between human and zebrafish can be seen in *Section 6*.

At the protein level zebrafish FLNA has 85% similarity to human FLNA, showing high conservation within the domains (**Figure 4.1 - B**). The complete amino acid (**Supplement Figure S2**) alignment between human and zebrafish is included in the *Section 6*.

Given the homology between human and zebrafish of FLNA and CBFβ, it is plausible to hypothesize that their function is conserved in humans and proceed with the studies using zebrafish as a model organism.

4.1.2 CBFβ knockdown leads to a heart failure phenotype

As previously described by our research group, translational blockade of CBFβ led to a heart failure phenotype in zebrafish embryos (Meder et al., 2010). Compared with the morpholino-injected control (MO-*control*) precardial edema (**Figure 4.2 - A ***), blood regurgitation from the atrium to the sinus venosus (**Figure 4.2 - A**), a reduced heart rate (MO-control vs MO-*cbfβ*; mean±SD: 148±6.9 vs 108±22.0 beats/min, respectively; $p<0.01$; **Figure 4.2 - C**) and a reduced ventricular systolic function (MO-control vs MO-*cbfβ*; mean±SD: 64.7±4.0 % vs 27.9±14.3 %, respectively; $p<0.001$; **Figure 4.2 - D**) were observed at 72 hours post-fertilization (hpf).

The knockdown was confirmed by Western blot (see *Section 3.8.5*, **Figure 4.2 - B**) using whole embryo protein extracts.

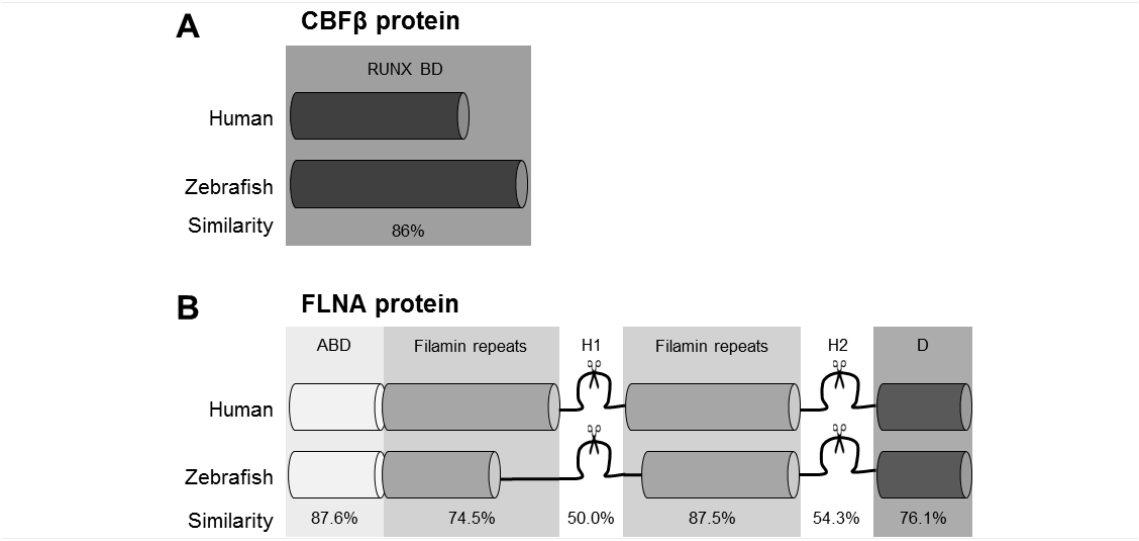

Figure 4.1: **FLNA and CBFβ protein conservation across species.** A - CBFβ protein with the RUNX binding domain (RUNX BD). B - FLNA protein with the actin binding domain (ABD), 1 to 15 filamin immunoglobulin-like repeats, hinge 1 (H1), 16 to 23 filamin immunoglobulin-like repeats, hinge 2 (H2) and the self-association domain (D). Zebrafish percentage similarity to the human sequence shown under each corresponding domain. Amino acid alignments accomplished by using CLC Main workbench (QIAGEN Bioinformatics).

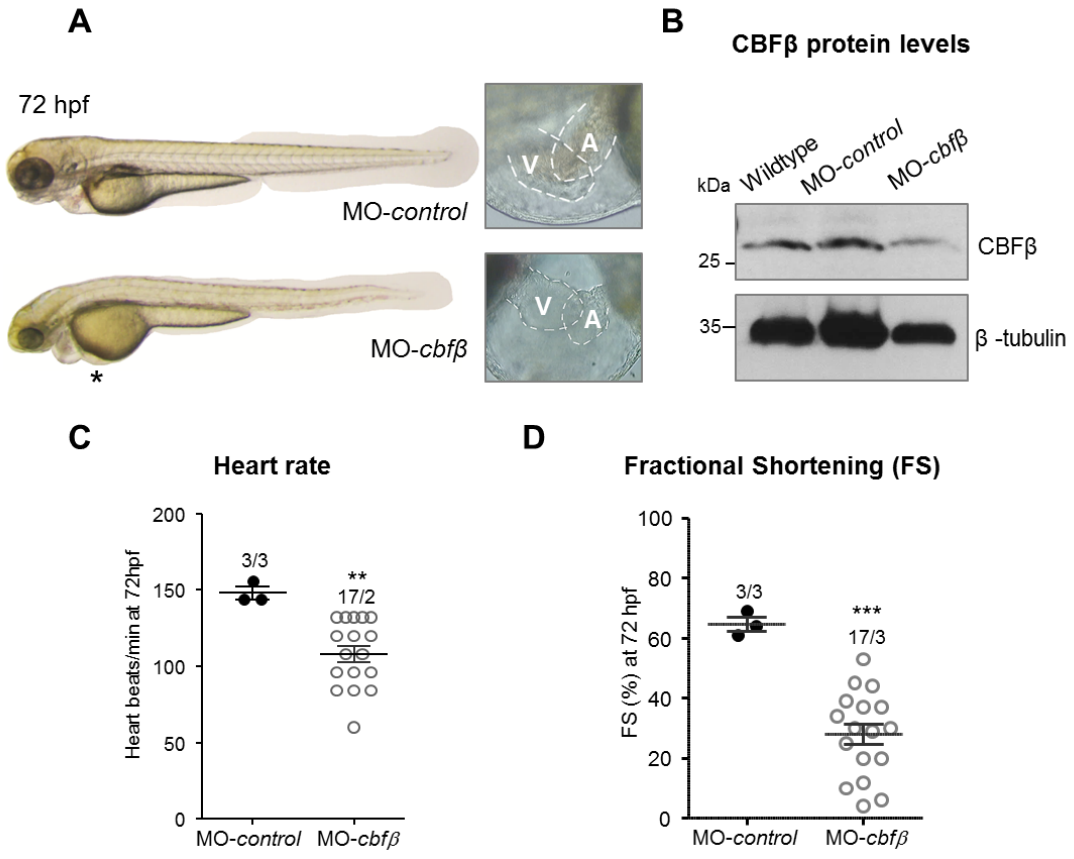

Figure 4.2: **Functional analysis of CBFβ knockdown at 72 hpf.** A - zebrafish embryo whole body and heart phenotype of injected morpholino control (MO-*control*) and injected *cbfβ* morpholino (MO-*cbfβ*); V - ventricle, A - atrium. B - Western blot confirming CBFβ knockdown at protein level. C - heart rate in beats per min of MO-*control* and MO-*cbfβ*. D - measured ventricular fractional shortening of MO-*control* and MO-*cbfβ*. $p<0.001$ (**) and $p<0.0001$ (***).

4.1.3 FLNA knockdown leads to systolic dysfunction

The FLNA knockdown (MO-*flna*) was performed by using a morpholino blocking the translational start site ATG. FLNA knockdown lead to systolic dysfunction, defects in re-absorption of cardiac matrix, a dilated atrium, blood regurgitation during ventricular contraction and maturation defects shown by uncompleted heart looping (**Figure 4.3 - A**). The heart rate (MO-control vs MO-*flna*; mean±SD: 148±6.9 vs 108±25.1 beats/min, respectively; $p<0.05$; **Figure 4.3 - C**) and ventricular fractional shortening (MO-control vs MO-*flna*; mean±SD: 64.7±4.0 vs 19.3±10.8 beats/min, respectively; $p<0.001$; **Figure 4.3 - D**) were significantly reduced in morphants.

The knockdown was confirmed by Western blot (see *Section 3.8.5*, **Figure 4.3 - B**) using whole embryo protein extracts.

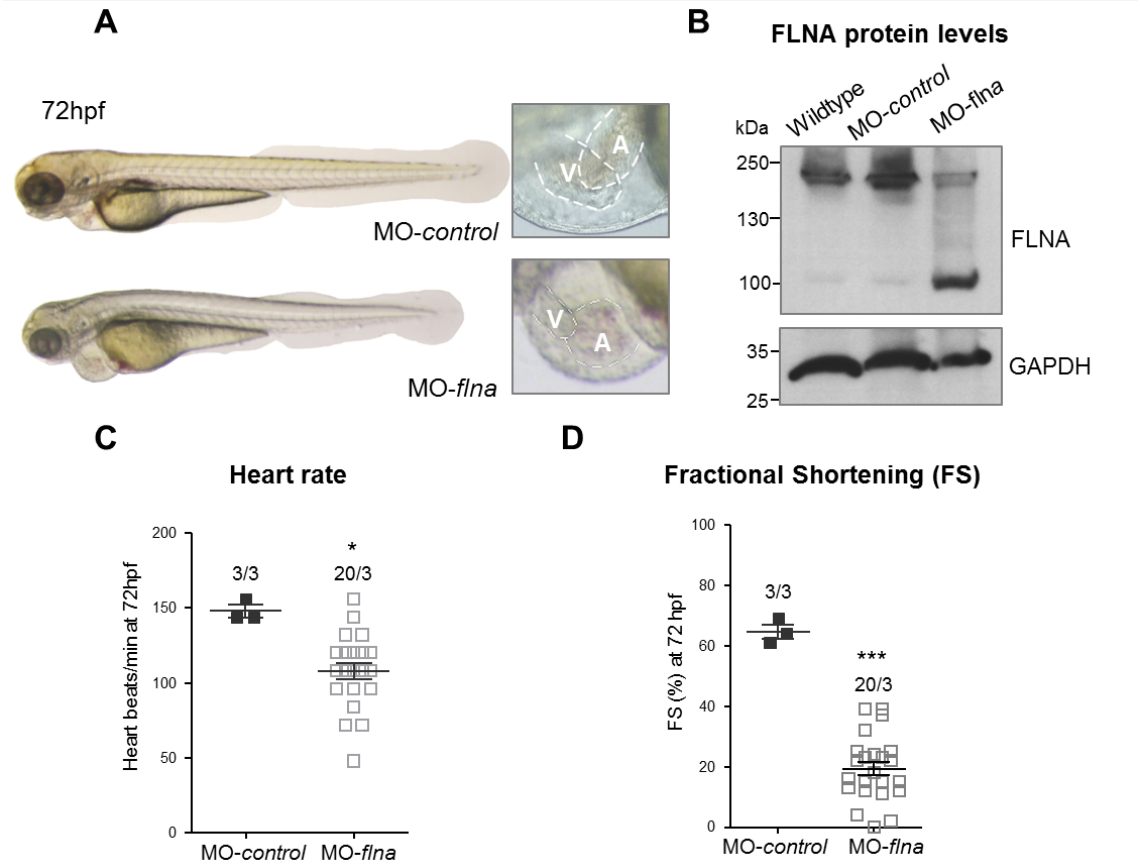

Figure 4.3: **Functional analysis of FLNA knockdown at 72 hpf.** A - lateral view of zebrafish embryo at 72 hpf either injected with morpholino control (MO-*control*) or with a morpholino specifically blocking the translation start site of *flna* (MO-*flna*); V - ventricle, A - atrium. B - Western blot confirming FLNA knockdown at protein level. C - heart rate in beats per min of MO-*control* and MO-*flna*. D - measured ventricular fractional shortening of MO-*control* and MO-*flna*. $p<0.05$ (*) and $p<0.001$ (**).

One of the most common non-specific effects of morpholino-mediated knockdown is the up-regulation of *tp53* gene. Next generation sequencing was used to analyse the transcriptome of FLNA knockdown whole embryos and hearts (see *Section 3.8.9*). The expression of *tp53* in morpholino-injected control and FLNA knockdown were not significantly different (MO-*control* vs MO-*flna*; mean±SD: 8.1±0.9 vs 9.7±0.9 normalized reads, respectively; non-significant; **Figure 4.4**).

Furthermore, taken into account the high similarity between *flna* and *flnb*, it was necessary to

evaluate if *flnb* was compensating for the lack of *flna*. The expression of *flnb* was not significantly different from the injected morpholino control (MO-*control* vs MO-*flna*; mean±SD: 7.9±1.5 vs 5.4±0.5 normalized reads, respectively; non-significant; **Figure 4.4**).

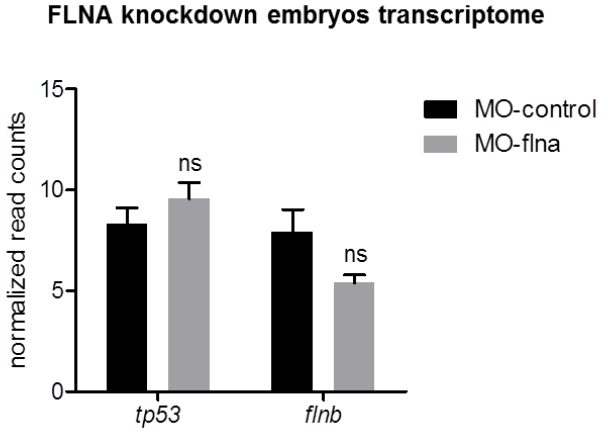

Figure 4.4: **Expression of *tp53* and *flnb* in wildtype and *flna* morphants.** Values presented as normalized read counts. Data shown as mean±SD, non-significant (ns).

Two different FLNA isoforms were detected by Western blotting and the isoforms present in several wildtype tissues were further investigate. FLNA was detected in whole embryo, adult heart, adult skeletal muscle (Skm) and adult fin tissues (**Figure 4.5 - A**). As FLNA antibody targets the self-association domain in the C-terminal of the protein, the detected fragments correspond to the whole FLNA protein (at approximately 270 kDa) and the cleaved fragment at the hinge 1 domain (at approximately 100 kDa, **Figure 4.5 - B**).

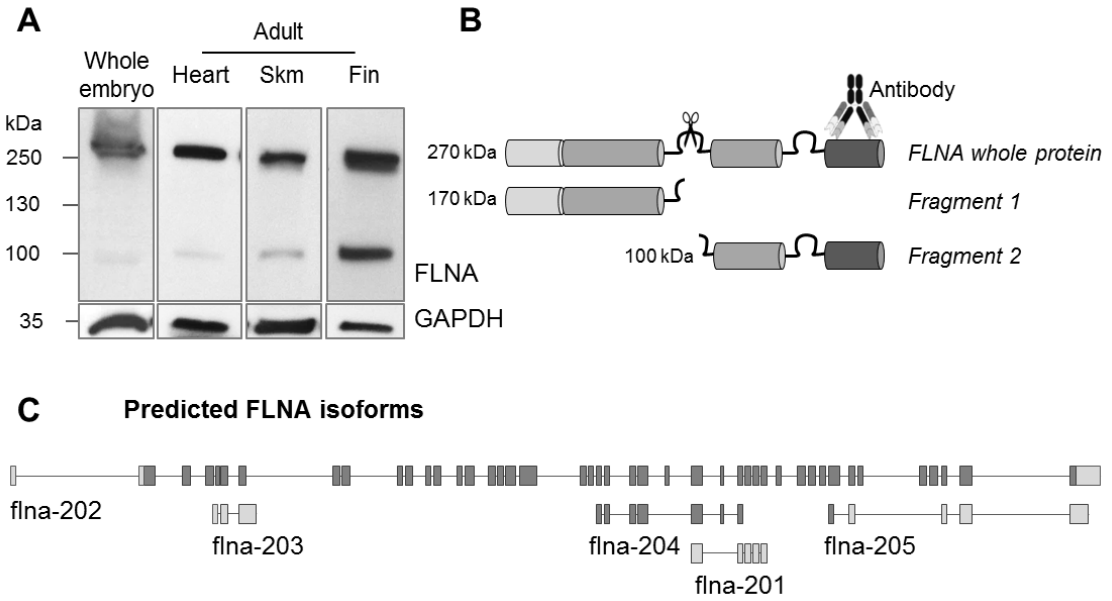

Figure 4.5: **Protein isoforms of FLNA in different zebrafish tissues.** A - FLNA protein levels detected with Western blot. B - scheme of the antibody binding and cleavage site. C - predicted *flna* isoforms from *Ensembl genome browser 97*.

While transcript flna-202 is the 270 kDa detected FLNA fragment, none of the *Ensembl genome browser 97* annotated transcripts (**Figure 4.5 - C** and **Table 4.1**) has a corresponding protein

predicted size that would explain the detected 100 kDa FLNA fragment.

Table 4.1: ***flna* transcripts annotated in *Ensembl genome browser 97***. For each transcripts the size in nucleotide (bp), amino acid (aa) and kilodaltons (kDa) is described.

	flna-202	**flna-204**	**flna-205**	**flna-201**	**flna-203**
Transcript (bp)	8551	1058	864	757	726
Protein (aa)	2553	353	No protein	No protein	No protein
Protein (kDa)	270	37	-	-	-

Taken from http://www.ensembl.org. Last accessed 6th September 2019.

Furthermore, given the structural function of FLNA, the sarcomeric structure in embryonic skeletal muscle was evaluated via electron microscopy. The analysis exposed no significant alterations in the sarcomere structure (MO-*control* vs MO-*flna*; mean±SD: 1.8±1.5 vs 3.9±6.6 ratio of thick filaments per sectioned sarcomeric unit, respectively; non-significant; **Figure 4.6**), with preserved primary organization of thick and thin filaments, in addition to these bundles organization in higher ordered sarcomeric units.

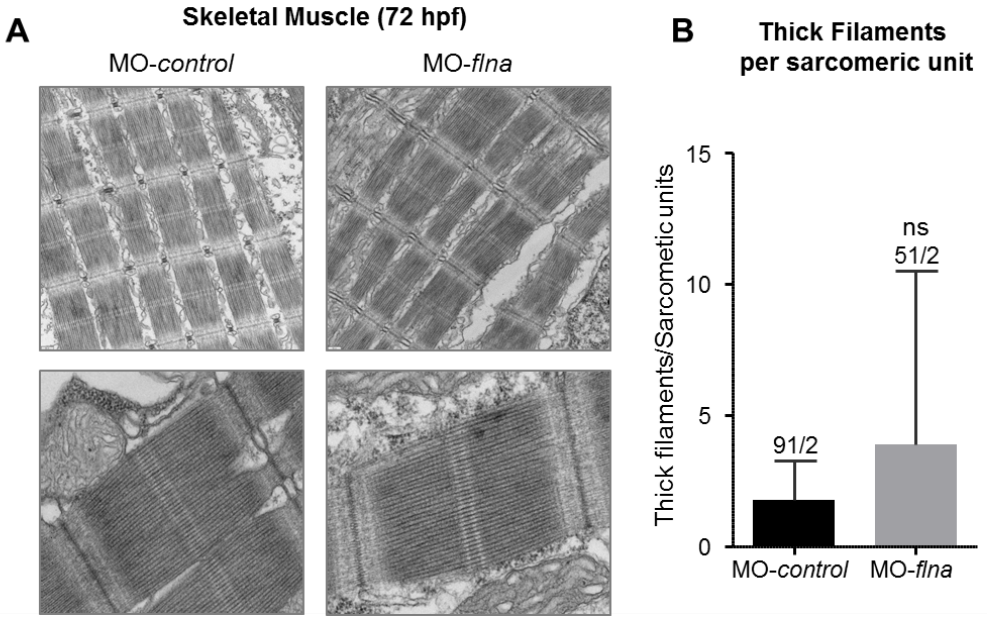

Figure 4.6: **Skeletal muscle analysis at 72 hpf with electron microscopy.** A - comparison between skeletal muscle structures of injected morpholino control (MO-*control*) and injected *flna* morpholino (MO-*flna*). B - plotted ratio of thick filaments per number of sarcomeric unit. Data shown as mean±SD, non-significant (ns).

4.2 Stable FLNA knockout resulted in altered heart morphology and heart failure

Morpholino induced FLNA knockdown is a transient method to evaluate gene function in embryos. The loss of FLNA through a stable knockout allows deeper phenotyping and the follow-up of disease progression and onset of symptoms also in adult fish.

4.2.1 CRISPR pipeline was established in zebrafish

FLNA knockout was accomplished using the bacterial CAS9, CRISPR (clustered regularly interspaced short palindromic repeats) technology. A single-stranded gRNA composed of a *flna* targeting gene sequence followed by the PAM (protospacer adjacent motif) sequence was designed. The gRNAs were designed to target *flna* exon 2 of transcript 202 using CHOPCHOP (Labun et al., 2016). The gRNA was cloned into a pT7-gRNA vector and the RNA produced using an *in vitro* transcription kit (**Figure 4.7 - A**). One cell stage embryos were injected with CAS9 protein complexed with gRNA. At 24 hours post-fertilization (hpf), 10 embryos were collected, genomic DNA extracted and the region of interest (ROI) analyzed for FLNA mutations (**Figure 4.7 - B**). This analysis provided an estimate of mutation efficiency, allowing us to predict the number of adults with genome-edited FLNA. The remaining alive embryos, were grown to adulthood.

At 72 hpf, the F0-injected embryos were screened, in detail, to define until which extent the embryos exhibit signs of heart dysfunction. Interestingly, the F0 injected embryos showed a heart failure phenotype, with a reduced heart rate (wildtype vs F0 embryos; mean±SD: 144.0±18.5 vs 106.2±12.8 beats/min, respectively; $p<0.001$; **Figure 4.8 - A**) and a reduced fractional shortening (wildtype vs F0 embryos; mean±SD: 63.7±9.7 % vs 42.9±9.2 %, respectively; $p<0.001$; **Figure 4.8 - B**). These embryos were grown to adulthood and tested for *flna* mutations. After reaching three months of age, adult mosaic fish were genotyped by clipping the fin, extracting the DNA with the NaOH method (see *Section 3.7.3*). ROIs were amplified with subsequently DNA sequencing (**Figure 4.7 - C**). Adult fish with a mutated *flna* allele were labelled as founders and outcrossed with wildtype adults to propagate the mutated line.

Different F0 mosaic founders carry different mutations, which lead to different penetrance and phenotypic outcomes. As expected, the phenotype varied greatly between F0 founders. The heart morphology and function of the F0 founders was analyzed with echocardiography (**Figure 4.8 - C**). F0 adults showed an approximately normal ventricular ejection fraction, but compared with the wildtype, also exhibited bradycardia and reduced velocity time integral (VTI). Mitral valve regurgitation due to the lack of coaptation as a result of the heart chambers' dilatation was also detected. Taken together, these parameters indicate a heart failure phenotype.

To establish one mutation per individual fish, the F0 adults were outcrossed with wildtype (giving rise to the F1 generation). F1 embryos were grown to adulthood and genotyped for mutations in the targeted area of *flna* (**Figure 4.9 - A**). The F1 generation consisted of 52 fish carrying different *flna* mutations. Since it was not feasible to propagate all these mutated fish lines, the fish were categorized in terms of *flna* knockout efficiency at mRNA and protein levels, as well as behavioural discrepancies. Overall, compared with wildtype, there was a significant reduction in *flna* transcript levels for most of the F1 founders (wildtype vs F1 founders; mean±SD: 119.7±38.9 vs 35.1±23.2-fold change, respectively; $p<0.001$; **Figure 4.9 - B**). At the protein level, not all individuals showed such an obvious difference compared to wildtype, which simplified selecting which mutated fish lines to propagate (**Figure 4.9 - C**). To add another layer of information, within the fish exhibiting reduced *flna* mRNA and FLNA protein levels, only the adults showing the highest levels of hyperventilation were selected (wildtype vs F1 founders; mean±SD: 7.3±4.2 vs 64.1±39.0 buccal movements, respectively; $p<0.001$; **Figure 4.9 - D, E**). To clear the genetic background of unwanted and unspecific mutations, two of the most promising F1 founders lines were propagated through outcross with wildtype, to generate an F2 generation. The process was repeated again to create an F3 generation.

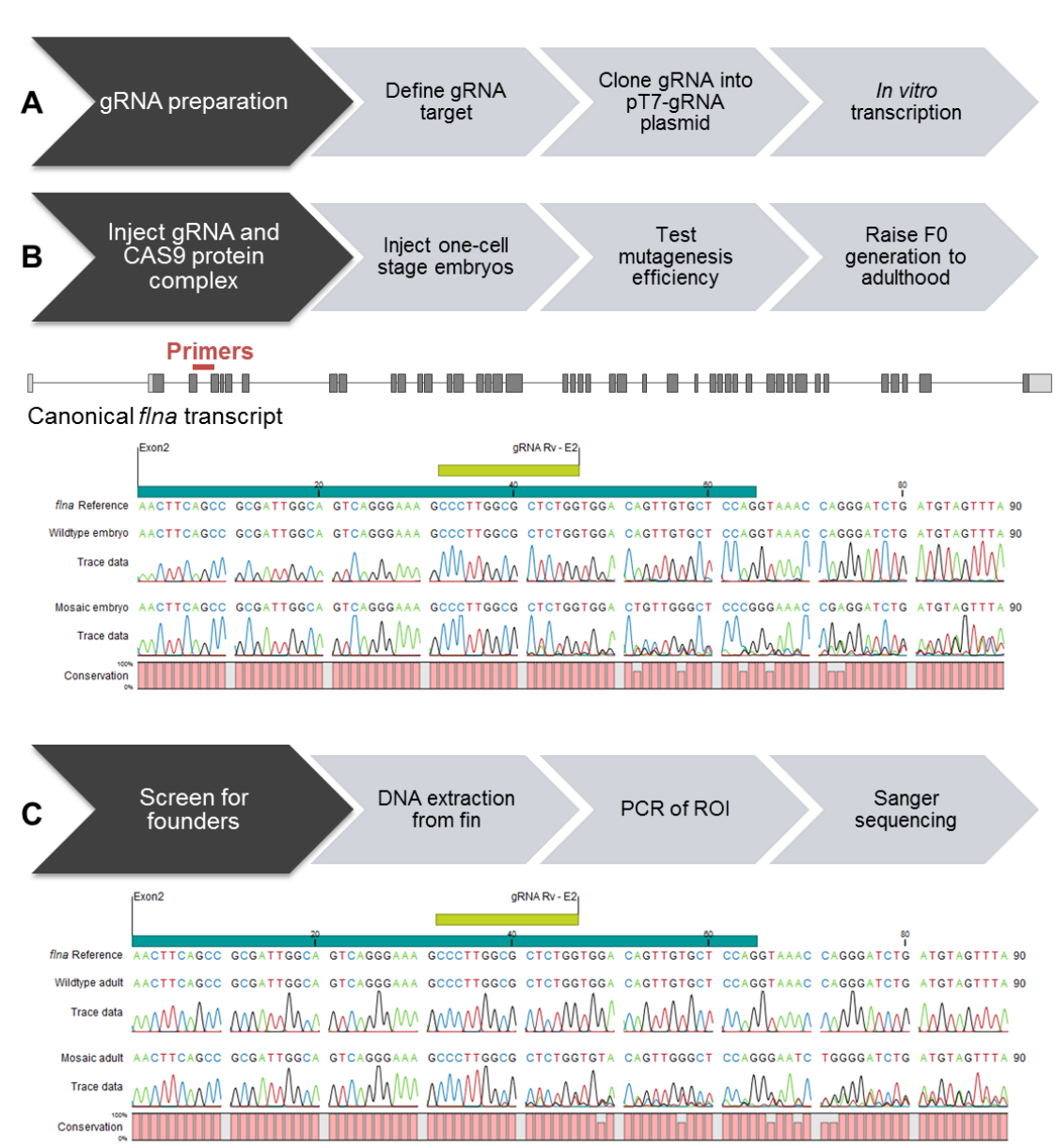

Figure 4.7: **CRISPR line generation pipeline**. A - design of a gRNA targeting *flna* exon 2, incorporation of the gRNA sequence into pT7-gRNA plasmid and *in vitro* transcription to produce the injectable gRNA. B (top) - one cell stage embryo injection of gRNA complexed with CAS9 protein, test of mutagenesis efficiency at 24 hpf and raise of the injected generation until adulthood. B (bottom) - the localization of the mutagenesis screening primers (in red) is shown in the schematic of the canonical zebrafish *flna* transcript. An example of the obtained Sanger sequencing results for the mutagenesis screening at 24 hpf is shown for an unedited *flna* exon 2 and an edited *flna* exon 2. C (top) - upon reaching adulthood, fin DNA was extracted and a PCR of the region of interest (ROI - *flna* exon 2) - was performed. C (bottom) - the PCR products were sent for Sanger sequencing and an example of a wildtype adult and an genome-edited fish, with multiple sequencing peaks per base is shown.

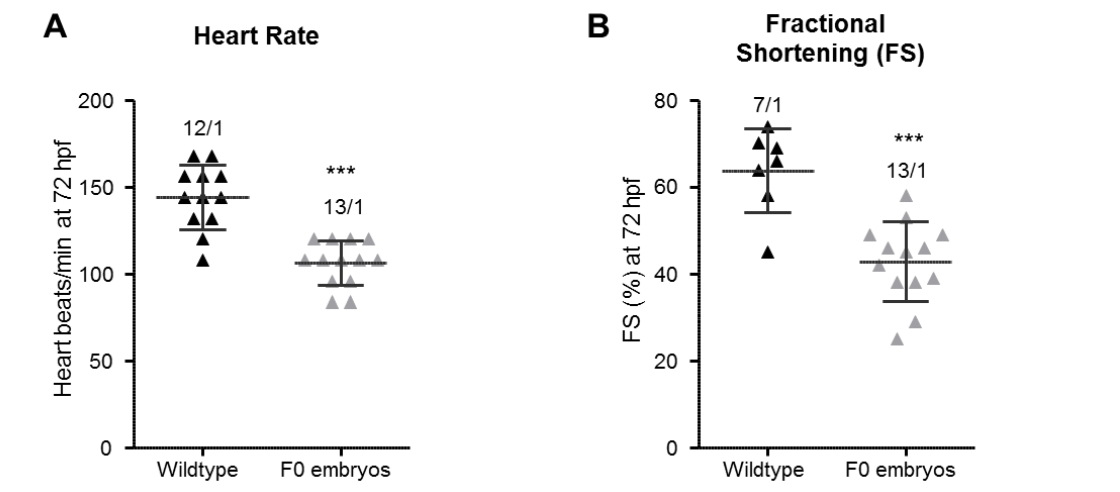

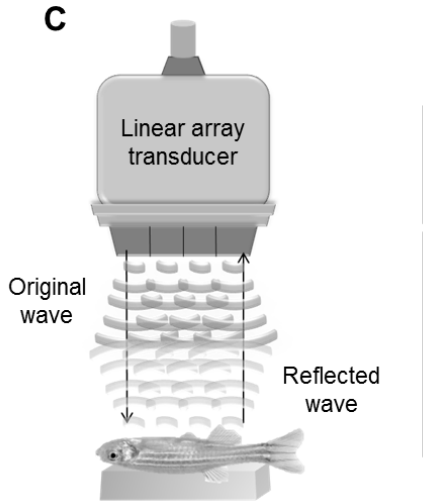

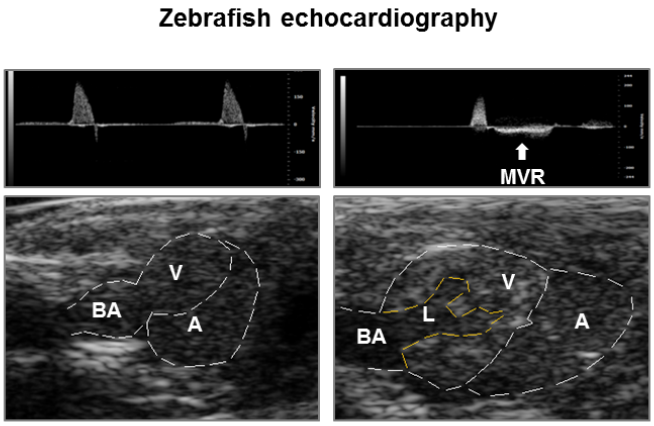

	Wildtype	Mosaic F0 Adult
Weight (g)	0.409	0.963
Length (cm)	3.5	3.6
Heart rate (bpm)	94.4	70
Ejection Fraction (%)	59	50
VTI (mm)	7.3	2.7

Figure 4.8: **CRISPR F0 generation analysis.** A - heart rate (beats/min) of wildtype embryos compared to F0 injected embryos at 72 hpf. B - ventricular fractional shortening (%) at 72 hpf of wildtype embryos compared to F0 injected embryos. C (left) - a schematic illustration of an echocardiography linear transducer and specimen. C (right) - a representative example of the echocardiogram results obtained from a wildtype adult and a mosaic F0 adult [top - pulse-wave imaging shows mitral valve regurgitation (MVR); middle - heart morphology with the following structures highlighted: bulbus arteriosus (BA), ventricle (V), lumen (L) and atrium (A) highlighted; bottom - table with the correspondent parameters weight (g), length (cm), heart rate (beats/min, bpm), ejection fraction (%) and velocity time integral (VTI, mm)]. $p<0.0001$ (***).

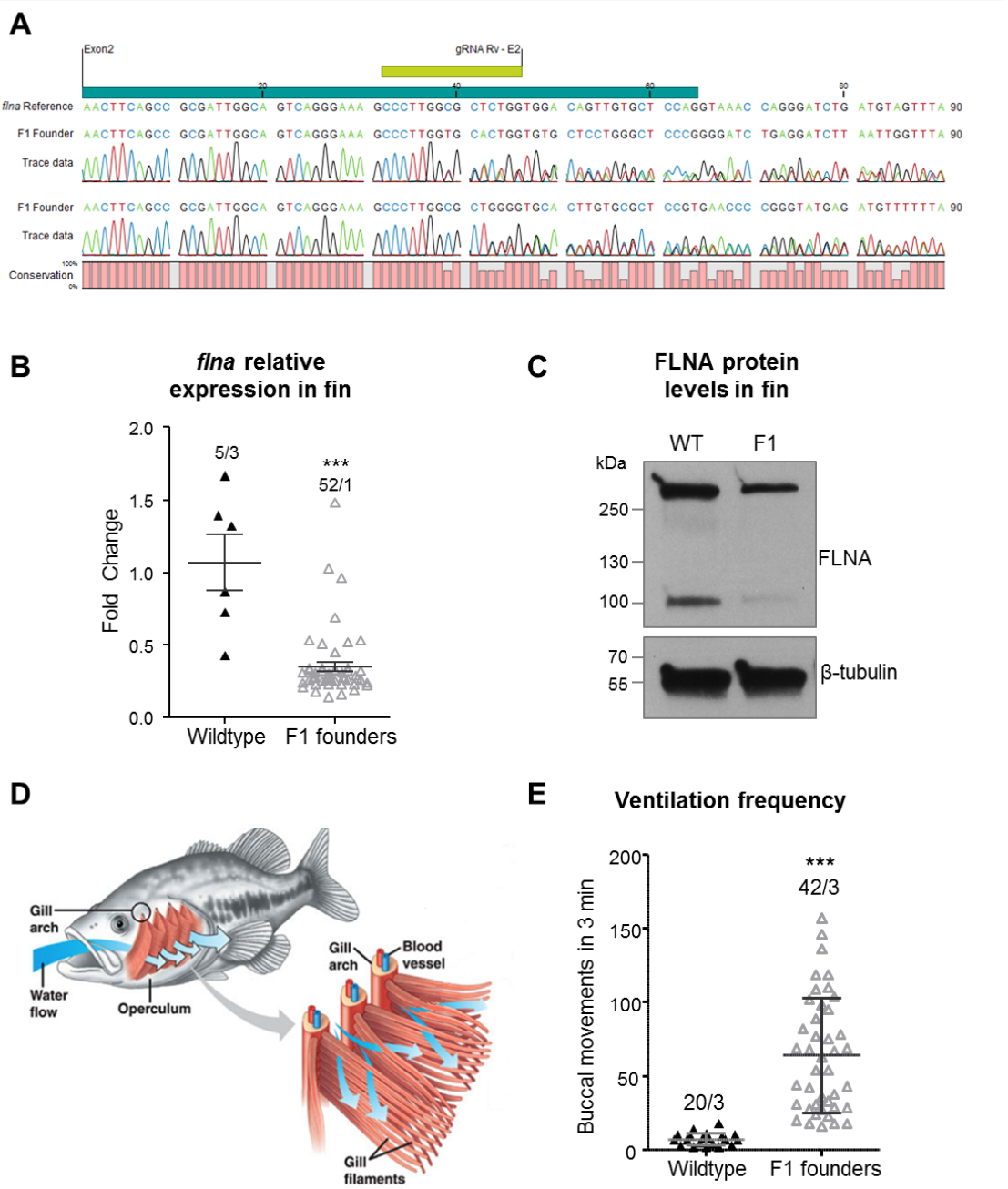

Figure 4.9: **Assessment of CRISPR F1 generation.** A - two representative examples of F1 founder Sanger sequencing results compared with the wildtype *flna* reference sequence. B - *flna* expression at mRNA level of wildtype adults compared to F1 founders [$p<0.0001$ (***)]. C - representative western blot of FLNA protein levels of a wildtype and an F1 founder zebrafish. D - schematic of fish gills illustrating oxygen exchange between ambient water and fish body (adapted from Taylor et al., 2019). E - behavioural analysis depicting the ventilation frequency [number of buccal movements in 3 min, $p<0.0001$ (***)].

As mentioned before, F0 adults were outcrossed with wildtype to generate the F1 generation. The F1 adults were analyzed as just described. Two F1 founders were selected for line propagation and will from now on be addressed as lines 1 and 2.

Members of line 1 carry a 46 bp insertion that leads to a frame shift starting with a missense mutation (c.606_607ins46; p.L203GfsX). The leucine (a neutral hydrophobic non-polar amino acid) at position 203 was replaced with a glycine (also a neutral hydrophobic non-polar amino acid). The frame shift is predicted to lead to a stop codon on exon 4 (**Figure 4.10 - A**).

Members of line 2 carry an 8 bp deletion, that also leads to a frame shift starting with a missense mutation (c.605_612del8; p.A202DfsX). At position 202, the alanine (a neutral hydrophobic non-polar amino acid) was replaced by aspartic acid (an negatively charged acid amino acid). With the frame shift, it is predicted that a stop codon is introduced in exon 4, leading to a truncated protein (**Figure 4.10 - B**). Both mutations, from line 1 and 2 are located in the actin binding domain (ABD).

Parallel to raising lines 1 and 2, an incross between the F1 founders of these two lines was made. The aim was to obtain a complete FLNA knockout and observe if a more prominent heart failure phenotype would be provoked. These inbred lines (addressed as line 1U2) generated compound heterozygous individuals, which had two distinct *flna* alleles carrying two separate mutations - c.[606_607ins46; 605_612del8]; p.[L203GfsX; A202DfsX] (**Figure 4.10 - C**).

4.2.2 FLNA knockout was confirmed for the selected lines

To confirm the FLNA knockout, each line was genotyped and the *flna* mRNA expression and FLNA protein levels analyzed.

Line 1 members harbor a 46 bp insertion, that could be clearly distinguished from the wildtype by agarose gel electrophoresis [**Figure 4.11 - B**]. The individual bands were excised from the gel, DNA was extracted and the PCR products cloned into a pCR4-TOPO vector. Samples were sent for Sanger sequencing, by which the wildtype and mutated allele presence in this zebrafish line could be confirmed [**Figure 4.11 - A**]. *flna* relative expression was significantly reduced in all generations (wildtype vs line 1 founders; mean±SD: 100.0±15.1 vs 45.4±10.7-fold change, respectively; $p<0.001$; **Figure 4.11 - C**). At the protein level, all individuals showed a reduction in FLNA levels (**Figure 4.11 - D**).

Line 2 genotyping, with only 8 bp deletion, was harder to distinguish from the wildtype in an agarose gel [**Figure 4.12 - B**]. Using a 3% agarose gel, the individual bands could be excised separately, DNA was extracted and the PCR products cloned into a pCR4-TOPO vector. Samples were sent for Sanger sequencing, by which the wildtype and mutated allele were confirmed [**Figure 4.11 - A**]. The relative expression of *flna* was significantly reduced in all generations (wildtype vs line 2 founders; mean±SD: 100.0±15.1 vs 39.0±32.8-fold change, respectively; $p<0.001$; **Figure 4.12 - C**). Is noteworthy that even though all fish had the same genomic *flna* mutation, the mRNA expression was distinct for each member. Furthermore, there seems to be a recovery of *flna* expression for the F3 generation (**Figure 4.12 - C**). All individuals showed a reduction in FLNA protein levels (**Figure 4.11 - D**), however not as pronounced as for line 1.

For line 1U2, the genotype of a compound heterozygous fish was confirmed by agarose gel electrophoresis and Sanger sequencing (**Figure 4.13 - A and B**). Compared with the wildtype, a bigger

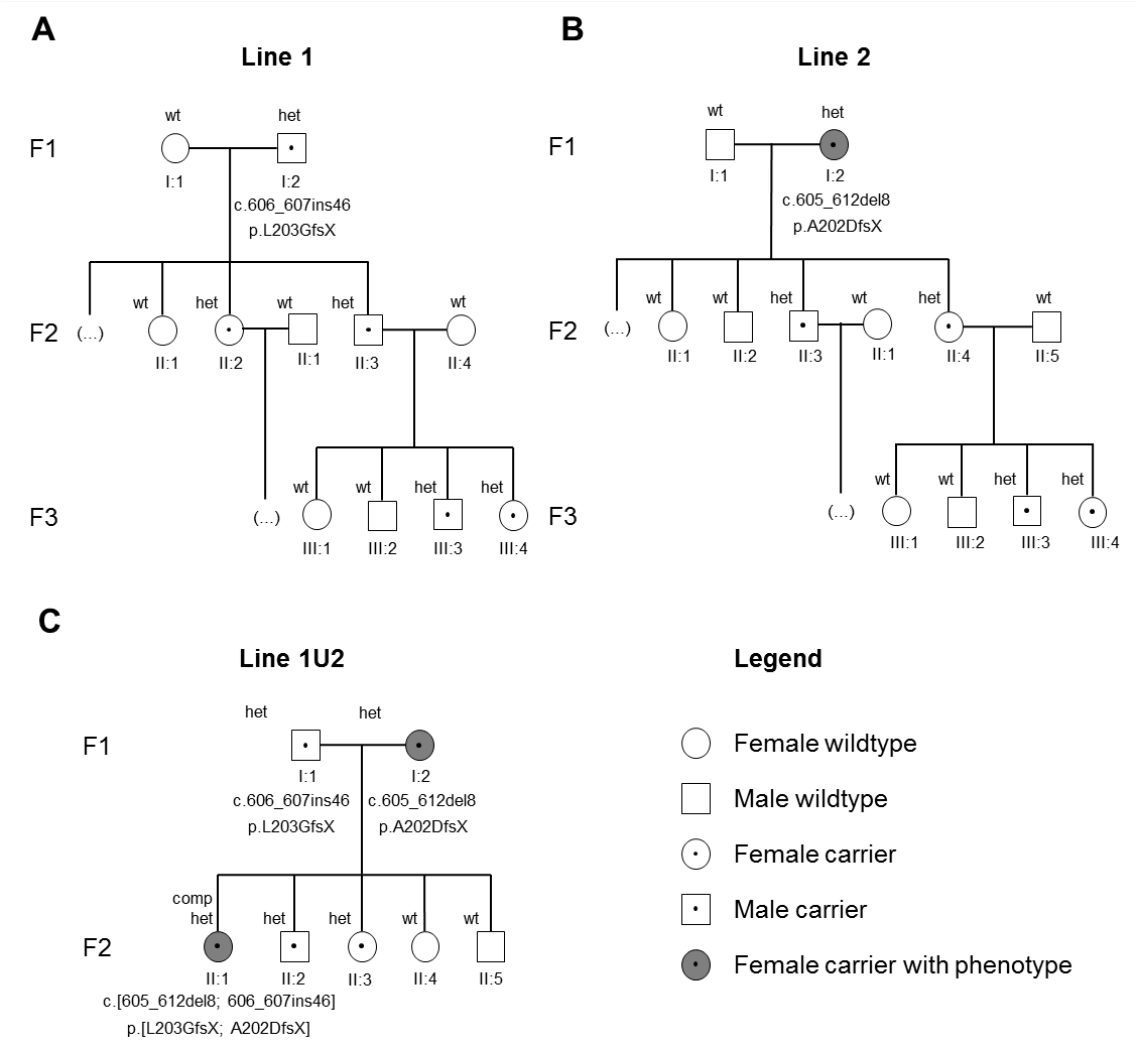

Figure 4.10: **FLNA knockout selected lines pedigree.** A - line 1 with a 46 bp insertion leading to a frame shift missense mutation, with a stop codon introduced in exon 4. B - line 2 with a 8 bp deletion also causing a frame shift missense mutation, with a stop codon introduced in exon 4. C - incross of line 1 and 2 producing a compound heterozygous with both *flna* alleles carrying a stop codon on exon 4. These pedigrees are merely representative of the wildtype (wt), heterozygous (het) and compound heterozygous (comp het) obtained for each line.

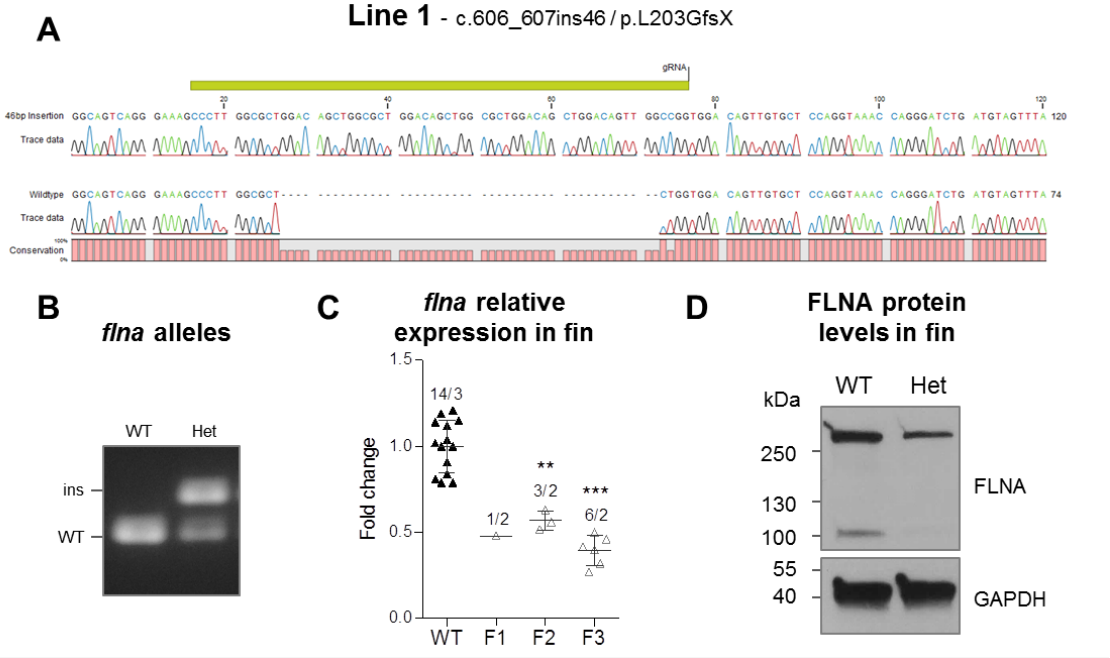

Figure 4.11: **Line 1 - FLNA knockout confirmation.** A - representative example of *flna* wildtype and mutated alleles by Sanger sequencing. B - genotyping confirmation with gel electrophoresis, clearly illustrating the wildtype (WT) and mutated allele with insertion (ins) for a wildtype adult (WT) and line 1 heterozygous (Het). C - *flna* relative expression analysis for all individuals of line 1 [$p<0.001$ (**) and $p<0.0001$ (***)]. D - representative example of FLNA protein levels of a wildtype and an heterozygous (Het).

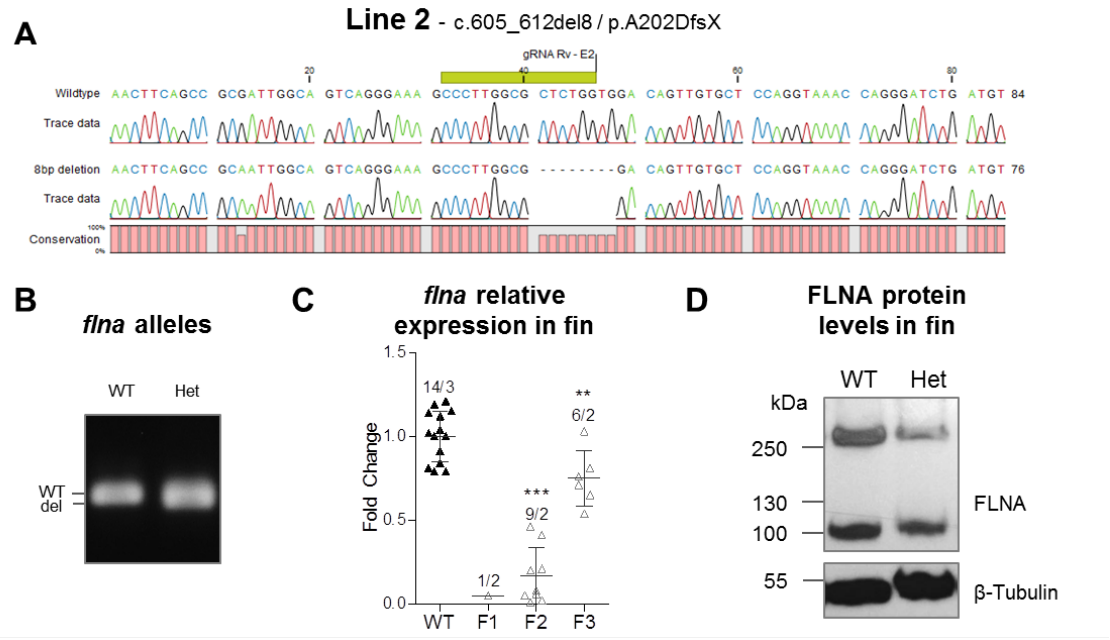

Figure 4.12: **Line 2 - FLNA knockout confirmation.** A - representative example of *flna* wildtype and mutated alleles by Sanger sequencing. B - genotyping confirmation with gel electrophoresis, clearly illustrating the wildtype (WT) and mutated allele with deletion (del) for a wildtype adult (WT) and line 2 heterozygous (Het). C - *flna* relative expression analysis, using qRT-PCR, for all individuals of line 2 [$p<0.001$ (**) and $p<0.0001$ (***)]. D - representative example of FLNA protein levels of a wildtype (WT) and an heterozygous (Het).

PCR product, corresponding to the 46 bp insertion, and a smaller PCR product, corresponding to the 8 bp deletion was detected. No FLNA protein could be detected as the FLNA antibody cannot bind to either of the produced truncated FLNA proteins (**Figure 4.13 - C**).

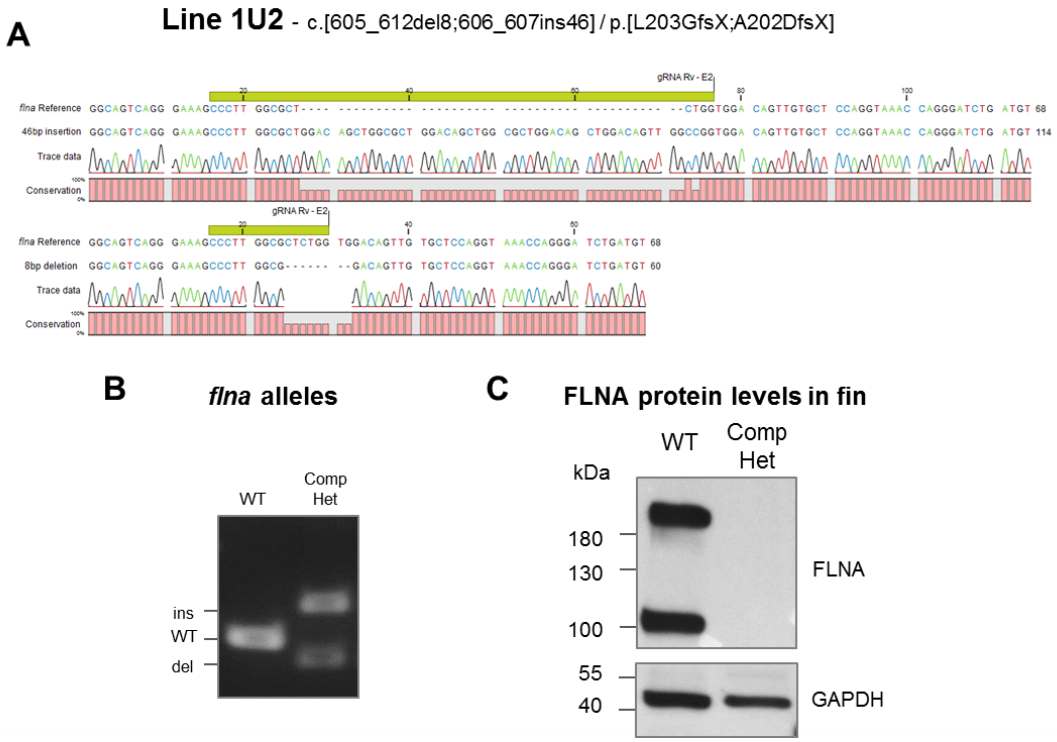

Figure 4.13: **Line 1U2 - FLNA knockout confirmation.** A - representative example of both *flna* mutated alleles by Sanger sequencing. B - genotyping confirmation with agarose gel electrophoresis, illustrating the wildtype (WT) and both mutated alleles with a deletion (del) and an insertion (ins) for a wildtype adult (WT) and line 1U2 compound heterozygous (Comp Het). C - FLNA protein levels of a wildtype (WT) and the compound heterozygous (Comp Het).

4.2.3 No off-target effects were detected in FLNA knockout lines

To ensure a clear correlation between the mutated *flna* gene and the observed phenotype, outcrossing with wildtype fish was performed. By outcrossing F1, F2 and F3 the probability that the genetic background remains wildtype while selecting for *flna* mutation carriers only is increased. This is important because only *flna* mutation contribution to the phenotype is relevant to these studies. Possible off-target mutations at the genomic level were predicted (see *Section 3.7.3*) and analyzed via PCR and Sanger sequencing. At the transcriptomic level, wildtype and FLNA knockout line members heart transcriptome was analyzed via NGS (see *Section 3.8.9*).

No CRISPR gene editing was visible in the analyzed potential off-target sites (**Figure 4.14 - A**) and their mRNA expression was similar to wildtype adults (**Figure 4.14 - B**).

4.2.4 FLNA knockout lines exhibited a heart failure phenotype

The phenotype of FLNA knockout adults was analyzed using echocardiography, behavioural analysis and by characterization of external features.

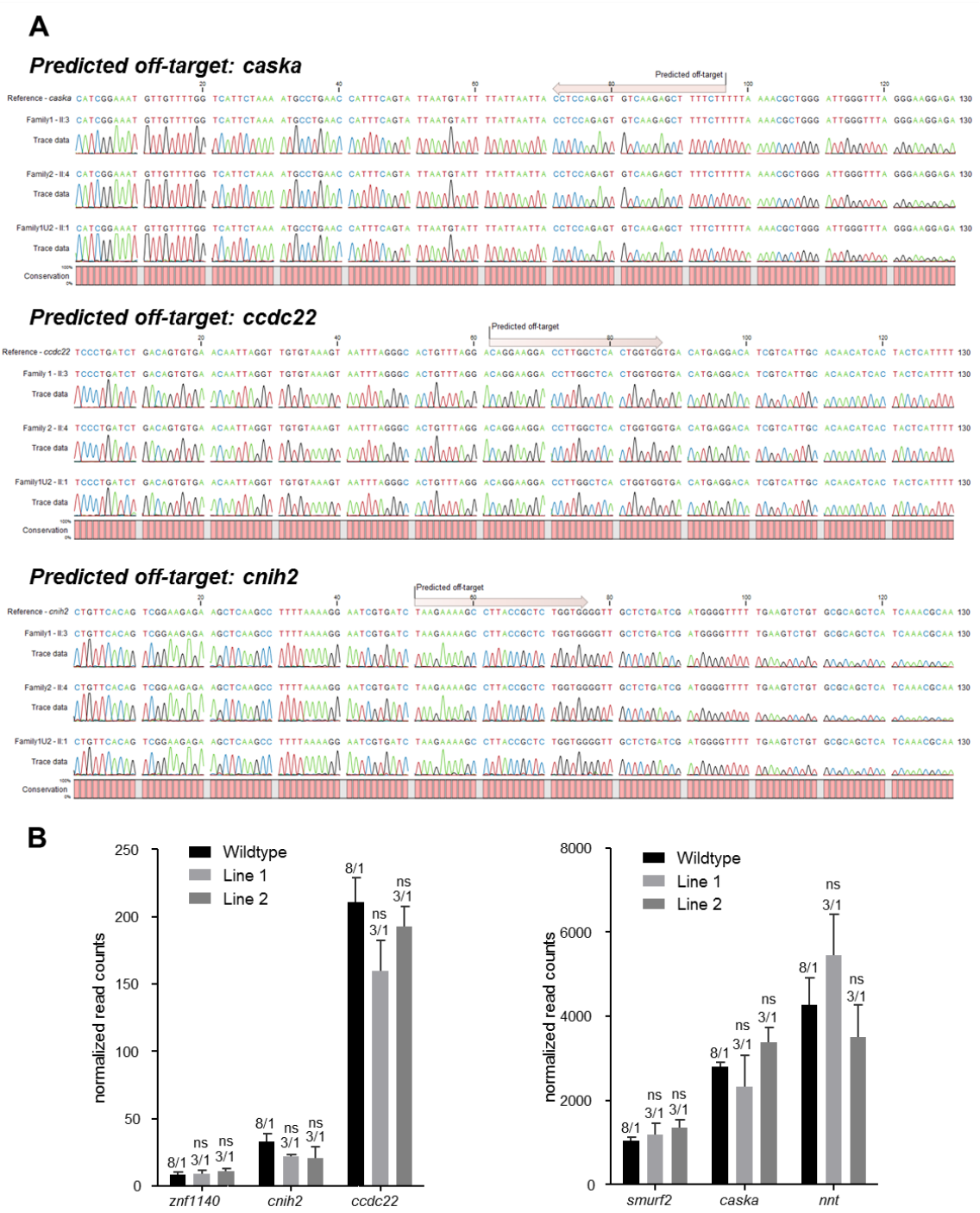

Figure 4.14: **Predicted off-targets analysis for FLNA knockout lines.** A - representative example of predicted off-target alignment of the Sanger results (top to bottom - *caska*, *ccdc22* and *cnih2*). B - heart transcriptome analysis for wildtype and FLNA knockout lines; normalized read counts for *znf1140*, *cnih2*, *ccdc22*, *smurf2*, *caska* and *nnt* [non-significant (ns)].

Line 1 individuals had a wildtype phenotype in regard to external features, such as fins, pigmentation and body shape (**Figure 4.15 - A**). Heart morphology naturally varies from individual to individual. Nevertheless, an 73% of line 1 members showed an enlarged bulbus arteriosus lacking the characteristic wildtype pear-shape. Enlarged ventricles were observed for 27% of line 1 members (**Figure 4.15 - B**). Heart rate was not affected in line 1 individuals (wildtype vs line 1 founders; mean±SD: 84.3±23.8 vs 100.2±27.6 beats/min, respectively; non-significant) but there was a significantly reduced ejection fraction (wildtype vs line 1 founders; mean±SD: 61.2±6.9 vs 42.7±12.1 %, respectively; $p<0.01$; **Figure 4.15 - C**).

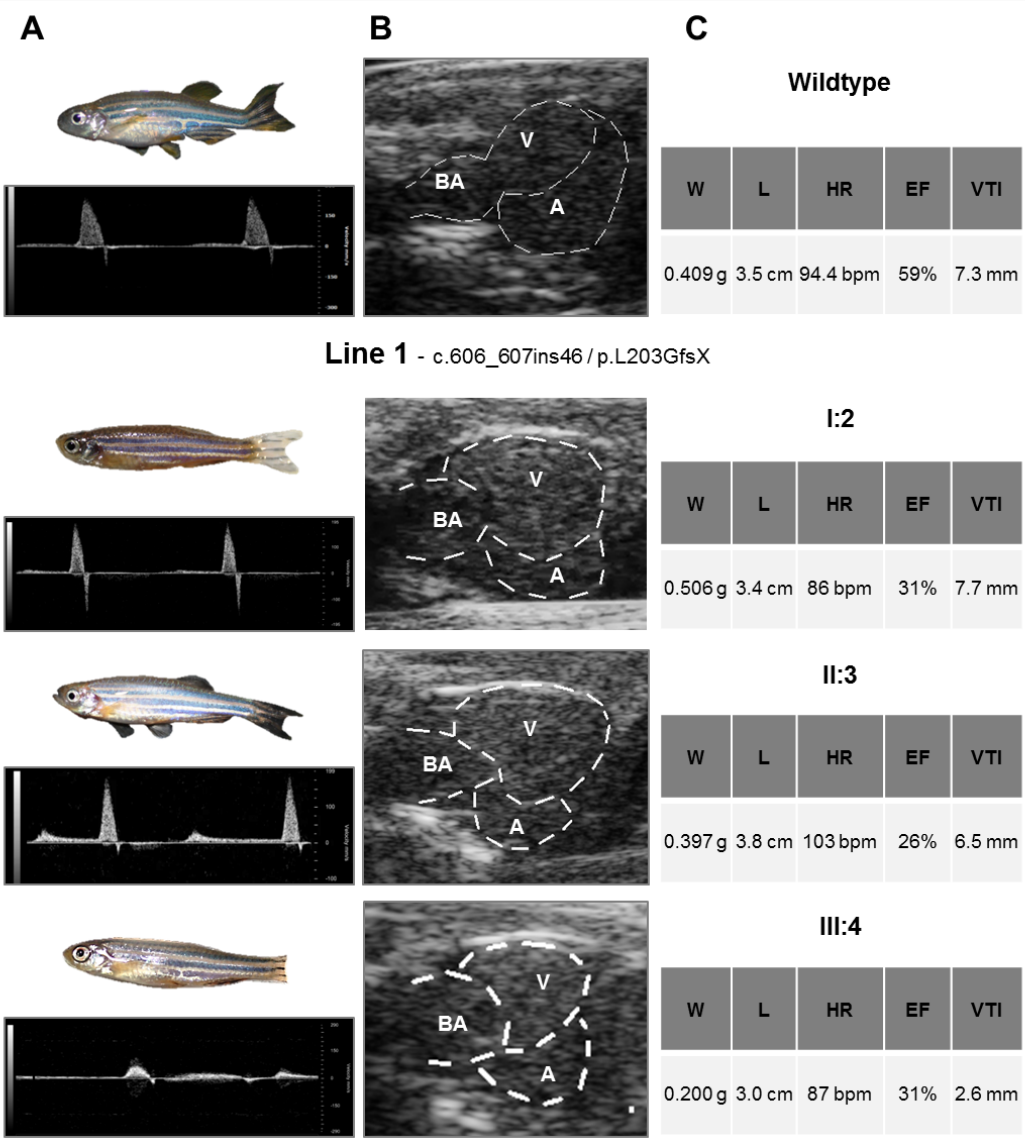

Figure 4.15: **Line 1 - Adult heterozygous phenotype.** Column A - representative examples of fish morphology (top) and Pulsed-Wave Doppler (PWD) recordings, from which the heart rate and velocity time integral were calculated (bottom). Column B - sagittal long axis view by B-Mode imaging, depicting heart morphology and chamber relative position to each other; BA - bulbus arteriosus, V - ventricle, A - atrium. Column C - measured parameters for both wildtype and FLNA knockout line 1; weight (W), length (L), heart rate (HR), ejection fraction (EF) and velocity time integral (VTI).

Line 2 individuals also showed an overall wildtype phenotype in regard to external features, however I:2 developed a noticeable pericardial edema (**Figure 4.16 - A**). Furthermore, I:2 showed an altered

pigmentation, probably due to the accumulation of blood in the pericardial area. The natural variability of the heart morphology also holds true for line 2. Nonetheless, 67% of line 2 members displayed an enlarged bulbus arteriosus. Moreover, 50% of line 2 fish had an enlarged ventricle compared to wildtype (**Figure 4.16 - B**). Heart rate was not affected in line 2 individuals (wildtype vs line 2 founders; mean±SD: 84.3±23.8 vs 102.9±27.6 beats/min, respectively; non-significant) but there was a significantly reduced ejection fraction (wildtype vs line 2 founders; mean±SD: 61.2±6.9 vs 40.1±12.4 %, respectively; $p<0.01$; **Figure 4.16 - C**) for most of the fish. Surprisingly, 57% of the F3 fish showed a wildtype like ejection fraction.

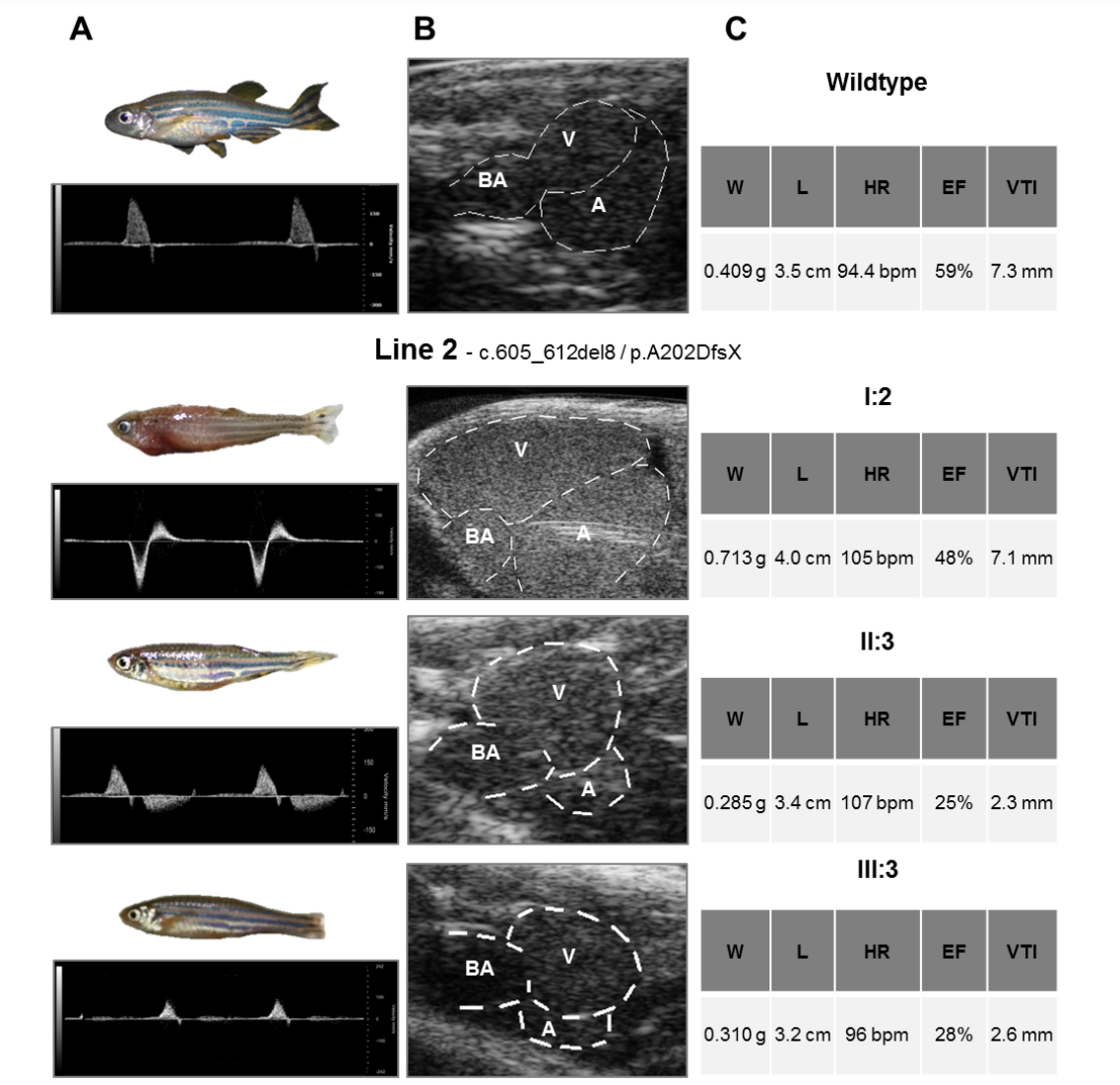

Figure 4.16: **Line 2 - Adult heterozygous phenotype.** Column A - representative examples of fish morphology (top) and Pulsed-Wave Doppler (PWD) recordings, from which the heart rate and velocity time integral were calculated (bottom). Column B - sagittal long axis view by B-Mode imaging, depicting heart morphology and chamber relative position to each other; BA - bulbus arteriosus, V - ventricle, A - atrium. Column C - measured parameters for both wildtype and FLNA knockout line 2; weight (W), length (L), heart rate (HR), ejection fraction (EF) and velocity time integral (VTI). EF and VTI for individual I:2 should be critically analyzed.

The purpose of the incross between line 1 and line 2 was to generate a compound heterozygous mutant. A stronger heart failure phenotype is expected from these individuals. The compound heterozygous led to a stronger phenotype with a higher death rate during embryonic stages. In

detail, only one compound heterozygous survived until adulthood (genotyping and FLNA protein levels shown in **Figure 4.13**). Compared to wildtype, this fish was small, had an altered fin structure and like fish I:2 from line 2, exhibited a noticeable pericardial edema. Once this individual died, the heart was dissected (**Figure 4.17 - A**). This heart showed massively enlarged chambers, both the ventricle and the atrium (**Figure 4.17 - B**). Furthermore, the blood accumulated outside of the heart chambers, probably within the pericardial cavity, suggesting a pericardial hemorrhagic effusion.

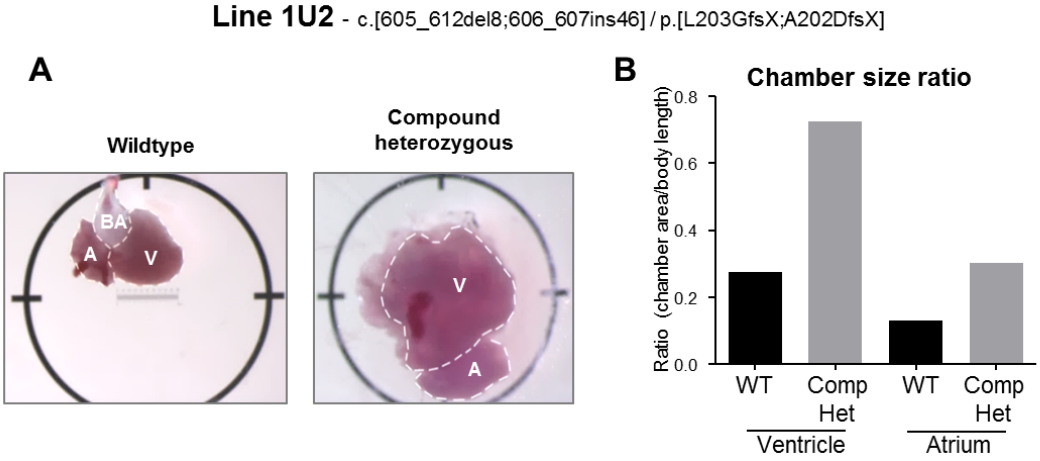

Figure 4.17: **Line 1U2 - Adult compound heterozygous phenotype.** A - dissected heart from a wildtype fish in comparison to the dissected heart from the compound heterozygous fish from the line 1 and 2 incross. B - chamber size ratio obtained by normalization of the chamber area to the body length.

Taken together, throughout all FLNA knockout (FLNA KO) generations, the adult heterozygous showed a tendency for reduced body weight (wildtype, mean±SD: 0.45±0.3 g; FLNA KO F1, mean±SD: 0.61±0.15 g, non-significant; FLNA KO F2, mean±SD: 0.31±0.1 g, non-significant; FLNA KO F3, mean±SD: 0.25±0.1 g, $p<0.05$) and length (wildtype, mean±SD: 3.3±0.3 cm; FLNA KO F1, mean±SD: 3.7±0.4 cm, non-significant; FLNA KO F2, mean±SD: 3.4±0.2 cm, non-significant; FLNA KO F3, mean±SD: 3.0±0.3 cm, non-significant; **Figure 4.18 - A and B**). This reduction might be due to the fact that the F1 and F2 fish were kept exclusively in individual 1L tanks, while F3 fish were kept in a 15 L tank, allowing feeding with no competition. A correlation between the FLNA knockout and the body weight and length was excluded.

As an indication for oxygen deprivation, the ventilation frequency was measured (number of buccal movements in 3 min; **Figure 4.18 - C**). Hyperventilation in F1 and F2 adult heterozygous fish was observed, while F3 coped better with the FLNA knockout in regard to oxygen deprivation (wildtype, mean±SD: 6.3±3.0 buccal movements; FLNA KO F1, mean±SD: 24.0±5.7 buccal movements, $p<0.0001$; FLNA KO F2, mean±SD: 17.5±6.4 buccal movements, $p<0.0001$; FLNA KO F3, mean±SD: 10.0±3.4 buccal movements, $p<0.001$).

Albeit individually the lines showed no significant heart rate reduction, when an analysis per generation was conducted, the heart rate was significantly increased for the F2, while the F1 and F3 remain not significantly different from the wildtypes (wildtype, mean±SD: 84.3±23.8 beats/min; FLNA KO F1, mean±SD: 95.3±13.1 beats/min, non-significant; FLNA KO F2, mean±SD: 121.3± 14.1 beats/min, $p<0.001$; FLNA KO F3, mean±SD: 94.2±19.2 beats/min, non-significant; **Figure 4.18 - D**).

The measured ejection fraction was significantly reduced for all generations, highlighting the heart failure phenotype in FLNA knockout lines (wildtype, mean±SD: 61.6±7.8 %; FLNA KO F1, mean±SD: 39.5±12.0 %, p<0.05; FLNA KO F2, mean±SD: 38.2±9.0 %, p<0.0001; FLNA KO F3, mean±SD: 46.2±13.3 %, p<0.001; **Figure 4.18 - E**). Interestingly, there was an increase in the SD (standard deviation) for the F3, accounting for the individuals with a wildtype-like ejection fraction mentioned before. The velocity time integral was significantly reduced for F2 and F3, ultimately reflected in the stroke volume and cardiac output (wildtype, mean±SD: 7.3±0.8 mm; FLNA KO F1, mean±SD: 7.4±0.4 mm, non-significant; FLNA KO F2, mean±SD: 4.7±1.4 mm, p<0.001; FLNA KO F3, mean±SD: 3.3±1.1 mm, p<0.0001; **Figure 4.18 - F**).

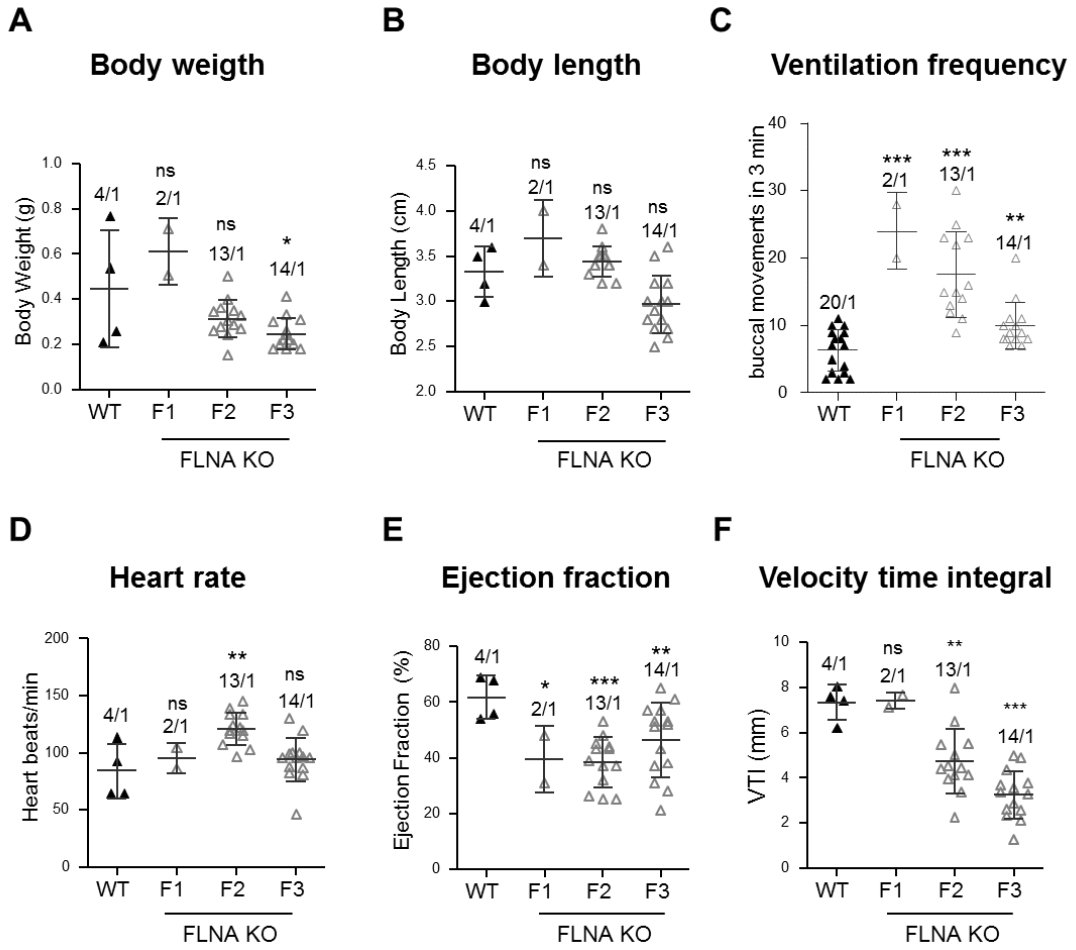

Figure 4.18: **FLNA knockout heterozygous adults analysis by generation.** A - body weight, in grams. B - body length, in cm. C - zebrafish ventilation frequency analysis (number of buccal movements in 3 min). D - heart rate, in heart beats per minute. E - ejection fraction, in %. F - velocity time integral, in mm. non-significant (ns); p<0.05 (*), p<0.001 (**) and p<0.0001 (***).

4.2.5 Homozygous embryos exhibited a wildtype phenotype

To investigate the consequences of FLNA knockout during heart development, F3 adults from each line were incrossed to generate F4 embryos. The only F3 male from line 2 was infertile. The outcross of line 2 F2 with wildtype was repeated to generate more F3 individuals. Nevertheless, the experiment was performed using the F3 heterozygous adults from line 1. In the F4 generation, was possible to identify wildtype, heterozygous and homozygous embryos (**Figure 4.19 - A**). According

to Mendel's laws of inheritance, 25 % wildtypes, 50 % heterozygous and 25 % homozygous is expected, which was approximately the ratios observed for FLNA knockout embryos (**Figure 4.19 - B**). Phenotypically, the embryos exhibit a wildtype body shape and heart morphology (**Figure 4.19 - C**), heart rate (wildtype, mean±SD: 123.0±18.0 beats/min; F4 heterozygous, mean±SD: 100.5±18.1 beats/min, non-significant; F4 homozygous, mean±SD: 108.0±12.0 beats/min, non-significant; **Figure 4.19 - D**) and fractional shortening (wildtype, mean±SD: 45.8±9.2 %; F4 heterozygous, mean±SD: 44.0±13.0 %, non-significant; F4 homozygous, mean±SD: 46.8±8.2 %, non-significant; **Figure 4.19 - E**).

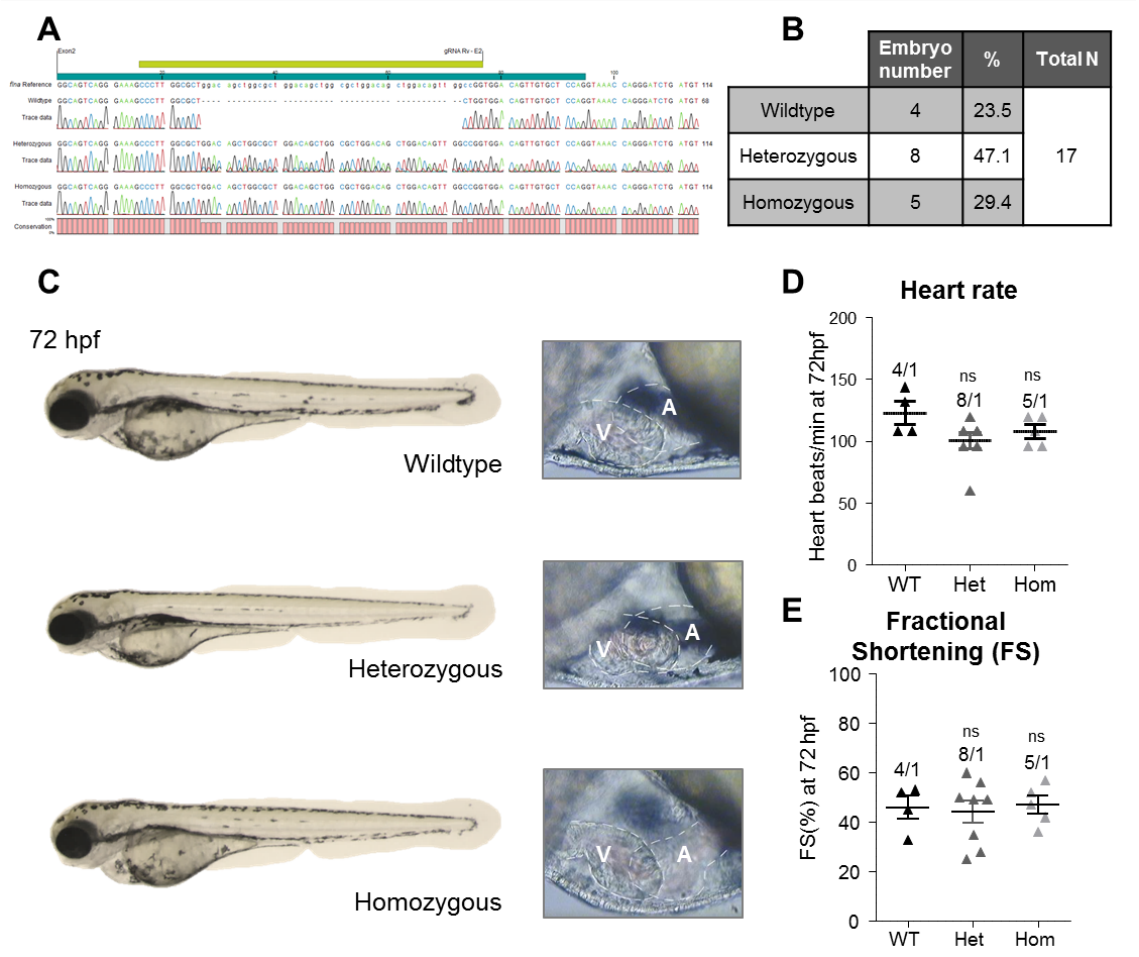

Figure 4.19: **Line 1 - F4 embryos analysis.** A - examples of the Sanger sequencing results for wildtype, heterozygous and homozygous embryos. B - incross embryo count per genotype. C - 72 hpf wildtype, heterozygous and homozygous embryos phenotype; V - ventricle, A - atrium. D - 72 hpf heart rate according to genotype. E - 72 hpf fractional shortening (FS) according to genotype. non-significant (ns).

4.2.6 Expression of *flnb* was up-regulated in FLNA knockout zebrafish

It was intriguing that the F3 incross yielded no heart failure phenotype embryos and that the heterozygous adults from both lines showed a phenotype compared to the compound heterozygous. Taken together, we hypothesised that an activation of compensatory mechanisms would lead to such results. In the zebrafish genome as annotated, no *flna* paralogues were found. Considering the filamin family, *flnb* expression was investigated in FLNA knockout lines.

RNA was extracted from zebrafish hearts of each generation of line 1 and 2 and using next generation sequencing the heart transcriptoms were obtained (see *Section 3.8.9*). A significant increase in *flnb* expression (**Figure 4.20 - A**) was detected. The expression of *flnb* was also analyzed in adult fin by qRT-PCR. These findings could be validated for line 1 but not line 2 (wildtype, mean±SD: 1.0±0-fold change; line 1, mean±SD: 4.8±13.0-fold change, p<0.0001; line 2, mean±SD: 1.8±2.1-fold change, non-significant; **Figure 4.20 - B**). However, analysing the **Figure 4.20** in more detail, it is possible to note that one individual (**Figure 4.20 - B, arrow**) has a high *flnb* expression (comparable to the *flnb* expression found in line 1 members). These results highlight the genetic and phenotypic heterogeneity in zebrafish, indicating that each fish will have an individual response to the FLNA knockout.

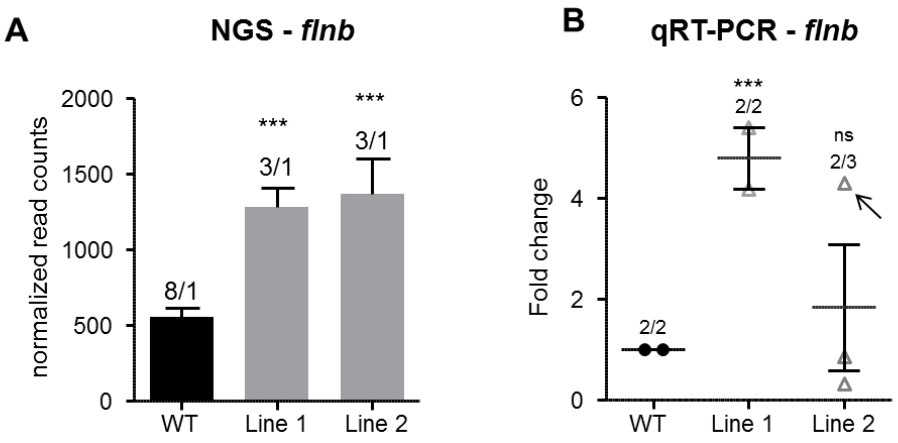

Figure 4.20: **Expression of *flnb* in FLNA knockout lines compared to wildtype.** A - heart transcriptome analysis of adult heterozygous from each line. Shown normalized read counts for *flnb* pooled per FLNA knockout line. B - fold change of the relative *flnb* expression for F2 founders of each line. Highlighted is the line 2 outlier (arrow). non-significant (ns) and p<0.0001 (***).

4.3 CBFβ localization was affected by β-adrenergic stress

As shown above, loss of FLNA leads to heart failure by yet unknown mechanisms. To gain insights into those, we used our model system described above to investigate if FLNA is a hub for CBFβ and if stressors that are known to induce heart failure act via this interplay. In order to further our knowledge regarding the interaction between CBFβ and FLNA their cellular localization were determined. FLNA was mainly detected in the cytoplasm of zebrafish embryos (**Figure 4.21 - A**). In wildtype conditions, CBFβ could also be detected in the cytoplasm. Furthermore, CBFβ is a structural protein located at the Z-disc, thus stripes in the sarcomere can be observed (**Figure 4.21 - B**).

Using a FLNA knockdown model these previous findings were corroborated by showing an increase of CBFβ in the nucleus, in the absence of FLNA (**Figure 4.21 - C**). In the wildtype setting, we strove to understand if stress could influence the location of CBFβ. Given the cardiomyopathy context of this thesis, β-adrenergic stress (through isoproterenol exposure) was investigated as a potential trigger of CBFβ translocation to the nucleus. Interestingly, the translocation from the sarcomere and cytoplasm to the nucleus did occur when the zebrafish embryos were under isoproterenol stress (**Figure 4.21 - D**). The number of CBFβ enriched nuclei were counted and divided by the total number of nuclei found in the section. These values were compared between wildtype, wildtype

stimulated with isoproterenol (ISO) and FLNA knockdown. According to these results, 39% of CBFβ translocated to the nucleus upon ISO stress, while 66% of CBFβ translocated to the nucleus upon FLNA knockdown.

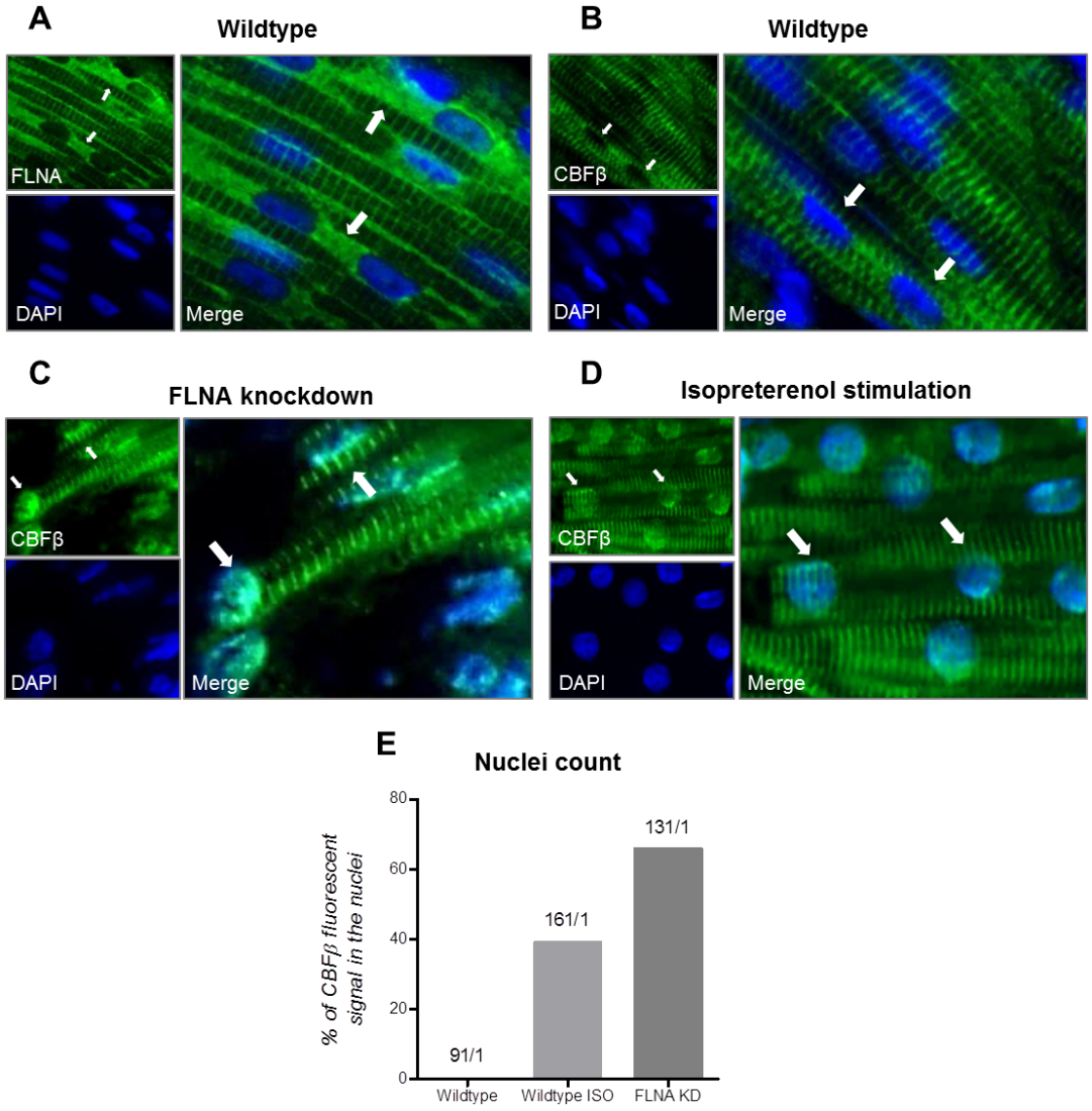

Figure 4.21: **Immunostainings using histological slices of 72 hpf zebrafish embryos.** A - location of FLNA (green) in wildtype. B - location of CBFβ (green) in wildtype. C - CBFβ localization (green) in FLNA knockdown (FLNA KD). D - CBFβ localization (green) in isoproterenol stimulated (ISO) wildtype zebrafish. E - percentage of CBFβ enriched nuclei, using immunostaining data.

Finally, to visualise the cellular localization of FLNA and CBFβ upon stress in a schematic manner, **Figure 4.22** was created. In the next steps, different stressors in embryos and adults will be investigated, in FLNA knockdown and knockout, respectively.

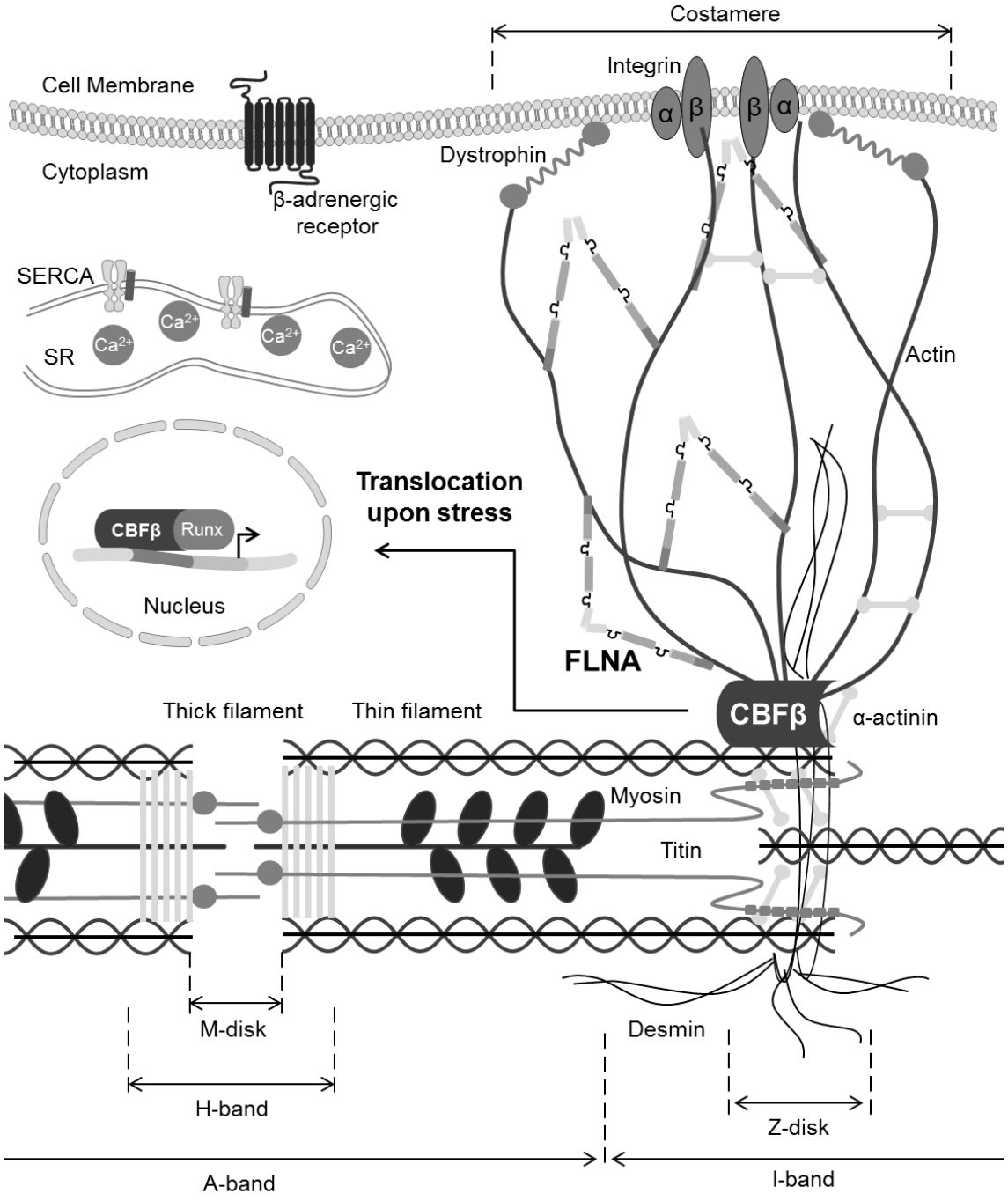

Figure 4.22: **Illustration of the cellular localization of FLNA and CBFβ.** Muscle cell scheme with cell membrane, cytoplasm, sarcoplasmic reticulum (SR) and nucleus represented. Adapted from Chien, 2000.

5 | Discussion

In this thesis, the function of FLNA was investigated using a zebrafish knockdown and knockout model. Our results showed that loss of FLNA, in both embryos and adults, resulted in a heart failure phenotype.

A member of the filamin family, FLNC was already associated with cardiomyopathies. Two different FLNC variants were correlated with restrictive cardiomyopathy when patients display an altered diastolic filling pattern and enlarged atria, but not with an abnormal systolic LV-function and wall thicknesses (Brodehl et al., 2015; Tucker et al., 2017). It was also shown that FLNC variants can result in hypertrophic cardiomyopathy derived from sarcomeric abnormalities and formation of FLNC aggregates in muscle cells (Valdés-Mas et al., 2014). Moreover, in a recent study a FLNC truncation variant was associated with dilated cardiomyopathy (DCM, Begay et al., 2018).

Given the similarities between FLNC and FLNA, it is expected that these proteins are involved in similar pathways. Hence, the role of FLNA in heart morphogenesis and function was thoroughly investigated in this thesis. There are several reports of FLNA variants in humans which showed a severe phenotype at different organ levels (Fox et al., 1998; Zhou et al., 2007; Kyndt et al., 2007; Goodwin et al., 2012; Robertson et al., 2006). Patients with human periventricular heterotopia exhibited congenital heart defects (Fox et al., 1998; Zhou et al., 2007), while patients affected by frontometaphyseal dysplasia and otopalatodigital syndrome also displayed cardiac malformations (Robertson et al., 2006; Goodwin et al., 2012). FLNA variants were further associated with familial cardiac valvular dystrophy (Kyndt et al., 2007).

A point mutation, as reported for FLNC (Brodehl et al., 2015; Tucker et al., 2017; Valdés-Mas et al., 2014; Begay et al., 2018), can have an extensive effect and might lead to heart failure. Unfortunately, only 30% to 50% of genetic dilated cardiomyopathies can be resolved by genetic testing because many of the DCM contributing genes remain unknown.

Phenotypic differences between the zebrafish FLNA transient knockdown and stable knockout

Discrepancies between morphant and mutant phenotypes have been reported (Rossi et al., 2015; El-Brolosy and Stainier, 2017; El-Brolosy et al., 2019; Stainier et al., 2017). At 72 hours post-fertilization (hpf), *flna* morphants and F0 CRISPR-injected embryos both showed a heart failure phenotype, with reduced heart rate and reduced fractional shortening (see *Section 4.1 and 4.2.1*).

However, the heterozygous F1, F2, F3 and homozygous F4 embryo generations exhibit none of the heart failure symptoms. There could be three main reasons for these differences between the knockdown and knockout lines: 1) the observed FLNA knockdown phenotype is due to unspecific effects; 2) the FLNA knockout phenotype is due to off-target effects and 3) in the FLNA knockout fish utilise compensatory mechanisms absent in the FLNA knockdown. These three reasons shall be discussed in the ensuing paragraphs.

One of the most common toxic effects of morpholino-mediated knockdown which may account for unspecific effects is the induction of cell death by activation of the p53 pathway (Robu et al., 2007). Using next generation sequencing to analyze the *flna* morphants' embryo transcriptome, no differences in the normalized read counts of *tp53*, between the morpholino control and MO-*flna*, could be detected.

Besides non-specific morpholino effects, the difference between morphants and mutants could also be attributed to mutant off-target effects. Six predicted gene off-targets were analyzed in mutant heterozygous adults and found to be unaffected (see *Section 4.2.3*). To comprehensively confirm the absence of unpredicted off-target effects with higher confidence, a whole genome sequencing analysis of each FLNA knockout line should be performed.

Up to date, multiple studies showed that phenotypic differences between morphants and mutants could be due to compensatory responses occurring in knockout animals (Rossi et al., 2015). In line with this data, an up-regulation of *flnb* was detected in different fish of line 1 and 2 that could explain the embryonic wildtype phenotype and the mild FLNA knockout phenotype observed in the heterozygous adults (see *Section 4.2.6*). A transcriptomic comparison between *flna* mutant and morphants was also conducted to confirm the mutant specific *flnb* overexpression. In morphants, *flnb* expression was not significantly different from the wildtype embryos. To further investigate the hypothesized compensatory mechanisms, a proteomic analysis should be conducted to verify the FLNB protein levels. FNLB protein levels in the mutant embryos and adults should be compared to wildtype zebrafish and additionally, to the *flna* morphants, the latter of which should not exhibit any compensation. Not all gene knockouts lead to an up-regulation of paralogues or same family genes; thus, genes with a function similar to FLNA (such as cytoskeletal proteins) should also be investigated as a possible alternative compensatory mechanism.

In conclusion, FLNA knockdown embryos showed a heart failure phenotype which was absent in FLNA knockout embryos. We hypothesize that the differences between morphants and mutants can be attributed to active compensatory mechanisms in the FLNA knockout lines.

FLNB as a compensatory gene in FLNA knockout lines

It has been reported that not every kind of DNA lesions was sufficient to trigger a compensatory response (El-Brolosy et al., 2019). El-Brolosy *et al.* (2019) showed that alleles that fail to produce a transcript is not sufficient to lead to an up-regulation of known compensatory genes. It was proposed that degradation of the mutant transcripts is the key to induce a transcriptional adaptation response. Such a mechanism has been reported for the *mt2* gene (Schuermann, Helker, and Herzog, 2015). A mutation in *mt2* exon 1 with high levels of nonsense-mediated mRNA decay displayed a mild angiogenesis phenotype. However, when the mutant transcripts were ablated with the use of an antisense-mediated knockdown, a much more severe phenotype emerged (El-Brolosy and Stainier, 2017).

FLNA knockout lines showed an overall reduction but not a complete ablation of *flna* expression levels. Based on the NGS data, all generations of each FLNA knockout line showed an up-regulation of cardiac *flnb* expression. Both filamins (FLNA and FLNB) share circa 90 % homology and have the same function although FLNB expression is much lower expressed compared to FLNA. Reported by Hu *et al.* (2017), loss of FLNA in mouse cartilage growth plate promotes FLNB expression and vice versa. Curiously, FLNA and FLNB can form functional heterodimers and stabilize the actin cytoskeleton. It was also suggested that this compensatory effect is cell-type specific, once loss of FLNB in lymphoblastoid cells did not stimulate an increase in expression of *flna* (Farrington-Rock et al., 2008). This emphasizes the need to study FLNA compensatory mechanisms specifically in cardiomyocytes.

It was observed that in the zebrafish heart, loss of FLNA leads to an overexpression of *flnb*. However, using qRT-PCR, different *flnb* expression levels within the same generation of line 2 individuals could be detected. A slight variation between individuals is expected due to naturally occurring divergences combined with technical inaccuracies. This stochastic variation can also be observed within the wildtype fish or within members of line 1. However, this natural variation does not account for the *flnb* 3-fold expression level changes found in one of line 2 members compared to the others (see *Section 4.2.6*). On the other hand, phenotypic heterogeneity could explain such wide variations in expression.

The line 2 fish that showed an increased expression of *flnb* demonstrates a similar compensatory mechanism to the one found in line 1. On the other hand, the other line 2 members, with wildtype levels of *flnb*, have an alternative compensatory response to FLNA knockout. Possibly, instead of a *flnb* overexpression, these individuals use an alternative compensatory gene or a different open reading frame or nonsense-mediated alternative splicing. The latter is a known event in which exons containing premature stop codons are skipped via alternative splicing (Hentze and Kulozik, 1999). Remarkably, the transcripts produced might escape the nonsense-mediated decay provided that the exon skipped does not contain essential motifs or that the newly formed transcript does not have a frame shift (Anderson et al., 2017). To study possible alternative *flna* transcripts found in FLNA knockout line 2 members, nanopore long-read sequencing is recommended.

Genetic and/or environmental variations lead to fluctuations in gene expression, which can impact the response mechanisms to loss-of-function mutations (Kasper et al., 2017). Like in humans, distinct genetic and phenotypic heterogeneity was observed. The members of line 1 and one particular individual of line 2 have different genomic mutations while presenting a similar compensatory mechanism. On the other hand, line 2 members with the same genomic mutation have discrete compensatory mechanisms.

Dilated cardiomyopathy phenotype in zebrafish

Zebrafish has been extensively used in cardiovascular research for the identification and validation of cardiomyopathy relevant genes (Vogel et al., 2009; Asnani and Peterson, 2014; Chen et al., 1996; Sehnert et al., 2002; Stainier et al., 1996; Driever et al., 1996; Xu et al., 2002). Different loss-of-function models were created for genes known to cause DCM in humans. Consistently these studies showed that the embryonic DCM phenotype in zebrafish is characterized by a reduced cardiac contractility and cardiac output, dilated ventricle and atrium, blood regurgitation from the ventricle to the atrium and blood congestion in the sinus venosus (Vogel et al., 2009). In

the FLNA transient knockdown model established, embryos showed similar results with reduced cardiac contractility, dilated chambers and blood regurgitation.

In human DCM there are gene-specific abnormalities. The same is observed in embryonic zebrafish DCM models; for example, the vinculin loss-of-function model exhibited impaired touch and flight response while the desmin loss-of-function model showed bradycardia (Vogel et al., 2009). In the FLNA transient loss-of-function model established in this thesis, besides the above mentioned features, embryos showed bradycardia and defects in re-absorption of the cardiac matrix.

Characterization of the embryonic phenotype is a crucial first step in unravelling the function of DCM relevant genes. However, embryos can only be investigated for a short time period and the mechanisms in action between embryos and adults most probably differ. Moreover, different techniques are available for the adult zebrafish such as swimming performance and drug tests which are not well established in embryos. Accordingly, it was relevant to evaluate adult zebrafish response to *flna* loss-of-function and a stable *flna* knockout line was created.

Up to date, adult zebrafish cardiomyopathy phenotype is characterized by changes in the heart morphology, with enlarged ventricles, for both hypertrophic cardiomyopathy (HCM) and DCM (Dvornikov, Tombe, and Xu, 2018). The described adult zebrafish DCM models are mainly characterized by hypocontractility and systolic dysfunction (Dvornikov, Tombe, and Xu, 2018). Also, in swimming performance test, fish with impaired cardiac function had a reduction in the maximal swimming velocity, compared to controls (Dvornikov, Tombe, and Xu, 2018). At the cellular level, the zebrafish HCM model showed reduced density and increased width of the isolated cardiomyocytes (Ding et al., 2011), while DCM hearts mostly exhibited elongated ones.

FLNA knockout lines showed a significantly reduced ejection fraction and velocity time interval, indicating a heart failure phenotype. Interestingly, F2 individuals displayed tachycardia which might be an attempt to compensate for the low cardiac output. The cardiac output is the product of the heart rate and the stroke volume (Young, 2010). Therefore, with reduced stroke volume the heart rate is increased to boost the volume of blood pumped to the organs (Young, 2010; Lymperopoulos, Rengo, and Koch, 2013). If the cardiac output is critically reduced for an extended period of time, even after the hormonal systems and the sympathetic reflexes have reached their maximum compensatory effects the progression of heart failure can not be counteracted (Young, 2010).

Our findings are consistent with previously described zebrafish DCM and heart failure phenotypes, both in embryos and in adults. It would be of interest to investigate the transcriptional levels of pathogenic cardiac remodelling genes, such as *nppa*, *nppb*, *vmhc* and *slc8a1a* (Dvornikov, Tombe, and Xu, 2018). Further research should also be conducted to understand how FLNA knockout adults perform under physical stress. Notwithstanding, to fully understand the extent of the cardiomyopathy observed in FLNA knockout lines, these hearts should be characterized at the cellular level.

β-adrenergic stimulation leads to CBFβ translocation to the nucleus

For the first time, β-adrenergic stimulation was identified as a stress factor inducing CBFβ translocation to the nucleus. A central role of the adrenergic nervous system (ANS) is the maintenance of a normal cardiac output (Kossack et al., 2017). When activated, the ANS increases heart rate, cardiac contractility, accelerates cardiac relaxation, decreases venous capacitance and leads to a

constriction of cutaneous arteries (Lymperopoulos, Rengo, and Koch, 2013). The ANS can be activated by two catecholamine neurotransmitters, norepinephrine and epinephrine; which are detected by cell surface adrenergic receptors (AR). Among the several types of adrenergic receptors, the human heart contains all subtypes of βAR in different proportions (75-80% of β_1, 15-18% of β_2 and 2-3 % of β_3). Upon activation of the cardiomyocyte β_1AR and β_2AR, the $G_{stimulatory}$ coupled protein triggers the adenylate cyclase to convert adenosine triphosphate (ATP) to cyclic adenosine monophosphate (cAMP). cAMP-dependent kinase (PKA) are thus activated and are able to phosphorylate different celullar targets. Among these targets are calcium channels, ryanodine receptors, phospholamban, hyperpolarization-activated cyclic nucleotide-gated channels, troponin I, myosin binding protein-C and phospholemman (Lymperopoulos, Rengo, and Koch, 2013). Ultimately, these events result in a significant increase in intracellular free Ca^{2+}, leading to alterations in cardiac muscle contractility. Furthermore, PKA can also phosphorylate the βAR which causes a functional desensitization. This can also be achieved by specialized G-protein-coupled receptor kinases (GRKs) that directly phosphorylate the βAR. β-arrestins bind to the phosphorylated receptor, promote its decoupling from the G-protein and target it for internalization.

With the help of β-adrenergic stimulation, the healthy heart can recover and maintain the cardiac output, such as during physical activity. On the other hand, an unhealthy heart with myocardial dysfunction could lead to a pathological hyperactivation of this pathway, resulting in increased cardiac toxicity culminating in an increased morbidity and mortality (Lymperopoulos, Rengo, and Koch, 2013).

In summary, β-adrenergic stimulation is an essential adaptation mechanism in the heart which needs to be fully understood. How this stimulation induced CBFβ translocation to the nucleus is not clear. Nonetheless, different hypothesis can be postulated: 1) the interaction between FLNA and CBFβ is disrupted by the calcium influx upon βAR activation; 2) FLNA and CBFβ can still interact but FLNA cleavage is increased and together FLNA and CBFβ translocate to the nucleus or, more likely, 3) a combination of the above two hypothesis.

Interestingly, it is known that PKA phosphorylates FLNA serine 2152 (located in Ig20, Peverelli et al., 2018). This FLNA phosphorylation impacts its conformation, dismantling the autoinhibitory structure formed between Ig21 and Ig19 when FLNA is not phosphorylated (Ithychanda et al., 2015). Curiously, FLNA S2152 phosphorylation facilitates the binding to integrins (Chen, Kolahi, and Mofrad, 2009), which might be relevant in a heart failure setting given the important role of integrins in different remodeling processes after myocardial infarction (Chen et al., 2016). It is thus conceivable that PKA-mediated FLNA phosphorylation might affect the ability of FLNA to bind CBFβ.

A direct correlation of FLNA phosphorylation and the β-adrenergic pathway was proposed by Pons *et a.* (2017), where phosphorylated FLNA serves as a scaffold that links cargo to endosomes, thereby promoting efficient recycling of β_2AR (Pons et al., 2017). Additionally, PKA activated by other ligand-activated G-protein-coupled receptors, were shown to increase FLNA phosphorylation of Ig domains 16-24 (Tirupula et al., 2015).

Furthermore, it is known that certain FLNA phosphorylations can inhibit calcium-dependent proteases (CAPNs) cleavage (Savoy and Ghosh, 2013). FLNA hinge 1 and 2 are known to be targeted by CAPNs (Zheng et al., 2014). It has been reported that upon activation of Wnt5a pathway, the resulting downstream signaling cascade leads to an increased calcium release from the sarcoplasmic reticulum into the cytoplasm, thereby activating the CAPN (O'Connell et al., 2009). The

activated CAPN cleaves FLNA into several fragments (O'Connell et al., 2009). In patients with heart failure, Wnt5a is up-regulated, which might promote myocardial inflammation and fibrosis (Abraityte et al., 2017). In a different context, Zheng *et al.* (2014) showed that in response to hypoxic stress, calpain-cleaved FLNA is increased. Moreover, unlike the uncleaved FLNA form, the cleaved FLNA fragments migrate together with their interacting partners to the nucleus and activate the transcription of downstream targets (Savoy and Ghosh, 2013). High levels of hypoxic stress are commonly found in late stages of hypertrophic and dilated cardiomyopathy.

As shown in *Section 4.1*, two different FLNA protein isoforms were detected in embryos and adult tissues; the predicted 270 kDa protein and also a 100 kDa fragment. This pattern has been previously observed in several studies (Zheng et al., 2014; Sorimachi and Ono, 2012; O'Connell et al., 2009; Abraityte et al., 2017; Savoy and Ghosh, 2013) and, using mass spectrometry, it was proven that both bands are indeed FLNA protein (Johnson et al., 2012). Nonetheless, FLNA cleavage status in cardiomyopathy patients is unknown and it would be interesting to investigate whether changes in the cleavage dynamics can be observed and correlated with the patients phenotype.

In zebrafish, it would be engaging to study the FLNA phosphorylation status after β-adrenergic stimulation and correlate it with FLNA cleavage status. If FLNA phosphorylation is increased, it would be of value to understand how FLNA and CBFβ interaction is affected. Possibly, by replacing FLNA serine 2152 with a phosphomimetic amino acid and performing immunoprecipitation experiments it would be possible to assess if FLNA and CBFβ could still interact. Moreover, analyzing FLNA and CBFβ nuclear and cytoplasmic localization, through protein fractionation, would allow a more accurate quantification of the translocation.

6 | Conclusions

Filamin A (FLNA) is an actin-binding cytoskeletal protein, mainly responsible for creating actin orthogonal networks. Additionally, FLNA interacts with multiple proteins and is therefore involved in several cellular processes and stress response mechanisms. A vast amount of FLNA mutations have been reported in humans and were even associated with cardiac malformations. Core Binding Factor β (CBFβ) is a structural protein of the sarcomeric Z-disc, essential to maintain its functional structure and thus essential for heart function. In different model systems, it has been shown that genetic abnormalities in genes involved in mechanical Z-disc stabilization lead to heart failure. Up to date, numerous genes are associated with primary cardiomyopathies but due to the individual genetic and phenotypic heterogeneity, the disease penetrance and expressivity vary greatly. Defining the cellular and molecular mechanisms by which gene variants lead to genetic cardiomyopathies will, ultimately, allow a finer understanding of the pathophysiology of heart failure.

This project was designed to assess the genomic and functional mechanism by which FLNA contributes to heart failure. Furthermore, one of FLNA proposed functions was to act as a regulatory layer of CBFβ shuttling, we sought to understand if a cardiac-relevant stress could interfere with FLNA/CBFβ interaction.

A morpholino-mediated knockdown of *flna* in zebrafish significantly impaired the embryos heart function. The observed morphant phenotype was not due to toxic effects of the morpholinos (given that the expression of *tp53* was not significantly elevated for the morphants) nor due to the interference from FLNA highly homologous counterpart FLNB (shown by the wildtype expression of *flnb* in the morphants). To elucidate the contribution of *flna* in adults, a stable *flna* knockout was created using CRISPR-CAS9 technology. Heterozygous FLNA knockout adults displayed a reduced ejection fraction and velocity time integral, indicating an impaired heart contractility and reduced cardiac output. In these adults, the heart morphology was altered revealing enlarged chambers, mainly the bulbus arteriosus and the ventricle. Differences between morphant and mutant embryos were observed and attributed to activated compensatory mechanisms in the FLNA knockout lines, through *flnb* overexpression. Off-target effects were mostly excluded given that the expression of all the predicted off-targets investigated was unaffected in FLNA knockout fish.

In humans, the main regulator of cardiac output is the adrenergic nervous system. In a heart failure setting, this pathway is overstimulated resulting in cardiotoxic effects. In zebrafish, it was shown that chronic β-adrenergic stimulation could induce cardiac dysfunction. Thus, we decided to investigate the localization of CBFβ upon such stimuli. Transduction of stress signals from the sarcomere to the nucleus is crucial to ensure an appropriate cell response to stress. CBFβ has been suggested as such a shuttling protein, but little is known about the stress factors that induce the aforementioned translocation. For the first time, β-adrenergic stimulation was shown to induce

CBFβ translocation to the nucleus.

Collectively, our results indicate that FLNA is essential for correct heart morphology and function. Notably, the same genetic and phenotypic heterogeneity seen with human variants was also observed for zebrafish FLNA knockout. Moreover, CBFβ, an essential sarcomeric structural protein necessary for proper heart function, was shown to translocate to the nucleus upon β-adrenergic stress. Further studies are needed to clarify the connection of both FLNA and CBFβ to heart failure. These would provide further possibilities to modulate pathogenic pathways in the heart and thereby potentially enabling the discovery of new therapies.

Bibliography

Abraityte, Aurelija et al. (2017). "Wnt5a is elevated in heart failure and affects cardiac fibroblast function." In: *J. Mol. Med.* 95.7, pp. 767–777.

Anderson, Jennifer L. et al. (2017). "mRNA processing in mutant zebrafish lines generated by chemical and CRISPR-mediated mutagenesis produces unexpected transcripts that escape nonsense-mediated decay." In: *PLoS Genet.* 13.11, pp. 1–18.

Anilkumar, Gopalakrishnapillai et al. (2003). "Prostate-specific membrane antigen association with filamin A modulates its internalization and NAALADase activity." In: *Cancer Res.* 63.10, pp. 2645–2648.

Asnani, Aarti and Randall T. Peterson (2014). "The zebrafish as a tool to identify novel therapies for human cardiovascular disease." In: *DMM Dis. Model. Mech.* 7.7, pp. 763–767.

Aster, Vinay Kumar Abul Abbas Jon (2014). *Robbins & Cotran Pathologic Basis of Disease.* Elsevier/Saunders.

Bakkers, Jeroen (2011). "Zebrafish as a model to study cardiac development and human cardiac disease." In: *Cardiovasc. Res.* 91.2, pp. 279–288.

Bartfeld, Deborah et al. (2002). "DNA recognition by the RUNX1 transcription factor is mediated by an allosteric transition in the RUNT domain and by DNA bending." In: *Structure* 10.10, pp. 1395–1407.

Bee, Thomas et al. (2010). "Nonredundant roles for Runx1 alternative promoters reflect their activity at discrete stages of developmental hematopoiesis." In: *Blood J.* 115.15, pp. 3042–3050.

Begay, Rene L. et al. (2018). "Filamin C truncation mutations are associated with arrhythmogenic dilated cardiomyopathy and changes in the cellâĂŞcell adhesion structures". In: *JACC Clin Electrophysiol* 4.4, pp. 504–514.

Blyth, Karen, Ewan R. Cameron, and James C. Neil (2005). "The RUNX genes: gain or loss of function in cancer." In: *Nat. Rev. Cancer* 5.5, pp. 376–387.

Bonow, Robert O. (2017). "Hypertrophic cardiomyopathy: past, present and future." In: *Trends Cardiovasc. Med.* 6.12.

Bresciani, Erica et al. (2014). "CBFbeta and RUNX1 are required at 2 different steps during the development of hematopoietic stem cells in zebrafish." In: *Blood J.* 124.1, pp. 70–78.

Bresnick, Anne R., Vivien Warren, and Jonh Condeelis (1990). "Identification of a short sequence essential for actin binding by Dictyostelium ABP-120." In: *J. Biol. Chem.* 265.16, pp. 9236–9240.

Brodehl, A. et al. (2015). "Mutations in Filamin C cause familial restrictive cardiomyopathy." In: *Can. J. Cardiol.* 31.10, S147.

Brown, Daniel et al. (2016). "Advances in the Study of Heart Development and Disease Using Zebrafish". In: *J. Cardiovasc. Dev. Dis.* 3.2, p. 13.

Cahill, Thomas J., Houman Ashrafian, and Hugh Watkins (2013). "Genetic cardiomyopathies causing heart failure." In: *Circ. Res.* 113.6, pp. 660–675.

Camacho, César López (2011). "A new role for Filamin A as a regulator of Runx2 function." PhD thesis. University of Manchester, pp. 1–195.

Chen, Chao et al. (2016). "Integrins na dintegrin-related proteins in cardiac fibrosis." In: *J Mol Cell Cardiol.* 93, pp. 162–174.

Chen, Harvey S., Kevin S. Kolahi, and Mohammad R.K. Mofrad (2009). "Phosphorylation facilitates the integrin binding of filamin under force." In: *Biophys. J.* 97.12, pp. 3095–3104.

Chen, Jau Nian et al. (1996). "Mutations affecting the cardiovascular system and other internal organs in zebrafish." In: *Development* 123, pp. 293–302.

Chen, Wei et al. (2014). "Cbfbeta deletion in mice recapitulates cleidocranial dysplasia and reveals multiple functions of Cbfbeta required for skeletal development." In: *PNAS* 111.23, pp. 8482–8487.

Chien, Kenneth R. (2000). "Genomic circuits and the integrative biology of cardiac diseases." In: *Nature* 407.6801, pp. 227–32.

Clark, Alice R. et al. (2009). "Skeletal dysplasias due to filamin A mutations result from a gain-of-function mechanism distinct from allelic neurological disorders." In: *Hum. Mol. Genet.* 18.24, pp. 4791–4800.

Czepluch, Frauke S., Bernd Wollnik, and Gerd Hasenfuß (2018). "Genetic determinants of heart failure: facts and numbers." In: *ESC Hear. Fail.* 5.3, pp. 211–217.

Dalkilic, I. et al. (2006). "Loss of FilaminC (FLNc) results in severe defects in myogenesis and myotube structure." In: *Mol. Cell. Biol.* 26.17, pp. 6522–6534.

Ding, Yonghe et al. (2011). "Haploinsufficiency of target of rapamycin attenuates cardiomyopathies in adult zebrafish". In: *Circ. Res.* 109.6, pp. 658–669.

Driever, W. et al. (1996). "A genetic screen for mutations affecting embryogenesis in zebrafish." In: *Development* 123, pp. 37–46.

Dvornikov, Alexey V., Pieter P. de Tombe, and Xiaolei Xu (2018). "Phenotyping cardiomyopathy in adult zebrafish". In: *Prog. Biophys. Mol. Biol.* 138, pp. 116–125.

Dyson, Jennifer M. et al. (2001). "The SH2-containing inositol polyphosphate 5-phosphatase, SHIP-2, binds filamin and regulates submembraneous actin." In: *J. Cell Biol.* 155.6, pp. 1065–1079.

El-Brolosy, Mohamed A. and Didier Y.R. Stainier (2017). "Genetic compensation: a phenomenon in search of mechanisms." In: *PLoS Genet.* 13.7, pp. 1–17.

El-Brolosy, Mohamed A. et al. (2019). "Genetic compensation triggered by mutant mRNA degradation." In: *Nature* 568, pp. 193–197.

Farrington-Rock, Claire et al. (2008). "Disruption of the Flnb gene in mice phenocopies the human disease spondylocarpotarsal synostosis syndrome." In: *Hum. Mol. Genet.* 17.5, pp. 631–641.

Feng, Yuanyi et al. (2006). "Filamin a (FLNA) is required for cell-cell contact in vascular development and cardiac morphogenesis." In: *PNAS* 103.52, pp. 19836–19841.

Forrester, A. Michael, Jason N. Berman, and Elspeth M. Payne (2012). "Myelopoiesis and Myeloid Leukaemogenesis in the Zebrafish." In: *Adv. Hematol.* Pp. 1–12.

Fox, Jeremy W et al. (1998). "Mutations in filamin 1 prevent migration of cerebral cortical neurons in human periventricular heterotopia." In: *Neuron* 21.6, pp. 1315–1325.

Gergen, J. Peter and Barbara A. Butler (1988). "Isolation of the Drosophila segmentation gene runt and analysis of its expression during embryogenesis." In: *Genes Dev.* 2, pp. 1179–1193.

Goodwin, Richard L. et al. (2012). "Developmental basis for filamin-A-associated myxomatous mitral valve disease." In: *Cardiovasc. Res.* 96.1, pp. 109–119.

Gravante, Biagio et al. (2004). "Interaction of the pacemaker channel HCN1 with filamin A." In: *J. Biol. Chem.* 279.42, pp. 43847–43853.

Grunwald, DJ and G Streisinger (1992). "Induction of recessive lethal and specific locus mutations in the zebrafish with ethyl nitrosourea." In: *Genet. Res.* 59.2, pp. 103–116.

Haas, J et al. (2015). "Atlas of the clinical genetics of human dilated cardiomyopathy." In: *Eur. Hear. J.* 36.18, pp. 1123–1135.

Hart, Alan W. et al. (2006). "Cardiac malformations and midline skeletal defects in mice lacking filamin A." In: *Hum. Mol. Genet.* 15.16, pp. 2457–2467.

He, Hua Jun et al. (2003). "Interaction of filamin A with the insulin receptor alters insulin-dependent activation of the mitogen-activated protein kinase pathway." In: *J. Biol. Chem.* 278.29, pp. 27096–27104.

He, Xiaoqing et al. (2000). "Identification of actin binding protein, ABP-280, as a binding partner of human Lnk adaptor protein." In: *Mol. Immunol.* 37.10, pp. 603–612.

Hein, Selina J. et al. (2015). "Advanced echocardiography in adult zebrafish reveals delayed recovery of heart function after myocardial cryoinjury." In: *PLoS One* 10.4, pp. 1–21.

Hentze, Matthias W. and Andreas E. Kulozik (1999). "A perfect message: RNA surveillance and nonsense-mediated decay." In: *Cell* 96.3, pp. 307–310.

Hershberger, RE E, DJ J Hedges, and A Morales (2013). "Dilated cardiomyopathy: the complexity of a diverse genetic architecture." In: *Nat. Rev. Cardiol.* 10.9, pp. 531–547.

Himmel, Mirko et al. (2003). "The limits of promiscuity: isoform-specific dimerization of filamins." In: *Biochemistry* 42.2, pp. 430–439.

Hobbs, F. D.Richard et al. (2007). "Prognosis of all-cause heart failure and borderline left ventricular systolic dysfunction: 5 year mortality follow-up of the Echocardiographic Heart of England Screening Study (ECHOES)". In: *Eur. Heart J.* 28, pp. 1128–1134.

Howe, Kerstin et al. (2013). "The zebrafish reference genome sequence and its relationship to the human genome." In: *Nature* 496, pp. 498–503.

Huang, Gang et al. (2001). "Dimerization with PEBP2beta protects RUNX1/AML1 from ubiquitin-proteasome-mediated degradation." In: *EMBO J.* 20.4, pp. 723–733.

Inoue, Ken-ichi et al. (2002). "Runx3 controls the axonal projection of proprioceptive dorsal root ganglion neurons." In: *Nat. Neurosci.* 5, pp. 946–954.

Ithychanda, Sujay Subbayya et al. (2015). "A mechanism of global shape-dependent recognition and phosphorylation of filamin by protein kinase A." In: *J. Biol. Chem.* 290.13, pp. 8527–8538.

Ito, Kosei et al. (2008). "RUNX3 attenuates beta-catenin/T cell factors in intestinal tumorigenesis." In: *Cancer Cell* 14.3, pp. 226–237.

Ito, Yoshiaki (2004). "Oncogenic potential of the RUNX gene family: 'Overview'." In: *Oncogene* 24.23, pp. 4198–4208.

Johnson, Kristen et al. (2012). "A stem cell-based approach to cartilage repair." In: *Science.* 336.6082, pp. 717–721.

Jonz, Michael G. and Colin A. Nurse (2005). "Development of oxygen sensing in the gills of zebrafish." In: *J. Exp. Biol.* 208.8, pp. 1537–1549.

Kamachi, Y et al. (1990). "Purification of a mouse nuclear factor that binds to both the A and B cores of the polyomavirus enhancer." In: *J. Virol.* 64.10, pp. 4808–19.

Kasper, Dionna M. et al. (2017). "microRNAs establish uniform traits during the architecture of vertebrate embryos." In: *Dev Cell* 40.6, pp. 552–565.

Kim, Chungho et al. (2005). "Filamin is essential for shedding of the transmembrane serine protease, epithin." In: *EMBO Rep.* 6.11, pp. 1045–1051.

Kim, Eun Joo, Jong Sup Park, and Soo Jong Um (2007). "Filamin A negatively regulates the transcriptional activity of p73α in the cytoplasm." In: *Biochem. Biophys. Res. Commun.* 362.4, pp. 1101–1106.

Knöll, R., M. Hoshijima, and K. R. Chien (2002). "Z-line proteins: Implications for additional functions." In: *Eur. Hear. J. Suppl.* 4, pp. I13–I17.

Komori, T et al. (1997). "Targeted disruption of Cbfa1 results in a complete lack of bone formation owing to maturational arrest of osteoblasts." In: *Cell* 89.5, pp. 755–764.

Kossack, Mandy et al. (2017). "Induction of cardiac dysfunction in developing and adult zebrafish by chronic isoproterenol stimulation." In: *J. Mol. Cell. Cardiol.* 108, pp. 95–105.

Krief, Stephane et al. (1999). "Identification and Characterization of cvHsp." In: *J. Biol. Chem.* 274.51, pp. 36592–36600.

Kyndt, Florence et al. (2007). "Mutations in the gene encoding filamin A as a cause for familial cardiac valvular dystrophy." In: *Circulation* 115.1, pp. 40–49.

Labeit, Siegfried et al. (2006). "Expression of distinct classes of titin isoforms in striated and smooth muscles by alternative splicing, and their conserved interaction with filamins." In: *J. Mol. Biol.* 362.4, pp. 664–681.

Labun, Kornel et al. (2016). "CHOPCHOP v2: a web tool for the next generation of CRISPR genome engineering." In: *Nucleic Acids Res.* 44.W1, W272–W276.

Li, Qing-Lin et al. (2002). "Causal relationship between the loss of RUNX3 expression and gastric cancer." In: *Cell* 109.1, pp. 113–124.

Liu, Gseping et al. (1997). "Cytoskeletal protein ABP-280 directs the intracellular trafficking of furin and modulates proprotein processing in the endocytic pathway." In: *J. Cell Biol.* 139.7, pp. 1719–1733.

Liu, P et al. (1993). "Fusion between transcription factor CBFbeta/PEBP2beta and a myosin heavy chain in actue myeloid leukemia." In: *Science.* 261.5124, pp. 1041–1044.

Lu, Jie et al. (2007). "Filamin B mutations cause chondrocyte defects in skeletal development." In: *Hum. Mol. Genet.* 16.14, pp. 1661–1675.

Lymperopoulos, Anastasios, Giuseppe Rengo, and Walter J. Koch (2013). "Adrenergic nervous system in heart failure: Pathophysiology and therapy." In: *Circ. Res.* 113.6, pp. 739–753.

Machol, Keren, Roberto Mendoza-Londono, and Brendan Lee (2006). "Cleidocranial Dysplasia Spectrum Disorder." In: *Gene Rev. Seattle, USA*, pp. 1993–2019.

Maron, Barry J., Antonio Pelliccia, and Paolo Spirito (1995). "Cardiac Disease in Young Trained Athletes". In: *Circ. Res.* 19.5.

Maron, Barry J. et al. (2006). "Contemporary definitions and classification of the cardiomyopathies: an American Heart Association Scientific Statement from the Council on Clinical Cardiology, Heart Failure and Transplantation Committee; Quality of Care and Outcomes Research and Functio". In: *Circulation* 113.14, pp. 1807–1816.

Marti, Amelia et al. (1997). "Actin-binding protein-280 binds the stress-activated protein kinase (SAPK) activator SEK-1 and is required for tumor necrosis factor-alpha activation of SAPK in melanoma cells." In: *J. Biol. Chem.* 272.5, pp. 2620–2628.

Meder, B. et al. (2010). "JunB-CBF signaling is essential to maintain sarcomeric Z-disc structure and when defective leads to heart failure." In: *J. Cell Sci.* 123.15, pp. 2613–2620.

Meder, Benjamin (2017). *Genetische Kardiomyopathien.* De Gruyter, p. 324.

Mestroni, Luisa et al. (2014). "Genetic causes of dilated cardiomyopathy." In: *Prog Pediatr Cardiol* 37, pp. 13–18.

Minsaas, Laura et al. (2010). "Filamin a binds to CCR2B and regulates its internalization." In: *PLoS One* 5.8.

Montague, Tessa G. et al. (2014). "CHOPCHOP: A CRISPR/Cas9 and TALEN web tool for genome editing." In: *Nucleic Acids Res.* 42, pp. 401–407.

Morales, Ana and Ray Hershberger (2017). "Clinical Application of Genetic Testing in Heart Failure". In: *Curr Hear. Fail Rep.* 14.6, pp. 543–553.

Nagata, Takashi et al. (1999). "Immunoglobulin motif DNA recognition and heterodimerization of the PEBP2/CBF Runt domain." In: *Nat. Struct. Biol.* 6.7, pp. 615–619.

Nakamura, Fumihiko, Thomas P. Stossel, and John H. Hartwig (2011). "The filamins: organizers of cell structure and function." In: *Cell Adhes. Migr.* 5.2, pp. 160–169.

O'Connell, Michael P et al. (2009). "Wnt5a activates the calpain-mediated cleavage of filamin A." In: *J Invest Dermatology* 129.7, pp. 1782–1789.

Onoprishvili, Irma et al. (2003). "Interaction between the mu opioid receptor and filamin A is involved in receptor regulation and trafficking." In: *Mol. Pharmacol.* 64.5, pp. 1092–1100.

Petrecca, K., D. M. Miller, and A. Shrier (2000). "Localization and enhanced current density of the Kv4.2 potassium channel by interaction with the actin-binding protein filamin." In: *J. Neurosci.* 20.23, pp. 8736–8744.

Peverelli, E. et al. (2018). "cAMP/PKA-induced filamin A (FLNA) phosphorylation inhibits SST2 signal transduction in GH-secreting pituitary tumor cells." In: *Cancer Lett.* 435, pp. 101–109.

Pons, Mònica et al. (2017). "Phosphorylation of filamin A regulates chemokine receptor CCR2 recycling." In: *J. Cell Sci.* 130.2, pp. 490–501.

Poon, Kar Lai and Thomas Brand (2013). "The zebrafish model system in cardiovascular research: A tiny fish with mighty prospects." In: *Glob. Cardiol. Sci. Pract.* 1, pp. 9–28.

Popowicz, Grzegorz M. et al. (2006). "Filamins: promiscuous organizers of the cytoskeleton." In: *Trends Biochem. Sci.* 31.7, pp. 411–419.

Robertson, Stephen P. et al. (2006). "Frontometaphyseal dysplasia: mutations in FLNA and phenotypic diversity." In: *Am. J. Med. Genet.* 140.16, pp. 1726–1736.

Robu, M E et al. (2007). "p53 activation by knockdown technologies." In: *PLoS Genet.* 3.5, pp. 0787–0801.

Rossi, Andrea et al. (2015). "Genetic compensation induced by deleterious mutations but not gene knockdowns." In: *Nature* 524, pp. 230–233.

Sampson, Laura J., Mark L. Leyland, and Caroline Dart (2003). "Direct Interaction between the Actin-binding Protein Filamin-A and the Inwardly Rectifying Potassium Channel, Kir2.1." In: *J. Biol. Chem.* 278.43, pp. 41988–41997.

Sasaki, Aya et al. (2001). "Filamin associates with Smads and regulates transforming growth factor-beta signaling." In: *J. Biol. Chem.* 276.21, pp. 17871–17877.

Sasaki, K. et al. (1996). "Absence of fetal liver hematopoiesis in mice deficient in transcriptional coactivator core binding factor beta." In: *Proc. Natl. Acad. Sci. U. S. A.* 93.22, pp. 12359–12363.

Savoy, Rosalinda M and Paramita M Ghosh (2013). "The dual role of filamin A in cancer: can't live with (too much of) it, can't live without it." In: *Endocr. Relat. Cancer* 20.6, R341–R356.

Sawyer, Gregory M. et al. (2009). "Disease-associated substitutions in the filamin B actin binding domain confer enhanced actin binding affinity in the absence of major structural disturbance: Insights from the crystal structures of filamin B actin binding domains." In: *J. Mol. Biol.* 390.5, pp. 1030–1047.

Schindelin, Johannes et al. (2012). "Fiji: an open-source platform for biological-image analysis." In: *Nat. Methods* 9.7, pp. 676–82.

Schuermann, Annika, Christian S.M. Helker, and Wiebke Herzog (2015). "Metallothionein 2 regulates endothelial cell migration through transcriptional regulation of vegfc expression." In: *Angiogenesis* 18.4, pp. 463–475.

Sedaghat-Hamedani, Farbod et al. (2017). "Clinical genetics and outcome of left ventricular noncompaction cardiomyopathy." In: *Eur. Heart J.* 38.46, pp. 3449–3460.

Sehnert, Amy J. et al. (2002). “Cardiac troponin T is essential in sarcomere assembly and cardiac contractility.” In: *Nat. Genet.* 31.1, pp. 106–110.

Sharif-Naeini, Reza et al. (2009). “Polycystin-1 and -2 dosage regulates pressure sensing.” In: *Cell* 139.3, pp. 587–596.

Sheen, Volney L. et al. (2002). “Filamin A and Filamin B are co-expressed within neurons during periods of neuronal migration and can physically interact.” In: *Hum. Mol. Genet.* 11.23, pp. 2845–2854.

Sorimachi, Hiroyuki and Yasuko Ono (2012). “Regulation and physiological roles of the calpain system in muscular disorders.” In: *Cardiovasc. Res.* 96.1, pp. 11–22.

Stahlhut, Martin and Bo Van Deurs (2000). “Identification of filamin as a novel ligand for caveolin-1: evidence for the organization of caveolin-1-associated membrane domains by the actin cytoskeleton.” In: *Mol. Biol. Cell* 11.1, pp. 325–337.

Stainier, Didier Y R et al. (1996). “Mutations affecting the formation and function of the cardiovascular system in the zebrafish embryo.” In: *Development* 123, pp. 285–292.

Stainier, Didier Y.R. et al. (2017). “Guidelines for morpholino use in zebrafish.” In: *PLoS Genet.* 13.10, pp. 6–10.

Stossel, Thomas P. et al. (2001). “Filamins as integrators of cell mechanics and signalling.” In: *Nat. Rev. Mol. Cell Biol.* 2.2, pp. 138–145.

Sverdlov, Maria et al. (2009). “Filamin A regulates caveolae internalization and trafficking in endothelial cells.” In: *Mol. Biol. Cell* 20, pp. 4531–4540.

Taylor, Martha R. et al. (2019). *Campbell biology: concepts and connections.* 9th editio. Pearson, p. 928.

Tirupula, Kalyan C. et al. (2015). “G protein-coupled receptors directly bind filamin A with high affinity and promote filamin phosphorylation.” In: *Biochemistry* 54.44, pp. 6673–6683.

Towbin, Jeffrey A. et al. (2006). “Incidence, causes, and outcomes of dilated cardiomyopathy in children.” In: *Am. Med. Assoc.* 296.15, pp. 1867–1876.

Tucker, Nathan R. et al. (2017). “Novel Mutation in FLNC (Filamin C) Causes Familial Restrictive Cardiomyopathy”. In: *Circ Cardiovasc Genet* 10.6.

Vadlamudi, Ratna K. et al. (2002). “Filamin is essential in actin cytoskeletal assembly mediated by p21-activated kinase 1.” In: *Nat. Cell Biol.* 4.9, pp. 681–690.

Valdés-Mas, Rafael et al. (2014). “Mutations in filamin C cause a new form of familial hypertrophic cardiomyopathy”. In: *Nat. Commun.* 5.

Vogel, Britta et al. (2009). “In-vivo characterization of human dilated cardiomyopathy genes in zebrafish”. In: *Biochem. Biophys. Res. Commun.* 390.3, pp. 516–522.

Wang, K. and S. J. Singer (1977). “Interaction of filamin with F-actin in solution.” In: *Proc. Natl. Acad. Sci. U. S. A.* 74.5, pp. 2021–2025.

Westerfield, Monte (1995). *The Zebrafish Book - A guide for the laboratory use of zebrafish.* University of Oregon Press, Eugene.

Xu, Xiaolei et al. (2002). “Cardiomyopathy in zebrafish due to mutation in an alternatively spliced exon of titin.” In: *Nat. Genet.* 30.2, pp. 205–209.

Yoshida, Koji et al. (2002). “Leucine-rich repeat region of decorin binds to filamin-A.” In: *Biochimie* 84.4, pp. 303–308.

Yoshida, Naomi et al. (2005). “Filamin A-bound PEBP2beta/CBFbeta is retained in the cytoplasm and prevented from functioning as a partner of the Runx1 transcription factor.” In: *Mol. Cell. Biol.* 25.3, pp. 1003–12.

Young, DB (2010). *Control of Cardiac Output.* San Rafael (CA): Morgan & Claypool Life Sciences.

Yuan, Yuan and Zhiyuan Shen (2001). “Interaction with BRCA2 suggests a role for filamin-1 (hsFLNa) in DNA damage response.” In: *J. Biol. Chem.* 276.51, pp. 48318–48324.

Zhang, Wanjiang et al. (1998). “Interaction of presenilins with the filamin family of actin-binding proteins.” In: *J. Neurosci.* 18.3, pp. 914–922.

Zheng, Xiaowei et al. (2014). “Hypoxia-induced and calpain-dependent cleavage of filamin A regulates the hypoxic response.” In: *Proc. Natl. Acad. Sci. U. S. A.* 111.7, pp. 2560–2565.

Zhou, Xianghua et al. (2007). “Filamin B deficiency in mice results in skeletal malformations and impaired microvascular development.” In: *Proc. Natl. Acad. Sci. U. S. A.* 104.10, pp. 3919–3924.

del Sol Keyer, Maria et al. (2015). “CCTop: an intuitive, flexible and reliable CRISPR/Cas9 target prediction tool.” In: *PLoS One* 10.4, pp. 1–11.

Supplements

Known interaction partners of FLNA, that bind the repeat 23 and the self-association domain, are listed in **Table S1**.

Table S1: **Filamin partners binding to the region from repeat 23 to repeat 24.** Table adapted from Nakamura, Stossel, and Hartwig, 2011.

Partner	Binding site	Significance	References
Signalling			
TRPP2	20-24	FLNA reduces the activity of strech-activated ion channels	Sharif-Naeini et al., 2009
MKK-4	21-23	Necessary for TNFα activation of SAPK	Marti et al., 1997
Phosphorylation			
SHIP-2	22-24	SHIP-2 membrane ruffles localization is dependent on FLNA	Dyson et al., 2001
PAK1	23	FLNA regulates PAK1-induced cytoskeletal reorganization	Vadlamudi et al., 2002
LNK	19-23	Its interaction with FLNA possibly leads T-cell activation	He et al., 2000
Proteolysis			
Epithin	14-24	FLNA is essential for the epithin shedding	Kim et al., 2005
PMSA	23-24	Regulates internalization of PMSA and its enzymatic activity	Anilkumar et al., 2003
Furin	13-24	FLNA is required for Furin trafficking	Liu et al., 1997
Ion channels			
Kv4.2	20-24	FLNA localizes Kv4.2 channel to filopodial roots and enhances its current density	Petrecca, Miller, and Shrier, 2000
Kir2.1	23-24	FLNA regulates surface expression of the Kir2.1 potassium channel	Sampson, Leyland, and Dart, 2003
HCN1	23-24	FLNA localizes HCN1 to specific neuronal areas and modulates its channel activity	Gravante et al., 2004
Transcription			
p73α	20-24	FLNA inhibits p73α transcriptional activity by retaining it in the cytoplasm	Kim, Park, and Um, 2007
BRCA2	21-24	Interaction with FLNA is required for efficient regulation of early stages of DNA repair processes	Yuan and Shen, 2001

Partner	Binding site	Significance	References
Smad5	20-23	FLNA facilitates TGFβ-mediated SMAD phosphorylation and nuclear transportation	Sasaki et al., 2001
Receptors			
μ opioid	H2-24	FLNA is required for agonist-induced receptor down-regulation and functional desensitization	Onoprishvili et al., 2003
Insulin	22-24	FLNA interacts with insulin signaling to inhibit MAPK cascade	He et al., 2003
CCR2B	19-24	FLNA is required for efficient internalization of the CCR2B receptor	Minsaas et al., 2010
Muscle development			
Titin	22-24	FLNA binds to the titin Z2-Zis1 domain in smooth muscle cells	Labeit et al., 2006
Others			
Caveolin-1	22-24	Interaction with FLNA promotes caveolae-mediated endocytosis and trafficking	Stahlhut and Van Deurs, 2000; Sverdlov et al., 2009
Decorin	22-24	FLNA binds to the leucine-rich repeat region of decorin	Yoshida et al., 2002
cvHsp	23-24	cvHsp interacts with FLNA in the human heart and insulin-sensitive tissues	Krief et al., 1999
Presenilins	21-24	FLNA interacts with the presenilin loop regions mutated in familial Alzheimer's disease	Zhang et al., 1998

CBFβ protein alignment between human and zebrafish showed a highly conserved *runx* binding domain (**Supplement Figure S1**).

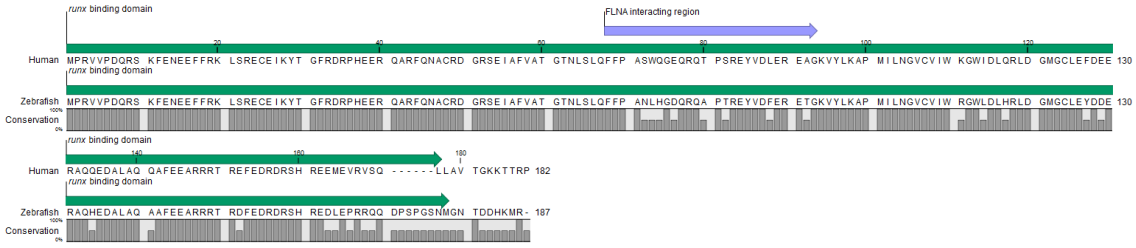

Figure S1: **Human and zebrafish CBFβ protein alignment**. Highlighted are the *runx* binding domain and the FLNA interaction region.

FLNA protein, with 86% similarity, is highly conserved between human and zebrafish (**Supplement Figure S2**).

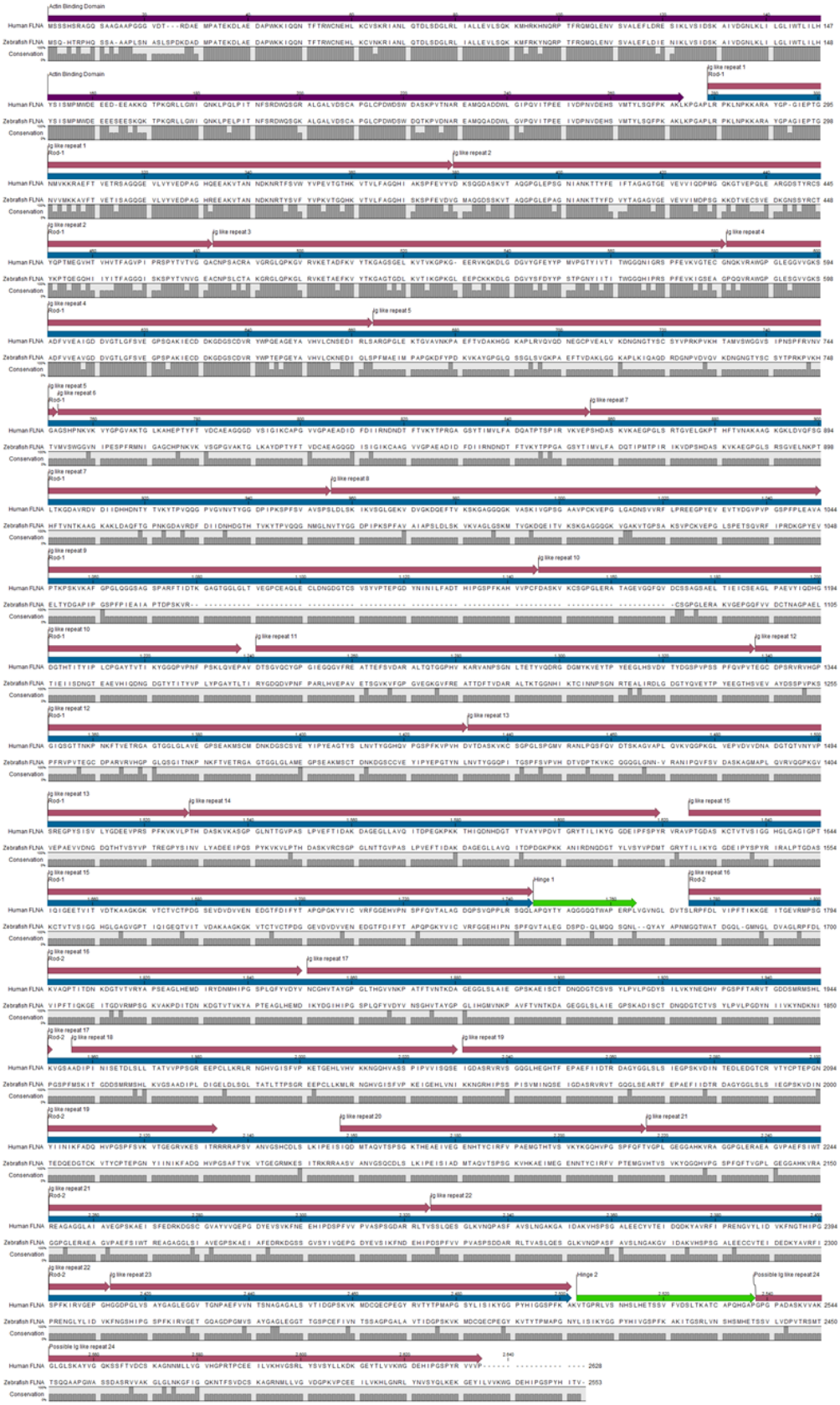

Figure S2: **Human and zebrafish FLNA protein alignment.** Marked in the alignment are the several FLNA domains: Actin binding domain (purple), Rod1 and 2 (blue) with its several Ig-like repeats (red) and hinge region (green).

List of Figures

List of Tables

List of Abbreviations

Abbreviation	Explanation
A	Atrium
aa	Amino acid
ABD	Actin binding domain
ACTB	Beta-actin
ADP	Adenosine diphosphate
AHA	American heart association
ANS	Adrenergic nervous system
AR	Adrenergic receptor
ARVC	Arrythmogenic right ventricle cardiomyopathy
ATP	Adenosine triphosphate
BA	Bulbus arteriosus
bp	Base pair
bpm	Beats per minute
BRCA	BRCA DNA repair associated
BSA	Bovine serum albumin
Ca^{2+}	Calcium ion
$CaCl_2$	Calcium chloride
cAMP	Cyclic adenosine monophosphate
CAPN	Calpain
CAS	CRISPR associated protein 9
CCR2B	C-C motif chemokine receptor
cDNA	Complementary DNA
CH	Calponin homology domain
cm	Centimeter
Comp Het	Compound heterozygous
CRISPR	Clustered regularly interspaced short palindromic repeats
D	Self-association domain
DAPI	4',6-Diamidine-2'-phenylindole dihydrochloride
DCM	Dilated cardiomyopathy
Del	Deletion
DMSO	Dimethyl sulfoxide
DNA	Deoxyribonucleic acid
dNTP	Nucleoside triphosphate
dpf	Days post fertilization

Abbreviation	Explanation
DTT	Dithiothreitol
ECL	Enhanced chemiluminescence
EDTA	Ethylenediaminetetraacetic acid
EF	Ejection fraction
EGFP	Enhanced green fluorescent protein
FCS	Fetal calf serum
FITC	Fluorescein isothiocyanate
FS	Fractional Shortening
GAPDH	Glyceraldehyde-3-phosphate dehydrogenase
GRK	G-protein-coupled receptor kinase
gRNA	guide RNA
h	Hour
H_2O	Water
H_2O_2	Hydrogen peroxide
HCl	Hydrochloric acid
HCM	Hypertrophic cardiomyopathy
HCN	Hyperpolarization activated cyclic nucleotide gated potassium channel
Het	Heterozygous
Hom	Homozygous
hpf	Hours post fertilization
HR	Heart rate
HRP	Horseradish peroxidase
HSPC	hematopoietic stem and progenitor cells
Ig	Immunoglobulin
Ins	Insertion
ISO	Isoproterenol
kb	Kilo base
KCl	Potassium chloride
KD	Knockdown
kDa	Kilo Dalton
KGN	Kartogenin
Kir	Inwardly rectifying potassium channel
KO	Knockout
L	Length
L	Liter
L	Lumen
LNK	Lymphocyte adapter protein
LVNC	Left ventricular non-compaction
M	Molar
mA	Milli ampere
MAPK	Mitogen activated protein kinase
$MgCl_2$	Magnesium chloride
$MgSO_4$	Magnesium sulfate
μg	Microgram
μL	Microliter

Abbreviation	Explanation
μM	Micromolar
min	Minute
MKK	MAPK kinase
mL	Milliliter
mm	Millimeter
mM	Millimolar
MO	Morpholino
mRNA	Messenger RNA
MW	Molecular weight
MYBPC	myosin binding protein C
MYH	β Myosin heavy chain
NaCl	Sodium chloride
NaF	Sodium fluoride
$NaHCO_3$	Sodium bicarbonate
$NaVO_3$	Sodium metavanadate
NGS	Next generation sequencing
NH_4OH	Ammonium hydroxide
NLS	Nuclear localization signal
NMTS	Nuclear matrix targeting signal
ns	non-significant
OMIM	Online mendelian inheritance in man
P_c	Compensation pressure
P_i	Injection pressure
PAGE	Polyacrylamide gel electrophoresis
PAK	P21 activated kinase 1
PAM	Protospacer adjacent motif
PCR	Polymerase chain reaction
PKA	Protein kinase A protein
pmol	Picomol
PMSA	Prostate-specific membrane antigen
PMSF	Phenylmethylsulfonyl fluoride
PTU	1-phenyl-2-thiourea
QA	Glutamine-alanine repeat domain
qRT	Quantitative real-time
RCM	Restrictive cardiomyopathy
RNA	Ribonucleic acid
ROI	Region of interest
rpm	Revolutions per minute
RQN	RNA quality number
SAPK	Stress-activated protein kinase
SD	Standard deviation
SDS	Sodium dodecyl sulfate
sec	Second
SEM	Standard error of the mean
SHIP	Phosphatidylinositol 3,4,5-trisphosphate 5-phosphatase

Abbreviation	Explanation
Skm	Skeletal muscle
SR	Sarcoplasmic reticulum
t_i	Injection time
TGFβ	Transforming Growth Factor Beta β
TNFα	Tumor necrosis factor α
TNNT	cardiac troponin-T
TPM1	α-tropomyosin
Tris	Tris hydroxymethyl aminomethane
TRITC	Tetramethylrhodamine
TRPP	Transient receptor potential polycystic
TUBB	Tubulin β
V	Ventricle
V	Volt
VTI	Velocity time integral
W	Watt
W	weight
WT and wt	Wildtype
%	Percent
°C	Degree Celsius

Nucleotide code

Abbreviation	Explanation
A	Adenine
C	Cytosine
G	Guanine
T (or U)	Thymine (or Uracil)

Amino acid code

Abbreviation	Explanation
G	Glycine (Gly)
P	Proline (Pro)
A	Alanine (Ala)
V	Valine (Val)
L	Leucine (Leu)
I	Isoleucine(Ile)
M	Methionine (Met)
C	Cysteine (Cys)
F	Phenylalanine (Phe)
Y	Tyrosine (Tyr)
W	Tryptophan (Trp)
H	Histidine (His)
K	Lysine (Lys)
R	Arginine (Arg)
Q	Glutamine (Gln)
N	Asparagine (Asn)
E	Glutamic Acid (Glu)
D	Aspartic Acid (Asp)
S	Serine (Ser)
T	Threonine (Thr)